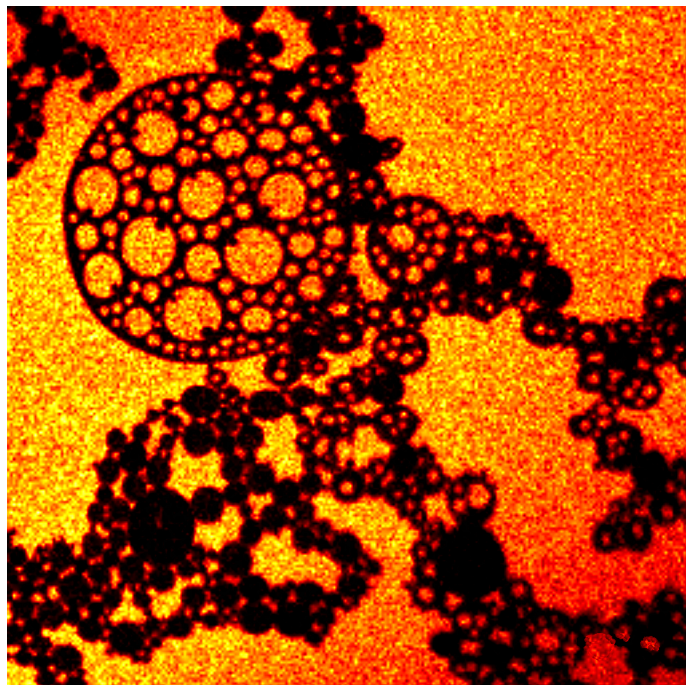


Interactions of FCHo2 with lipid membranes



Dissertation

Submitted to TU Dresden, Department of Biology for the degree of
Doctor rerum naturalium
(Dr. rer. nat.)

By Grzegorz Chwastek
Born on March 22nd, 1984 in Wrocław, Poland

6th February 2013

'And if I have prophetic powers, and understand all mysteries and all knowledge, and if I have all faith, so as to remove mountains, but have not love, I am nothing.'

1Cor.13:2 ESV

Abstract

Endocytosis is one of the most fundamental mechanisms by which the cell communicates with its surrounding. Specific signals are transduced through the cell membrane by a complex interplay between proteins and lipids. Clathrin depended endocytosis is one of the most important signalling pathways which leads to budding of the plasmalemma and a formation of endosomes. The FCHo2 is an essential protein at the initial stage of the this process. It is a membrane binding protein containing BAR (BIN, Amphiphysin, Rvs) domain which is responsible for membrane binding. Although numerous valuable studies on BAR proteins were published recently, the mechanistic description of BAR domain functionality is missing. In the present work, we applied *in vitro* systems in order to gain knowledge about the molecular basis of the activity of the FCHo2 BAR domain. In our studies, we used supported lipid bilayers (SLBs) and lipid monolayers as s model membrane system. The experiments were carried out with a minimal number of components including the purified FCHo2 BAR domain. Using SLBs, we showed that the BAR domain can bind to entirely flat bilayers. We also demonstrated that these interactions depend on the negatively charged lipid species incorporated in the membrane. We designed an assay which allows to quantify the membrane tubulation. We found out that the interaction of the FCHo2 BAR domain with the lipid membrane is concentration dependent. We showed that an area of the bilayer deformed by the protein depends on the BAR domain concentration.

In order to study the relation between the mobility of the lipids and the activity of FCHo2 BAR domain, we designed a small-volume monolayer trough. The design of this micro-chamber allows for the implementation of the light microscopy. We demonstrated that the measured lipid diffusion in the monolayer by our new approach is in agreement with the literature data. We carried out fluorescence correlation spectroscopy (FCS) experiments at different density of lipids at the water-air interface. We showed that the FCHo2 BAR domain binding affinity is proportional to the mean molecular area (MMA). We additionally demonstrated that the increased protein binding is correlated with the higher lipid mobility in the monolayer. Additionally, by curing out high-speed atomic force microscopy (hsAFM) we acquired the structural information about FCHo2 BAR domains orientation at the membrane with a high spatio-temporal resolution. Obtained data indicate the BAR domains interact with each other by many different contact sites what results in a variety of protein orientations in a protein assemble.

Motivation and outline

BAR proteins are a big family of membrane binding proteins. Due to their multi-functionality, these proteins take part in a variety of processes. Among them, the endocytosis is of fundamental importance (1). This process is initiated by the FCHo2 protein (2) and it is a sequence of recruitment events leading to invagination of the plasmalemma and a formation of the lipid vesicle (3), (4), (5), (6). Among many proteins involved in the endocytosis, BAR proteins are the least studied. While some of biological functions of this group of proteins are known from *in vivo* studies (7), (3), (2), (8), (6), (9), (10) the molecular mechanism by which BAR proteins specifically bind to cell membranes is still unclear. Recent experiments which revealed the ternary structure of many BAR domains (11), (12), (13), (14) and molecular dynamics simulations (15), (16), (17) were pioneering studies helping in understanding the mechanism of interactions between those proteins and the lipid bilayer. The main focus in these studies so far was on proteomics. On the other hand, not much is known about the role of the lipid composition and other membrane properties in the binding and the bilayer tubulation activity of BAR proteins. Gaining information on these details is crucial for understanding how the activity of BAR proteins is regulated. Due to complex protein-protein and protein-lipid interactions in the cell, questions regarding the basic BAR domain behaviour are extremely difficult to address with *in vivo* methodology. Therefore, we found that a bottom-up approach in such a case will be of a great use. Using a purified protein together with minimal lipid systems was shown to be a powerful tool in the investigation of protein-lipid interactions (18), (19), (20), (21), (22).

In part I of this work, a general introduction to the proteomics is given. It is focused on the relation between the structure, biochemical properties and the functionality of molecules. Further, the *in vitro* systems used in this work are described. The general introduction to the field of lipids is given and it is followed by a discussion on advantages and drawbacks of each lipid system. At the end of this section the theoretical introduction to the phenomenon of fluorescence is described. Basic concepts of absorption and emission are presented and their relation to the emission spectrum is discussed. Further, the fluorescence correlation spectroscopy is described with a focus on basic diffusion models and possible artifacts.

Part II describes the practical realisation of the concepts described theoretically in part I. Furthermore, the protein purification protocols and descriptions of other wet-lab procedures used in this work are discussed.

Part III presents the results obtained in present work. The order of the presentation is in accordance of the development of the project and it reflects the time-line of the work. Firstly, experiments with SLBs system are presented and the quantitative tubulation assay is described. Then the monolayer system is introduced as an alternative and supplementary method by which an investigation of BAR domains properties can be carried out more thoroughly. The last chapter of this part comprises the results of the collaboration with the research group of prof. Toshio Ando where high speed AFM was used in order to gain knowledge about the structural features of the protein ensemble.

List of publications

1. Chiantia S., Ries J., Chwastek G., Carrer D., Li Z., Bittman R., Schwille P. (2008)
Role of ceramide in membrane protein organization investigated by combined AFM and FCS. *Biochim Biophys Acta*.
2. Carrer D., Kummer E., Chwastek G., Chiantia S., Schwille P. (2009)
Asymmetry determines the effect of natural ceramides on model membranes. *Soft Matter*.
3. Gubernator J., Chwastek G., Korycińska M., Stasiuk M., Gryniewicz G., Lewrick F., Süß R., Kozubek A. (2010)
The encapsulation of idarubicin within liposomes using the novel EDTA ion gradient method ensures improved drug retention in vitro and in vivo. *J. Control. Release*.
4. Arumugam S., Chwastek G., Schwille P. (2011)
Protein-membrane interactions: the virtue of minimal systems in systems biology. *Wiley Interdiscip Rev Syst Biol Med*.
5. Herold C., Chwastek G., Schwille P., Petrov EP. (2012)
Efficient electroformation of super-giant unilamellar vesicles containing cationic lipids on ITO-coated electrodes. *Langmuir*.
6. Arumugam S., Chwastek G., Fischer-Friedrich E., Ehrig C., Mönch I., Schwille P., (2012).
Surface topology engineering of membranes for mechanical investigation of tubulin homologue FtsZ. *Angew Chem Int Ed Engl*.
7. Chwastek G., Schwille P.,
New approach to study protein interactions with lipid monolayer. (*submitted*)
8. Sezgin E., Chwastek G., Levental I., Simons K., Schwille P.,
Photoconversion of fluorescent lipid analogs. (*in preparation*)

Table of Contents

Abstract	5
Motivation and outline	7
List of publications	9
I. Theoretical Basis	13
1. BIN/Amphyphysin/Rvs proteins	15
1.1. Introduction	15
1.2. Membrane binding domains	17
1.3. The origin, function and properties of BAR proteins	18
2. Lipid systems for <i>in vitro</i> studies	24
2.1. Introduction	24
2.2. Lipids	24
2.3. Monolayer systems	26
2.4. Bilayer systems	28
3. Fluorescence based techniques	30
3.1. Fluorescence	30
3.2. Fluorescence Correlation Spectroscopy	31
4. Atomic Force Microscopy	35
II. Materials and Methods	37
5. Protein expression, purification and labelling of BAR domains	39
5.1. Vectors and bacterial expression systems	39
5.2. Purification protocol	40
5.3. Labelling procedure	41
5.4. Other proteins used in this studies	42
6. Model membrane systems	43
6.1. Lipid handling	43
6.2. Supported Lipid Bilayers (SLBs)	43
6.3. Langmuir monolayers	46
6.4. Monolayers troughs for FCS	47

Table of Contents

7. Atomic force microscopy measurements	53
7.1. Instrumentation	53
7.2. Procedure	53
8. Confocal Microscopy	54
8.1. Fluorescent probes	54
8.2. Imaging instrumentation	54
8.3. Fluorescence correlation spectroscopy instrumentation	54
III. Results	57
9. BAR protein binding to SLBs	59
9.1. Introduction	59
9.2. Tubulation of SLBs by FCHo2 BAR domain	59
9.3. Quantitative tubulation assay	60
9.4. Influence of negatively charged lipids on protein affinity	62
9.5. Phase separation and membrane tubulation	65
9.6. Discussion	67
10. BAR domain binding to monolayers	68
10.1. Introduction	68
10.2. Mobility of lipids in monolayers	69
10.3. FCHo2 binding assay	71
10.4. Discussion	74
11. Quaternary structure of BAR ensemble investigated by high-speed AFM	75
Conclusions	77
Acknowledgements	79
Abbreviations	81
Bibliography	82
Declaration (Erklärung)	89

Part I.

Theoretical Basis

1. BIN/Amphyphysin/Rvs proteins

1.1. Introduction

Cell is a fundamental form of living organisms. From bacteria to mammals, cell is the most versatile functional unit. Over the years of evolution this simple, single cell organisms 'learnt' how to adjust to constantly changing environment conditions and became more resistant and competitive. During this process, grouping together was the phenomenon which provided additional advantages giving the origin of the multicellular organism. Cells started to differentiate into specialised groups which took over more complex tasks. On every step of the mentioned processes the essential feature which allowed cells to survive was the ability to sense and react to changes in the surrounding. This required many complex mechanisms to be developed which would help to exchange the information through the wall barrier inwards the cell (Figure 1.1).

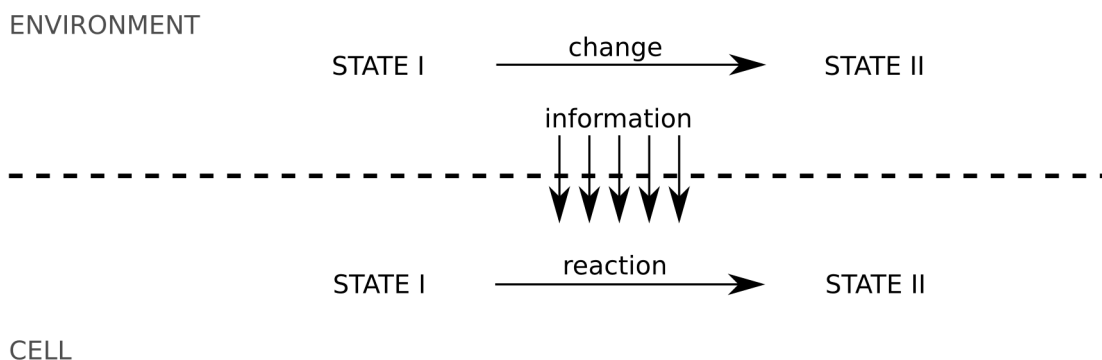


Figure. 1.1.: The schematic graph showing the basic information flow between the environment and the cell. Upper part represents the environment of the cell. At the starting point, conditions are in state I corresponding to equilibrium state I of the cell. Once the surrounding undergoes changes the cell senses the current conditions and reacts respectively in order to adjust to the new local environment.

While proteins, the so called 'cellular tools', are the essential element of almost every biochemical process in the cell they are not sufficient and, by the work of many scientists over last century, revealed the importance of plasmalemma. It is mostly made by lipid bilayer (23), contains almost 50% w/w of proteins within its lipid core (24) and shows structural and functional heterogeneity proposed by the so called lipid-raft model (25). Since the beginning of the twentieth century, cellular membrane is not only considered as a mechanical barrier, but rather like a sophisticated organelle which actively participates in the communication between the cell interior and the environment. One of the most straightforward way, to recognise current conditions of the surrounding is to probe its chemical composition. In order to do so, cells developed variety of mechanisms which are mostly based on the internalisation of the molecules of interest. This process called endocytosis, it is one of the most fundamental and complex phenomenon taking place in the cell (1). Any alteration of the endocytosis causes severe, often lethal, changes in the cell metabolism. In the case of multicellular organisms, it

1. BIN/Amphiphysin/Rvs proteins

was shown that many of mutations of proteins involved in endocytosis have implication in diseases including Alzheimer's disease or Down's syndrome and cancers. Comprehensive review on the diseases and syndromes connected with abnormalities of endocytic pathways is given in (26).

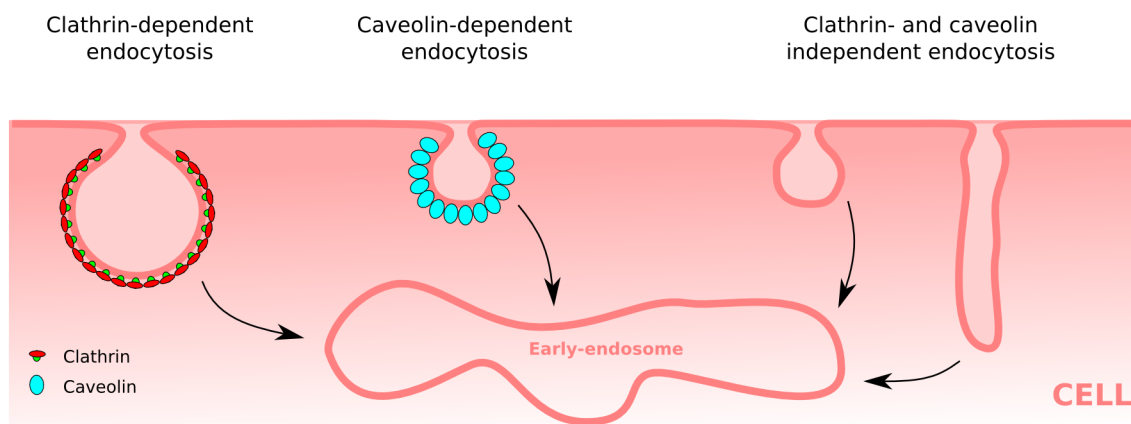


Figure. 1.2.: Three types of edocytic pathways. The clathrin-dependent internalisation is one of the most studies endocytosis gateways. It requires adaptor proteins and clathrin which assembles around the engulfed plasmalemma which is then cut off by the dynamin and forms endocytic vesicle. Another known path of endocytosis is mediated by caveolin which also assembles on the budding vesicles at the cell membrane. Besides these two ways, there is evidence that the cell can internalise molecules also independently from clathrin and caveolin.

During evolution cell developed variety of proteins which are used to co-ordinate complex interactions network. Proteins are polymers folded in unique manner which defines their function and specificity. Across all protein structures known two main secondary motifs are very abundant. These are α -helix and β -sheets (Figure 1.3A, B respectively).

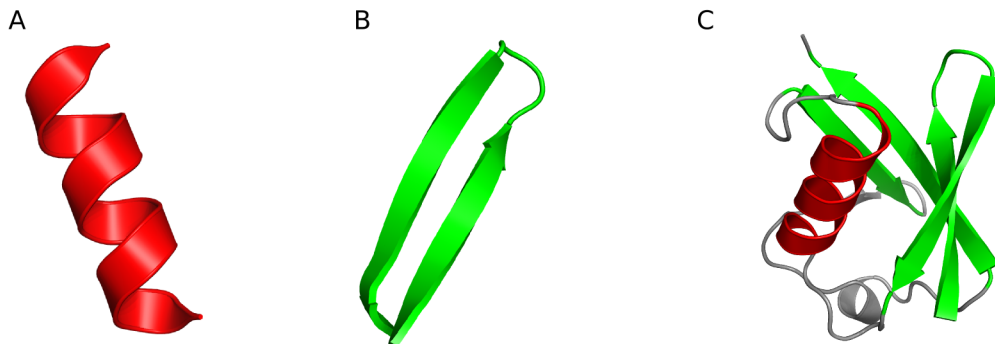


Figure. 1.3.: The 3D representation of two common secondary structures. A) α -helix structure. B) β -sheet structure. C) Both α -helix (red) and β -sheet (green) marked in the structure of ubiquitin (27).

The unique size, orientations and specific amino-acid sequence determines the overall structure of the protein (figure 1.3. C) While there are plenty of small proteins like ubiquitin existing, such a protein can be used to synthesise multi-domain structures. In many cases the domains preserve their original functionality and the resulting multi-domain protein exhibits increased functionality. Cholera

Toxin is one of the best studied examples of such a multi-domain organisation of the protein (28). It consists of one subunit A and pentameric subunit B which is responsible for the binding of the whole protein to the sugar moiety of lipids present at the cell membrane. After the protein binds to the membrane it is internalised by endocytic pathway. In the cell, subunit A becomes active and ADP-ribosilate G proteins which are turned into permanent active state.

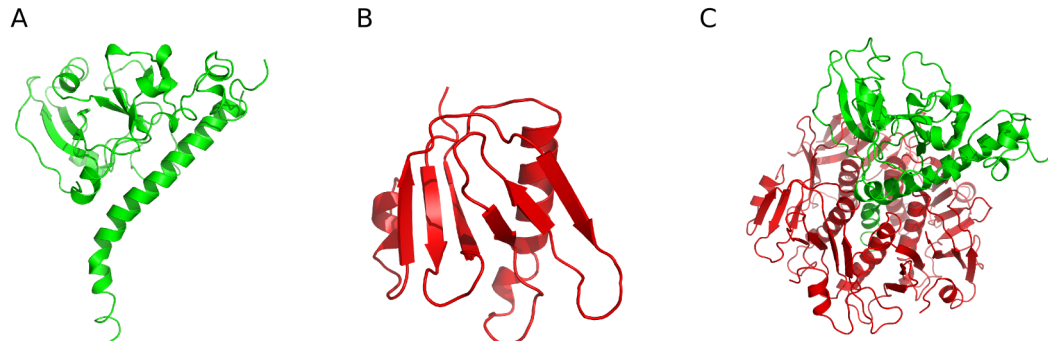


Figure 1.4: The multi-domain structure of the cholera toxin. A) Subunit A which has ADP-ribosylation activity with exposed extended α -helix that helps to dock to the pentameric subunit B. B) Single subunit B which has high affinity towards sugar moieties of gangliosides. C) The cholera toxin structure with visible subunit A (green) and B5 (red).

Proteins like cholera toxin are widely spread and used to accomplish more complex tasks. During the endocytosis where signaling pathways cross the membrane, multi-domain proteins are often used in order to perform the specific task at particular place on the membrane. In such a case one domain is used to dock the protein to the lipid bilayers while the second domain has specific enzymatic activity. It is also possible that the already bound protein recruits another molecules. This sequence method of protein binding ensures that the specific task will be performed in the right order which often is required for successful accomplishing of the biochemical pathway.

1.2. Membrane binding domains

Among the many proteins involved in the endocytic machinery, membrane binding proteins are one of the greatest importance. These proteins coordinate the enzymatic activity of many proteins at the plasmalemma so that each step of the endocytosis occurs in the right place and at the right moment. Over the evolution, cells developed variety of membrane binding domains - a functional subunit of the protein which task is to anchor the protein to the lipid interface. These domains are very abundant in nature and are a part of such essential proteins like: protein kinase C (PKC) (29), epsin (5), early endosome antigen 1 (EEA1) (30) or amphiphysin (31). Example structures of lipid binding domains are shown in figure 1.5. Although all of these domains provide the same functionality to the protein, they exhibit different anchoring mechanisms (32). While the pleckstrin homology domain (PH) specifically binds to phosphatidylinositols (PtdIns) by amphipathic helices (33), FYVE domains use rather coordinated zinc ions incorporated in their structure (34). Epsin N-terminal homology domain (ENTH) on the other hand forms positively charged pocket which accommodates specifically PtdIns(4,5)P₂ (5). BAR domains belong to another very interesting super-family. BAR domains have form of an elongated coiled-coil α structure which is a dimer. It usually has banana-shape (12) and depending on the

1. BIN/Amphiphysin/Rvs proteins

subgroup of the particular domain, it can interact with the lipid membrane by electrostatic interaction (11) or rather using hydrophobic residues which anchors into the bilayer (7).

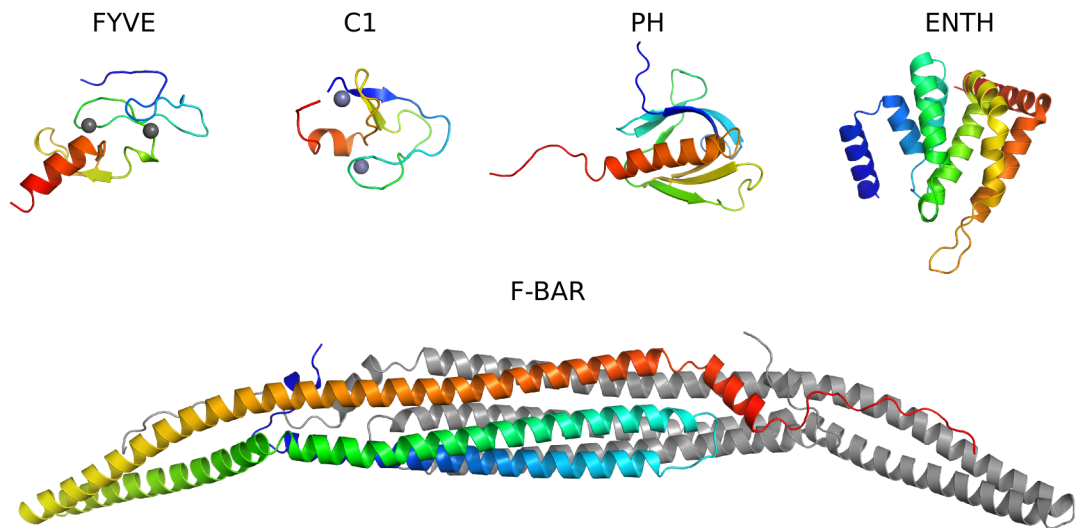


Figure 1.5.: Example structures of membrane binding domains: Fab1/YOTB/Vac1/EEA1 (FYVE, PDB ID: 1VFY), diacylglycerol binding domain (C1, PDB ID: 1PTR), pleckstrin homology domain (PH, PDB ID: 1PLS) Epsin N-terminal homology domain (ENTH, PDB ID: 1H0A) and FER-CIP4 BAR domain (F-BAR, PDB ID: 2V0O).

1.3. The origin, function and properties of BAR proteins

The BAR domain family takes its origin from studies on BIN1 (box-dependent myc-interacting protein-1) by group of George Prendergast (35). That work describes newly identified protein BIN1 as an interaction partner of MYC oncprotein. Further analysis of the protein sequence and an alignment with other known proteins revealed that BIN1 shares a homologous fragment with amphiphysin and Rvs167. While that time there was no evidence for high ternary similarities of those three proteins, the N-terminal sequence homology was recognised as a BAR (BIN1/Amphiphysin/RVS167) domain (Figure 1.6).

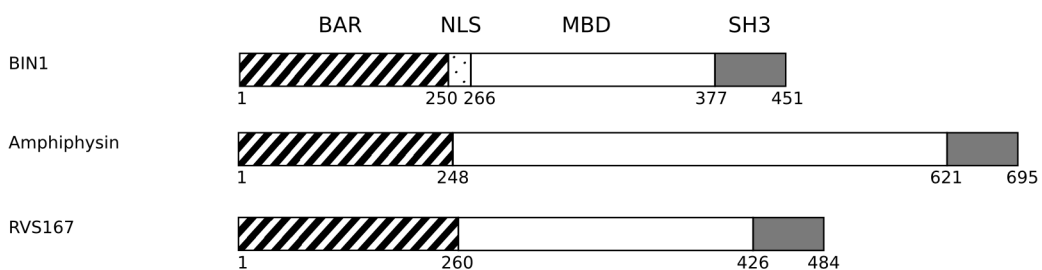


Figure 1.6.: Schematic drawing of protein amino-acid sequences (adopted from (35)). All of proteins contain the SH3 domain (dark grey) and newly identified N-terminal BAR domains (dashed area).

The first insight into the ternary/quaternary organisation of the BAR domain came from the work of Peter in which the first structure of BAR domain, amphiphysin, was resolved (12). In the following year, the structure of endophilin was published (14) - the second BAR protein which revealed in fact high structure similarities of both proteins. Furthermore, it was found that adjacent N-terminal region of BAR domains corresponds to α -helix with amphipathic properties, i.e. the residues on one side of the helix are mostly polar/charger whereas on other side they have rather hydrophobic characteristic. Studies by EPR showed that this not structured fragment of the protein becomes folded once the protein is bound to membrane (7). To emphasise this feature BAR domains with adjacent amphipathic α -helix were named N-BAR domains. In chorus with studies on N-BAR domains *per se*, many groups were focus on finding actin regulatory proteins. Syndapin was the protein which was shown to participate at the very early stage of the endocytosis and that it binds to dynamin, synaptosomal and N-WASP protein which is an activator of an actin nucleation complex (36), (37). Additionally, it was discovered that syndapin comprises of (Fer/CIP4) FCH homology domain with adjacent aa. sequence of a predicted coiled-coil structured. Identification of a new proteins FBP17 and FCHo2 with the same FCH-CC tandem was a motivation for De Camilli group to analyse mentioned proteins not only as the important part of the endocytic machinery but additionally as a potential members of a new class of proteins (38). Similar membrane tubulation activity and an important role in dynamin and actin networking suggested that FCH-CC might in fact be a distinct protein family. Itoh et al. estimated that FCH-CC is of about 300 aa. long and predicted that the secondary structure of combined domains comprises of three α -helices. Because of many similarities in functions and ternary structure of BAR domains and FCH-CC domains, it became obvious that the FCH might be a part of BAR-related structure with additional CC motif. To emphasise the functional similarity to BAR domains the newly identified motif was named F-BAR.

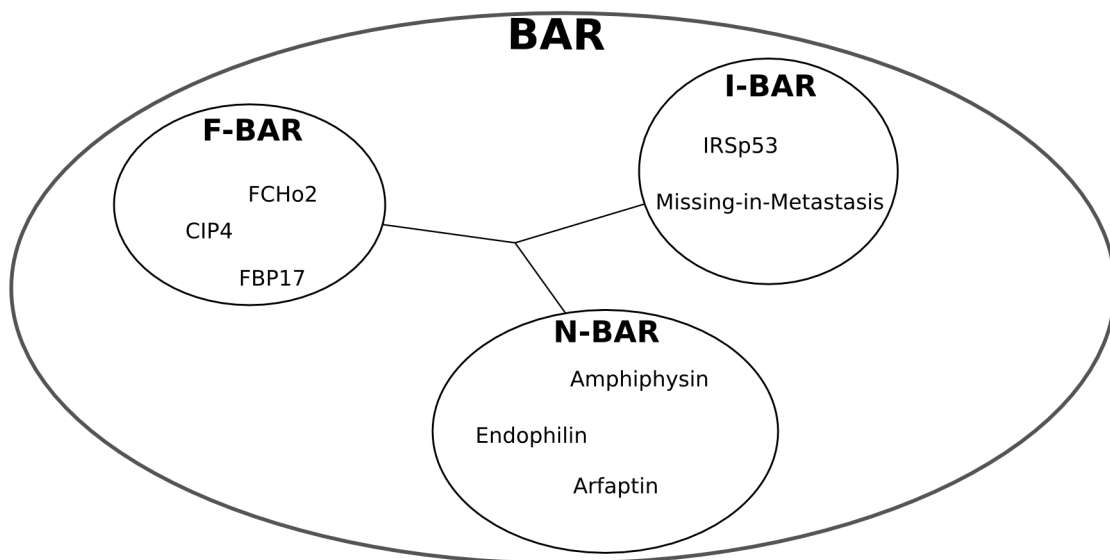


Figure. 1.7.: Schematic representation of relations between N-BAR, F-BAR and I-BAR groups of domains. Lines connecting all three subfamilies indicate the probable common ancestor (38).

Completely independently, the third class of BAR domains was identified at the same time. After identification of new proteins (IRSp53 and MIM) involved in cytoskeleton remodelling (39),(40) it was shown that these two molecules share the extended homology N-terminal region IMD (IRSp52/MIM domain). Additionally, the overexpression of any of these proteins in cell leads to extensive

1. BIN/Amphiphysin/Rvs proteins

filopodia formation (39). Striking functional similarities and high degree of IMD homology became a motivation for group of Roberto Dominguez to solve the structure of homologous region (41). It was revealed that the IMD fold is closely related to the BAR domain shape. It was shown that at the IMD interface, patches of positive charges are located which are known from BAR domains. Further investigations revealed that IMD proteins bind to the PtdIns(4,5)P₂-rich membranes and tubulate them in the way very similar to known BAR domains. The most striking difference between BAR and IMD folds was that whereas BAR proteins bind to the lipid bilayers by their concave surface, IMD proteins use convex interface. Since the functionality and the structure of BAR and IMD domains appeared to be similar, it was proposed to rename IMD domains in order to emphasize this close relationship between these two groups of protein domains into I-BAR (IMD/BAR) (22). The most studied members of each group of BAR proteins and their belonging to particular BAR subfamily are shown in figure 1.7.

The structural similarities and differences among the BAR domains are shown in figure 1.8. Looking from top to bottom on the side view of protein structures (in the figure dimers are presented) changes from the most curved (N-BAR proteins - endophilin, amphiphysin) through more extended and shallower fold of F-BAR proteins (FBP17, FCHo2 and Syndapin) towards inverted, very shallow structure of I-BAR protein. All the structures are presented in the way that the membrane binding interface is always pointing downwards. When domains are seen from top view, it is striking that the shape of N-BAR and I-BAR proteins remains straight. Only F-BAR proteins tend to vary in this matter from completely straight structure of FBP17 dimer throughout the moderately s-shaped FCHo2 to strongly bent fold of syndapin. Recently, it was shown that this shape might play an important role in accommodation of SH3 domain. Interaction of these two folds is proposed to be a key element of the auto-inhibition of F-BAR proteins activity (42). While this mechanism was shown only for syndapin further studies are needed to get better insight of the regulation of the -BAR proteins activity. While many partners of BAR proteins were identified (3) the exact role of particular BAR proteins still remains under discussion. Moreover, it is still not clear what is the difference between three groups of BAR domains and how their structural variety is related to their functions. In a very recent paper, Taylor et al. (6) conducted series of experiments in which they followed with high temporal resolution the arriving of different proteins at the endocytic pits. Among 34 proteins tested were FCHo1/2, endophilin2, amphiphysin2, BIN1, SNX9, syndapin2, APPL1 and FBP17. FCHo1/2 are proposed to be clathrin nucleators (2) and accordingly they bind as one of the first proteins to the clathrin pits. It was also shown that N-BAR proteins like endophilin and amphiphysin bind to the endocytic but at the same moment as the dynamin. While all of these proteins are plausibly taking part in scission of the vesicle, the exact mechanism of that event remains still unknown. Even more intriguing is the post-scission recruitment of FBP17 and SNX9 (both are F-BAR proteins) to the endocytic spot. It shows that the BAR domain does not determine itself the binding order of proteins, since F-BAR proteins might be recruited at the very beginning and very end of the endocytosis process. To be able to interact with many different partners, often at the same time, BAR proteins usually bear many other domains like SH3 (Src 3 homology) or PDZ. SH3 domain is particularly interesting since it can interact with proteins like dynamin (43), N-WASP (44), (45) or synaptojanin (9) which are the key players in endocytosis. While there are more and more studies trying to elucidate the biological role of many different BAR proteins, the mechanism by which the protein binds the lipid bilayer and how the specificity of this process is maintained is still unclear. Recent experiments and computer simulations show the importance of the protein-protein interaction and the flexibility of the domain (46), (47), (48), (13), (17), (17), (16).

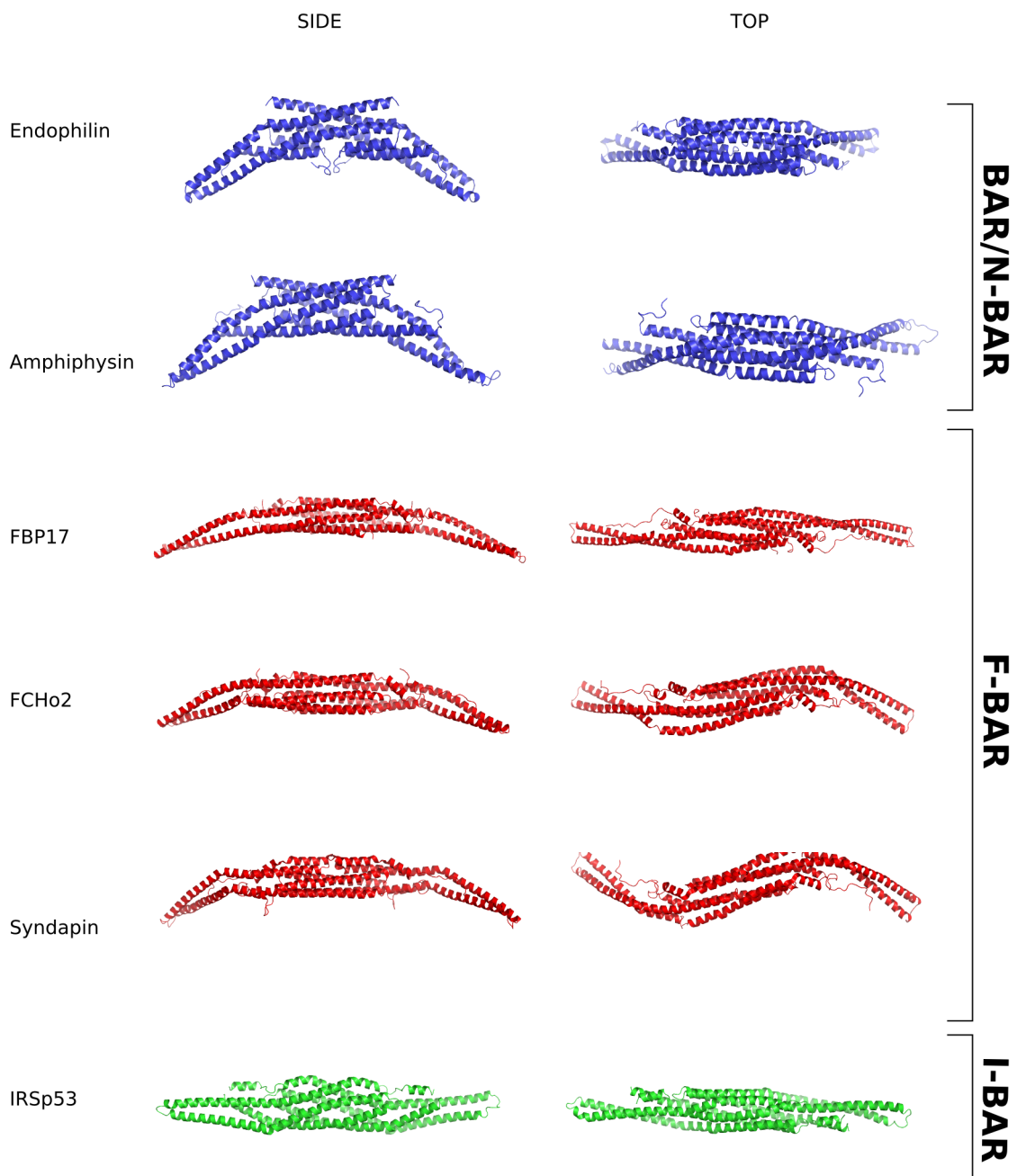


Figure 1.8: Example of well studied BAR domains. At the 'SIDE' view domains are presented with membrane-interacting interface downwards, while 'TOP' view means that this interface is not seen. N-BAR subfamily is marked in blue, F-BAR domains in red and I-BAR domain in green. PDB ID used to generate the images were as follows: endophilin: 2C08, amphiphysin: 1URU, FBP17: 2EFL, FCHo2: 2V0O, syndapin: 2X3V, IRSp53: 1Y2O.

1. BIN/Amphyphysin/Rvs proteins

1.3.1. FCHo2 BAR domain and its properties

From many BAR proteins, FCHo2 is an especially attractive molecule for *in vitro* studies. This protein comprises only from two domains: Fer/CIP4 homology and identified recently μ -MD (2) (Figure 1.9). By F-BAR domains the protein anchors to the lipid membrane whereas μ -HD (8) domains serves as a biding site for intersectin and eps15 (2). This recruitment is the first stage of the formation of the clathrin coated pits (CCPs) which are the functional unit of clathrin mediated endocytosis.

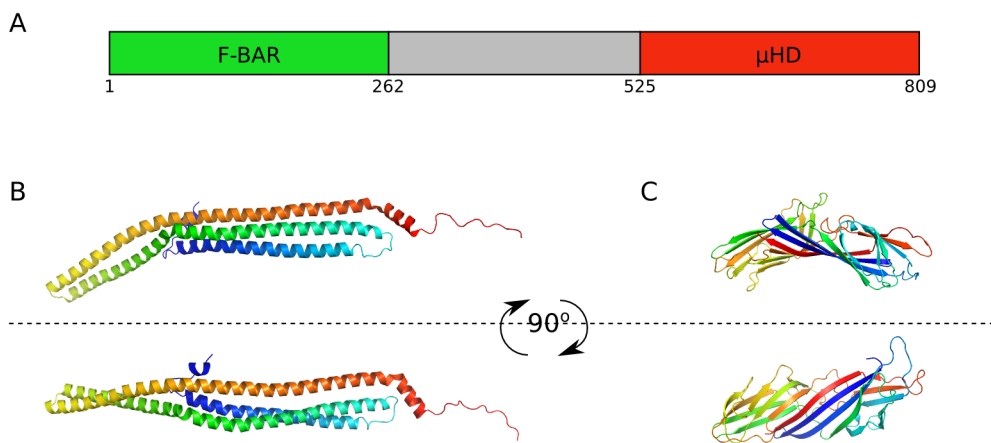


Figure. 1.9.: A) Domain organisation of FCHo2. N-terminus marked in green shows FCH and coiled-coil sequenced (F-BAR domain). On C-terminus sequence of μ -HD is depicted in red. B) Ternary structure of the monomeric FCHo2 domain. The bottom view is turned of 90° in respect to the top view. C) The structure of μ -HD domain seen from two different angles.

FCHo2 monomer has three Cys from which two make thiol bridge within the dimer. As shown by Henne and co-workers these Cys are not essential for the dimerisation and that the truncated construct without unstructured C-terminal (aa. 261-274) sequence is still able to form dimers (11). Interestingly, in contrast to N-BAR domains (7) the first aa. of the FCHo2 fold into α -helix (figure 1.10) also in the solution. This helix interacts with helix 5 of the adjacent monomer and its mobility is relatively low. The mutants without helix 1 are still able to bind to the membrane. FCHo2 binding to the lipid bilayers depends on the ionic strength of the buffer solutions. Substantial decrease in membrane affinity occurs at the concentration above 250 mM of NaCl. The deletion of the helix 1 does not alter general binding of the protein, but the protein seems to be more sensitive to ionic conditions (11).

Ionic interactions between the FCHo2 BAR domain and the membrane are mainly determined by clusters of positively charged residues at the concave surface of the protein (Figure 1.11). Similarly to N-BAR proteins (12), double mutations of the positively charged residues (K146E + R152E) strongly inhibits membrane binding (40 %) (11). As it was mentioned earlier, BAR proteins are able to tubulate the lipid membrane both *in vivo* and *in vitro*. Although there is a number of publications which imply that the size of formed lipid-protein tubes is correlated with the dimension of the BAR domain (13), (48), in case of FCHo2 it was shown that it is possible to obtain lipid tubes of diameter smaller than predicted by the size of the concave surface of the domain (11). So far, the exact mechanism by which the protein polymerise at the membrane surface is unknown. Moreover, the role of the lipid bilayer on the protein activity was investigated only with the focus on specificity of the lipid partners of the BAR domains (49).

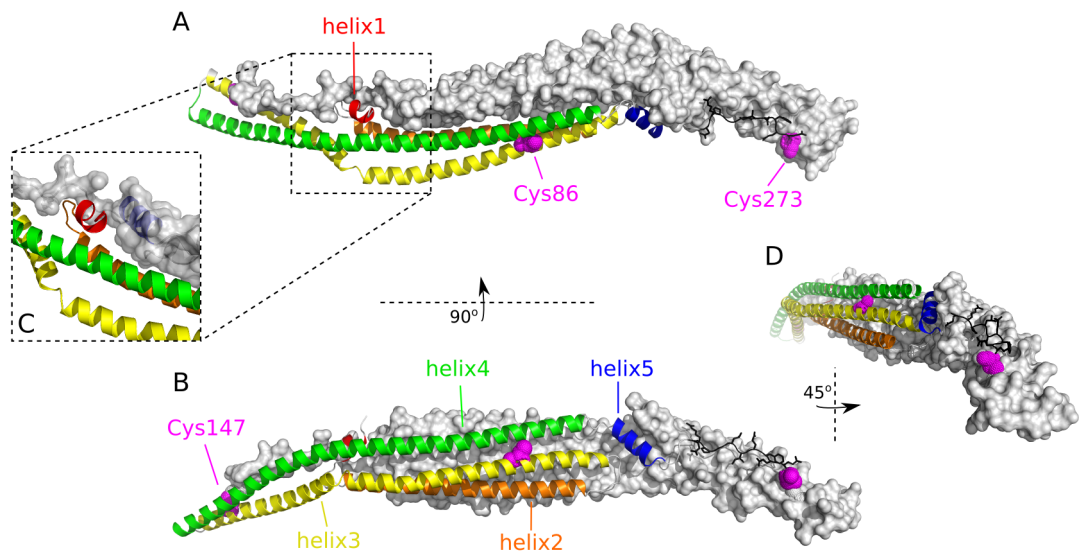


Figure. 1.10.: Structure of FCHo2 BAR domain. A) View on convex surface. For clarity one monomer molecular surface was used in light gray. B) The same molecule seen from 90° angle. Each of five helices is depicted with different colour. The C-terminal unstructured part of the protein is marked in black (D). Cys residues are coloured in magenta. The orientation of the Helix 1 in relation with Helix 5 of other monomer is shown in C.

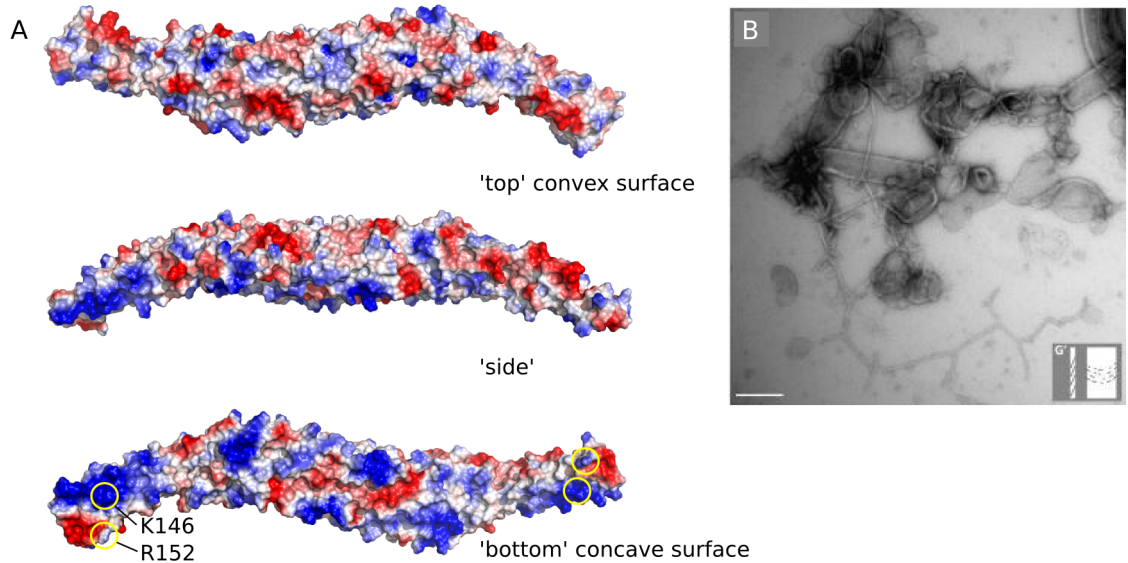


Figure. 1.11.: A) The charge distribution on the surface of the FCHo2 BAR domain. The blue colour indicates positive and red negative charge. The map was generated using Pymol software and it is the estimation of local charges in vacuum. B) Electron micrograph of lipid tubes formed as consequence of the FCHo2 presence (adopted from (11)).

2. Lipid systems for *in vitro* studies

2.1. Introduction

Together with the development in biology and biophysics more complex questions were addressed. It became obvious that many of these problems cannot be answered by direct *in vivo* studies. In order to simplify experimental conditions *in vitro* systems were applied. In this approach all the essential elements of interest are separated and studied under well controlled conditions (pH, ionic strength, temperature etc.). This bottom-up approach helped to gain knowledge in fields like endocytosis (4), bacterial cell division (19) or phase separation of the lipid membrane and protein partitioning (50), (51). In this chapter, the most common lipid systems will be presented. Their characteristic features will be pointed out and followed by examples of application and eventual drawbacks in context of this work.

2.2. Lipids

Lipids are the broad group of molecules including: fats, waxes, sterols, vitamis, mono-, di- and triglycerides and phospholipids. Although the name 'lipid' comes from Greek 'lipos' meaning fat, fats are only one of many subgroups of lipids. Lipid membranes are mostly composed of phospholipids and sterols (figure 2.1). The exact composition of the lipid bilayer varies greatly from species to species and is also specific to particular groups of organisms.

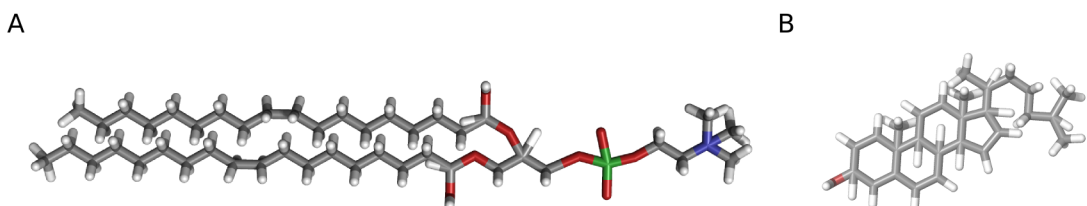


Figure. 2.1.: Structure of two common lipids: A) DOPC and B) cholesterol. Oxygen is labelled in red, phosphorus in green, nitrogen in blue and hydrogen in white.

The fundamental feature of the lipids, which constitute the membrane, is amphiphaticity. It means that the molecule cannot be easily classified as water-soluble or oil-soluble. The main reason for that is that one part of such a molecule is usually hydrophobic whereas second part is rather hydrophilic. As such, amphiphatic molecules rather try to localise at the hydrophobic-hydrophilic interfaces (like oil-water or water-air) (figure 2.2). One way to characterise the lipids is the measurement of partitioning of the particular lipid in between oil-water suspension (commonly used are octanol-water systems). To be able to induce lipid bilayers the amphiphaticity is not the only requirement. Considering lipid membrane as a geometric shape, one can conclude, that lipids have to exhibit specific shape. In reality

this 'shape' is not determined only by the structure geometry, but it is the result of the chemical nature of the headgroup and molecule dimensions (52):

$$S = V/A_o L_c \quad (2.1)$$

where S is the shape factor, V is the volume of the molecule, A_o is the 'optimum' area of the lipid headgroup taking into account dimensions of the molecule and its chemical properties and L_c is the length of the straight acyl chain. Lipids of a different shape form spontaneously different phases. When $S>1$ (cone shape) the inverted H_{II} phase is favourable (inverted micelle). Lipids with $S=1$ (cylindrical shape) spontaneously form lamellar structures (for example bilayers). When $S<1$ (inverted cone shape) micelles are formed. A_o parameter depends mostly on the charge the molecule bears. While mostly this charged is a result of the protonation state of acid or base moiety it is related to pH of the surrounding. The L_c and A_H parameters are mainly dependent on saturation of the acyl chain (in case of phospholipids).

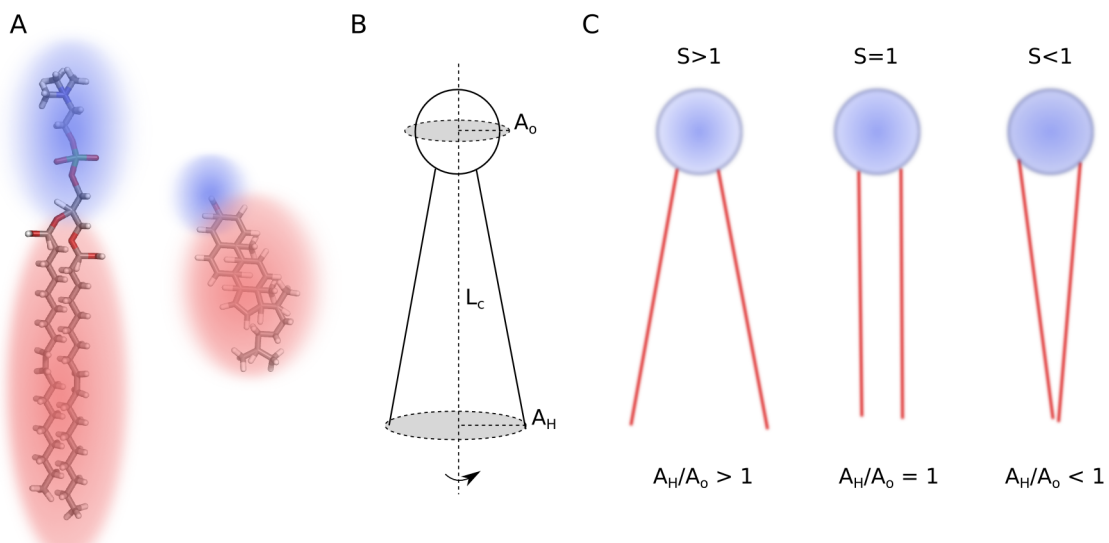


Figure. 2.2.: Features of lipids. A) Schematic representation of the amphipathic properties of lipids: blue area depicts polar part of the molecules (left DOPC, right cholesterol), red shade shows hydrophobic area of lipids. B) Drawing presenting schematically orientation of A_o , A_H and L_c parameters with respect to lipid molecule. C) Demonstration of types of lipids with different shape factor (from left to right): cone shaped, cylindrical shape, inverted cone shape.

While the shape of the lipid molecule determines the spontaneously formed phase, it has to be mentioned that this is the case only for pure lipid compositions. In nature, lipid membranes are composed of many different lipid species from which many have different shape factors. This allows to form lamellar structures in which the cone shape of one lipid species can be compensated by inverted cone shape of another lipid species. It is also important to notice, that properties of lipid layers are changing with a temperature. The most ordered state of lipid membrane is the so called gel phase. Lipids in this phase align with each other and the acyl chains show no mobility. Once the temperature is elevated over certain value (phase transition temperature, specific to particular lipid species) the ordering of the lipids decreases (lipids can freely move in the plane of the membrane) acyl chains exhibit higher mobility (liquid phase). In some of lipid mixtures it is possible to identify two subphases: liquid ordered

2. Lipid systems for in vitro studies

L_d and liquid disordered L_o . While in general in both phases lipids are mobile in plane of the bilayers, it is seen that the liquid disordered phase usually forms thicker membranes and the diffusion of the lipids in such a phase is relatively high (53). This is of great biological importance since these two phases can co-existence with each other and there is growing number of evidence that this property of the lipid bilayer is an important mechanism in many signalling pathways in the cell (25).

2.3. Monolayer systems

Lipid monolayer are historically one of the firsts lipid systems. Their origin monolayers take from fundamental property of the lipids which spread at the water-air interface form thin layers over available surface. It was probably Benjamin Franklin who first showed scientific interest in mono-molecular layers of lipid spread over the water. Among may scientist working on monolayers, Irving Langmuir was the most influential. He was the one who investigated the surface pressure as function of density of the molecules on the water surface. Collaborating with Langmuir, Katherine Blodgett designed the method to transfer lipid films on to solid surfaces - the so called Langmuir-Blodgett films. Since first developments in monolayer field in the beginning of the 20th century, the technology and as well as understanding of lipid properties have been improved substantially. Nevertheless, the principle of the method stayed the same. All the molecules of a hydrophobic/amphipathic properties orient on the water surface in that way, that the more hydrophilic part of the molecule faces the water phase whereas the hydrophobic part stick out to the air. This alignment minimises the overall energy of the whole system (2.3).

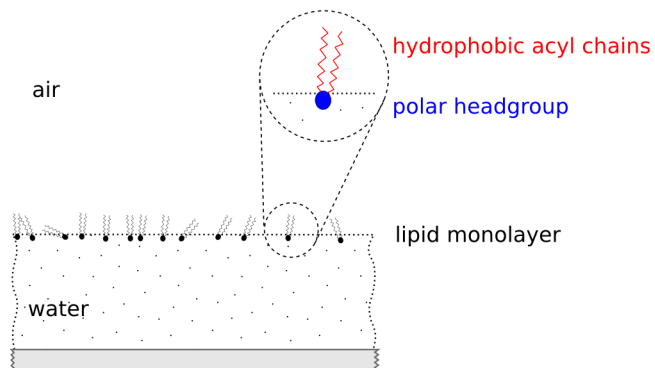


Figure. 2.3.: An orientation of phospholipids at the water-air interface. Water molecules penetrate the mono-molecular layers of lipids to some extend (polar headgroup) whereas hydrophobic acyl chains are completely excluded from water subphase sticking out towards the air.

Modern monolayer trough, known as Langmuir trough is composed of container made of a resistant material (PTFE), movable barriers and micro-balance 2.5. In order to measure the surface pressure (SP) very thin plate made of platinum or ash-free filter paper is attached to the micro-balance. Plate (Wilhelmy plate) is immersed in the subphase. Once the surface pressure of the monolayers increases the Wilhelmy plate experiences the force generated by compressed lipid molecules. This force is strictly related to surface tension (ST) by relation:

$$Force = (\rho_P l w t)g - (\rho_L d w t)g + 2(w + t)(ST)\cos\theta \quad (2.2)$$

where the ρ_P is the density of the plate, $l/w/t$ are dimensions of the plate, ρ_L is the density of the subphase $d/w/t$ is the upthrust volume, g represents the gravity and the last term describes the change in the surface tension - surface pressure (SP). Since the weight of the plate (the first term) and the upthrust (the second term) do not change during the measurement, we can eliminate them from the equation as a constant. $\cos\theta$ is the contact angle of the subphase liquid to the plate and in case of paper Wilhelmy plate equals 0° . Hence the force generated by lipids upon the compression can be described by the following relation:

$$\text{Force} = \text{PlatePerimeter} \cdot ST \quad (2.3)$$

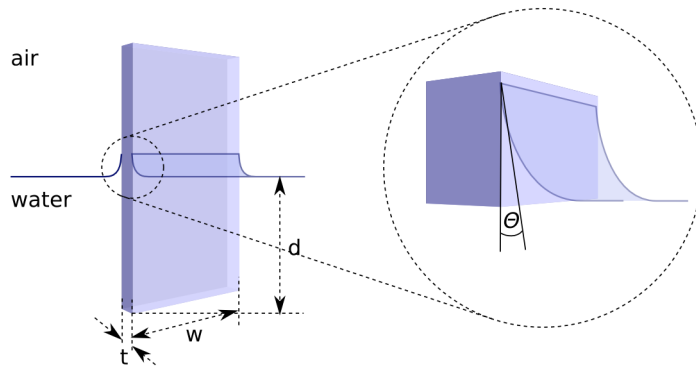


Figure. 2.4.: Wilhelmy plate with its dimensions and depicted contact angle of subphase θ

The surface pressure is the change in surface tension and the sum of both these parameters is constant, i.e. an increase of one is related with the decrease of another. Knowing that ST of water at standard condition equals 72.8 mN/m it is possible to calculate the surface pressure.

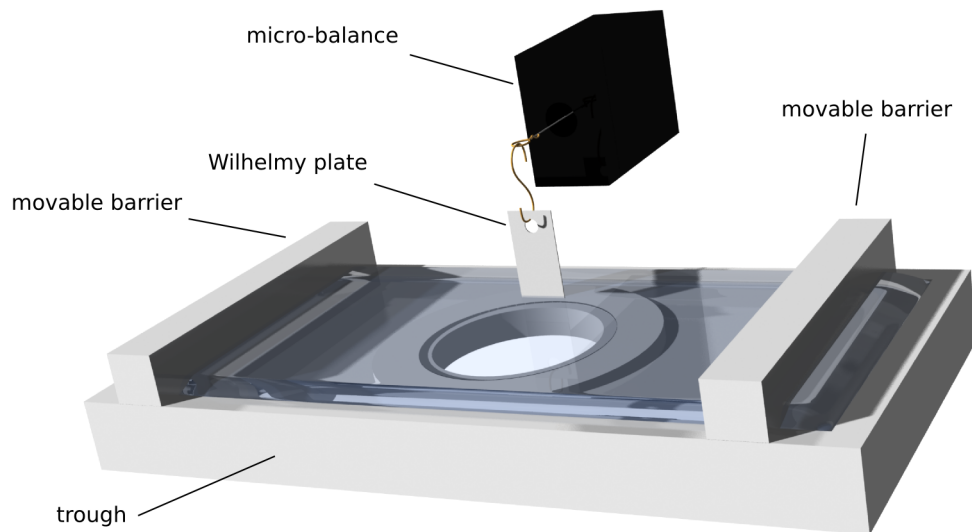


Figure. 2.5.: 3D drawing of the Langmuir trough with depicted components.

2.4. Bilayer systems

Lipid bilayers are lamellar structures which have a form of a vesicle or entirely flat sheet of membrane (figure 2.6). Lipid vesicles called liposomes were first commonly used bilayer system (54). Lipid vesicles have a form of the sphere made of lipid membrane. Liposomes can be divided into several subgroups taking into account the preparation method and the morphology of vesicles. Common abbreviations used nowadays are as follows:

MLVs - multilamellar lipid vesicles

SUVs - small unilamellar lipid vesicles

LUVs - large unilamellar lipid vesicles

GUVs - giant unilamellar lipid vesicles

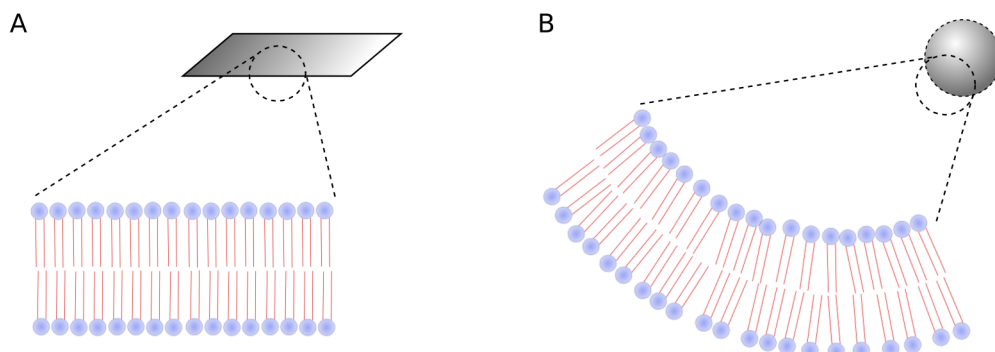


Figure. 2.6.: Two common conformations of the lipid bilayer: flat sheet (A) and spherical (B).

2.4.1. Lipid vesicles

SUVs are considered usually as liposomes of a diameter smaller than 100 nm. LUVs are the vesicles between 100 nm and 1 μm . GUVs usually are vesicles bigger than 1 μm , but practically they usually have diameter of 20 μm or more and in some cases their dimensions can exceed 100 μm (55). SUVs and LUVs are usually prepared using thin lipid film method where desired organic lipid mixtures are dried in the glass surface forming thin film. After complete removal of the organic solvent, lipids are hydrated with the buffer solution. During hydration layers of lipids pinch off and form vesicles (56). During this process MLVs are formed. These liposomes usually have a very broad distribution of diameter and usually have multiple membranes and smaller vesicles in their interior. To obtain SUVs or LUVs multilamellar vesicles are sonicated (no control over the size of the vesicles) or are extruded through the polycarbonate filter with pores of the desire size (57). In order to improve the size distribution and the capacity volume of vesicles freezing-after-thawing (FAT) protocol can be used (58) before the extrusion. Small vesicles usually are used in measurements where spatial information is not needed. Since they can be prepared in big quantities, they became a perfect system for batch experiments using spectrophotometer and spectrofluorometer (21). GUVs are usually prepared by electroformation (59). In this method a thin lipid film is made on a conductive surface. Usually, a platinum wire or ITO (indium-tin-oxide) coated glass is used. During hydration an alternating current is applied to the sample and the whole process lasts at least for one hour. While GUVs have rather broad distribution of diameter and are relatively fragile, they are extremely useful when investigated by

fluorescent microscope. Since their big dimensions they are a great tool to investigate the membrane surface with high spatial resolution. As such they became an alternative approach to SUVs/LUVs. Using GUVs it was possible for example to elucidate the partitioning of membrane proteins among different lipid phases (51).

2.4.2. Supported lipid membranes - SLBs

Although lipid vesicles were shown to be versatile and very useful model, their spherical shape did not allow to combine this model membrane with methods like atomic force microscopy (AFM) and robust confocal microscopy. To overcome these problems supported lipid membranes (SLBs) were designed (60). In this model, small vesicles were used to form an entirely flat sheet of bilayer deposited on the support. Material of the support can be varied, but commonly used are mica, glass or gold. In order to obtain SLB, one have to prepared firstly SUVs. Their high curvature is energetically not favourable and promotes liposomes fusion to minimise the membrane tension. Such unstable vesicles deposited on the charged surface easily fused with each other. To further accomplish the fusion divalent calcium ions are introduced to the system. Such prepared membrane is characterise by a very big flat area which can be easily investigated by confocal microscopy or TIRF microscopy (61). Additionally, AFM can be applied to such a sample and topographical image can we acquired. This was extremely useful in studies of two dimensional crystals of bacteriorhodopsin (62).

3. Fluorescence based techniques

3.1. Fluorescence

Any substance can absorb energy in the form of light. After the energy has been absorbed, the molecule/or atom gets excited to a higher quantum state. A spontaneous relaxation of the excited substance connected with a light emission is call luminescence. Depending on the quantum mechanism of the relaxations luminescence can be divided into two phenomena: fluorescence and phosphorescence. Fluorescence is the process which occurs between excited singlet state and the ground singlet state of the molecules. It is a very fast process which lasts on the scale of nanoseconds. Phosphorescence is an result of the so called intersystem crossing conversion to the triplet state and it takes place on the scale of milliseconds to seconds. The schematic representation of quantum processes involved in luminescence is called the Jabłoński diagram (figure 3.1).

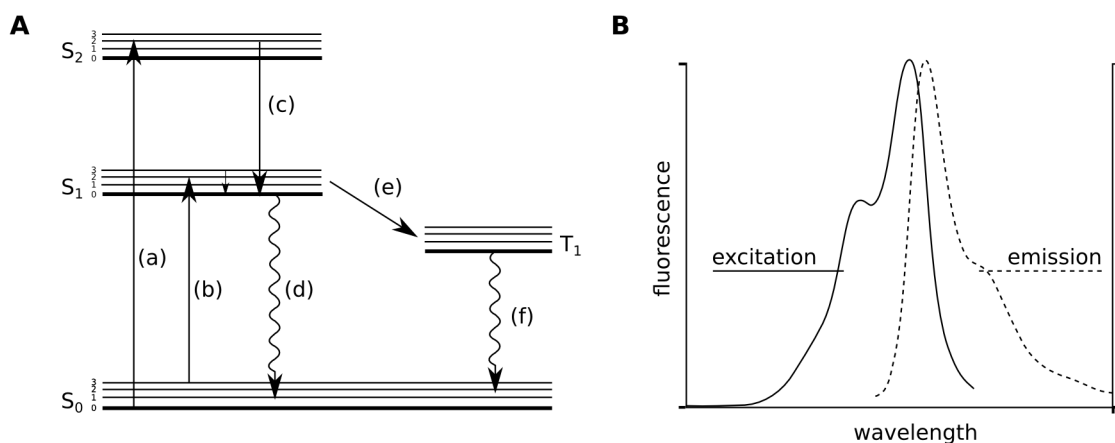


Figure. 3.1.: A) Jabłoński diagram. S_0 stands for singlet ground states, S_1 and S_2 refers to excited singlet states. 0, 1, 2 and 3 depict different vibrational energy levels. T_1 is an excited triplet level. When the molecule absorbs a light, the energy state of the molecules changes to one of the vibrational levels at S_1 (b) or S_2 (a) state. Excited molecules undergo fast relaxation to the ground vibrational level of S_1 (c) - the so-called internal conversion. From S_1 state the further relaxation can occur in two ways: as a direct immediate light emission called fluorescence (d) or trough the so-called intersystem crossing to the triplet state (e). Transition to the triplet state is related to the flip of the electron spin and it is relatively slow process. As a result, the following radiative relaxation to the S_0 level call phosphorescence (f) is characterised by much longer lifetime (on the scale of seconds). B) Emission and excitation spectra. It can be seen that the emission spectrum is shifted towards longer wavelengths (Stokes shift) and it is close in shape to a mirror reflection of the excitation spectrum demonstrating the Frank-Condon rule.

Due to the fast non-radiative internal conversion the energy of the emitted photos is usually lower than one of absorbed ones. This conversion refers not only to S_2 to S_1 conversion but also to the energy decay from higher vibrational states to the ground level of S_1 . Additionally, the radiative relaxation

often occurs to higher vibrational states of S_0 what further decrease of dissipated energy. The difference between the energy of the absorbed and emitted light is reflected in the shift of the radiation towards longer wavelength. This effect is called Stokes' shift - after George Stokes who first described this phenomenon. Practically, the Stokes shift is demonstrated as a red-shift of the emission spectrum with respect to the excitation spectrum (figure 3.1 B). Main parameters connected with fluorescence are quantum yield and fluorescence life time. The quantum yield is the ratio of a number of emitted photons to the total number of absorbed photons:

$$Q = \frac{D_r}{D_r + D_{non}} \quad (3.1)$$

where Q stands for quantum yield, D_r is the rate of S_1 to S_0 decay and D_{non} is the rate of all the processes leading to the non-radiative way of energy dissipation. Fluorescence lifetime is the average time which molecules stays in the excited state:

$$F(t) = F_0 \cdot e^{-t/\tau} \quad (3.2)$$

where $F(t)$ is a fluorescence intensity at time t , F_0 is the initial fluorescence intensity and τ is the fluorescence lifetime.

3.2. Fluorescence Correlation Spectroscopy

3.2.1. Principle of FCS

Principles of FCS were published for the first time by Magde, Elson and Webb (63). FCS is based on the correlation of the fluctuations in the fluorescence intensity. Fluorescent light is emitted by diffusing molecules which are excited by a focused laser beam. The movement of fluorophores in and out of the detection volume give rise to the fluctuation of the acquired signal and is strictly related to the particular particle species 3.2:

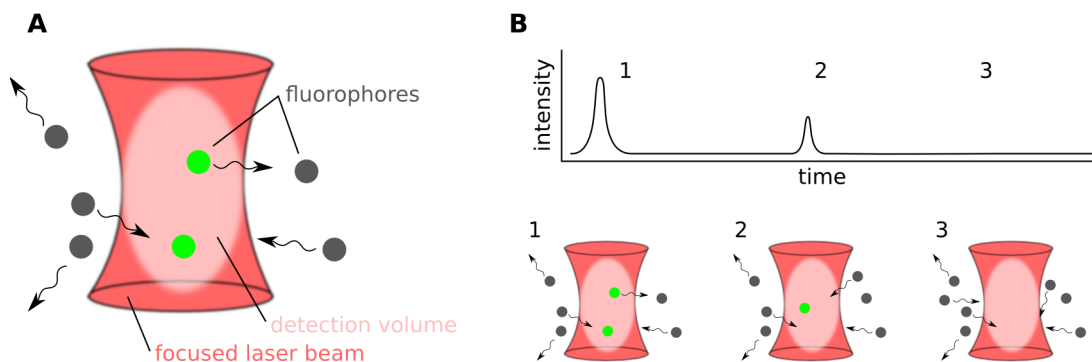


Figure. 3.2.: Principle of FCS. A) Laser beam (red) is strongly focused and the fluorophores (grey) are randomly entering the excitation volume (pink) where they absorb the laser light. Fluorophores immediately start to emit fluorescent (green) light as a result of energy dissipation. B) Drawing shows schematically connection between the number of fluorophores in the detection volume and the signal acquired at the detector. Numbers depicted at drawings correspond to numbers on a graph.

3. Fluorescence based techniques

Since FCS analysis is based on the signal collected from single molecules, the saturation of the detection volume with a fluorophore has to be avoided. In order to do so, usually the measurements are conducted at a very low concentration at which the mobility of single molecules can be resolved. Significant improvement of this method was proposed by Rigler and co-workers who implemented the confocal detection into the FCS setup (64). In such a system the detection volume is below one femtoliter which means that at the same concentration of fluorophore the average number of detected molecules is relatively smaller. This allows to perform FCS measurements at higher, biologically relevant concentrations.

3.2.2. The autocorrelation function

The fluorescence fluctuations $\delta F(t)$, assuming constant excitation power, are deviations from the average number of molecules, hence the average fluorescence signal:

$$\delta F(t) = F(t) - \langle F(t) \rangle \quad (3.3)$$

These fluctuations take their origin from temporal changes of the number of molecules in the detection volume. When compare the fluctuation at time t with itself at time $t + \tau$ one can obtain the temporal similarity of the signal with characteristic decay. This goal can be achieved by autocorrelation the signal over time:

$$G(\tau) = \frac{\langle F(t)\delta F(t + \tau) \rangle}{\langle F(t) \rangle^2} \quad (3.4)$$

Assuming that fluorophores undergo Brownian motion, one can conclude that the average observation time of molecules in the detection volume is strongly dependent on the mobility of particles. Hence, the characteristic decay of the temporal autocorrelation function is strictly connected to the diffusion of the fluorophore. The mentioned detection volume, the so called effective focal volume V_{eff} is the tree dimensional Gaussian approximation which is describe by the following relation:

$$V_{eff} = \pi^{\frac{3}{2}} \cdot r_0^2 \cdot z_0 \quad (3.5)$$

r_0 is the waist of the focal spot at which the Gaussian approximation of the emitted light decays to $1/e^2$ and z_0 is the dimension along the z axis. The final autocorrelation function which describes one diffusion species of fluorophores has a following form:

$$G(\tau) = \frac{1}{V_{eff}\langle C \rangle} \left(1 + \frac{\tau}{\tau_D}\right)^{-1} \left(1 + \frac{\tau}{\frac{r_0^2}{z_0} \tau_D}\right)^{-1/2} \quad (3.6)$$

where $V_{eff}\langle C \rangle$ is the average number of molecules $\langle N \rangle$ in the detection volume, τ_D is the characteristic diffusion time of the fluorescence species. Knowing that the D is the diffusion time of the molecule which is independent of the setup and that the τ_D is follows the relation:

$$\tau_D = \frac{r_0^2}{4 \cdot D} \quad (3.7)$$

It is possible to estimate the dimension of the the effective focal volume. This gives an opportunity to estimate the concentration of the fluorophore:

$$G(0) = \frac{1}{\langle N \rangle} = \frac{1}{V_{eff} \cdot \langle C \rangle} \quad (3.8)$$

and finally:

$$\langle C \rangle = \frac{1}{V_{eff} \cdot G(0)} \quad (3.9)$$

While the assumption that the motion of molecules is the most important factor which determines the fluorescence fluctuation in the detection volume more accurate experiments demand to consider other aspects of the fluorescence. During the light absorption the fluorophore gets to the exited singlet state.

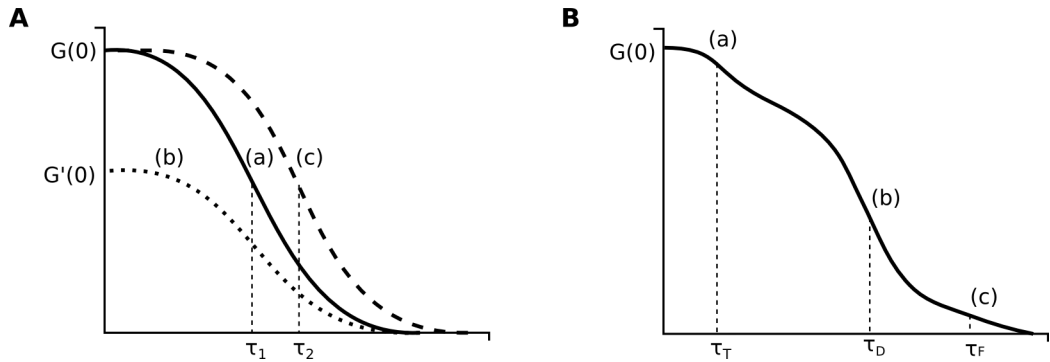


Figure 3.3: Influence of different factors on the shape of the autocorrelation curve. A) (a) shows the autocorrelation curve with the amplitude $G(0)$ and τ_1 characteristic time. When the concentration of the same species increases (b) the overall signal increases, but the amplitude of the correlation $G'(0)$ drops down what accordingly with the first therm of the model equation (3.6, 3.8). It is important to notice that the, since is the same fluorophore species, the characteristic diffusion time τ_1 stays the same. Giving the same concentration as in (a), the autocorrelation curve of the molecule with relatively lower mobility will have the same amplitude $G(0)$ but will be shifted towards longer diffusion times τ_2 (c). A) Shows the influence of a triplet blinking and membrane undulations on the shape of the correlation curve. For given particle with a characteristic diffusion time τ_D (b), its triplet state will appear at shorter lag times (a) (blinking is a relatively fast process in comparison to lateral diffusion of the molecule) with characteristic τ_T . On other hand membrane undulation are a relatively slow process with regards to molecule diffusion and will give rise to additional component on the right side of the curve τ_F (c).

As mentioned earlier, the relaxation of this state can occur in two ways: direct transition form excited singlet state to ground single state or through intersystem conversion to excited triplet state. While the first contributes into the fluorescence the second is a the same time scale is a non-radiative process which leads to dark state of the molecule. This phenomenon appears in the measurement as a fluorophore blinking and interferes with fluctuation arose from lateral mobility of the particle. While the triplet blinking is inherent property of the dye, the only way to obtain more accurate measurements is to change the model function so that triplet state is considered:

$$G(\tau) = \frac{1}{N} \left(1 + \frac{T}{1-T} e^{-\tau/\tau_T} \right) \left(1 + \frac{\tau}{\tau_D} \right)^{-1} \left(1 + \frac{\tau}{S^2 \tau_D} \right)^{-1/2} \quad (3.10)$$

where N is the particle number, T corresponds to the triplet fraction, τ_T and S is the so called structure parameter and it is the ration of r_0/z_0 and the triplet blinking is describe by an exponential

3. Fluorescence based techniques

decay (65). In order to be able to measure diffusion of the molecules in plane, lamellar structures like membrane the mention one component three dimensional model can be simplified as follows:

$$G(\tau) = \frac{1}{N} \left(1 + \frac{T}{1-T} e^{-\tau/\tau_T} \right) \left(1 + \frac{\tau}{\tau_D} \right)^{-1} \quad (3.11)$$

In this model the shape of the detection volume is estimated as a circular 2D Gaussian, hence the the third term of the equation for the 3D diffusion can be reduced. While 2D model is used commonly for membranes it has to be noticed that in this case additional fluctuations of the fluorescence can occur because of a thermal instability of the membrane which moves in and out of the focal volume. While in case of supported membranes this issue can be neglected, in case of free standing bilayers in can give rise to the second component. To overcome this problem, two dimensional two component model is used (66):

$$G(\tau) = \frac{1}{N} \left(1 + \frac{T}{1-T} e^{-\tau/\tau_T} \right) \left(\frac{F}{1+\tau/\tau_F} + \frac{1-F}{1+\tau/\tau_D} \right) \quad (3.12)$$

where fluctuations arisen from membrane undulations are the F fraction with τ_F characteristic diffusion time.

4. Atomic Force Microscopy

Atomic force microscopy is a type of the raster microscope where the sample surface is scanned by a tip attached to the elastic cantilever (67). During the scan the cantilever which senses the topography of the sample is deflected when it hits the three dimensional feature on the surface. This deflection is monitored by a laser which is pointed at the back side of the cantilever. Reflected laser beam is directed on the detector, which is subdivided into four areas so both up and down as well twisting movements can be recorded. The cantilever works like a spring of a certain spring constant K and it fulfils the relations of the Hooke's law:

$$F = K \cdot l \quad (4.1)$$

Since the deflection of the cantilever l can be controlled and the spring constant of the cantilever K is known it is possible to calculate the force applied to the sample. Typical K for cantilever used for soft biological samples is below 0.1 N/m. While setting the certain force applied to the sample is the common way to control the system it needs additional feedback loop which would prevent any deviations from this 'set point' value. Since the sample is not ideally flat and there are protruding features on its surface, the temporal force applied to the sample might significantly exceed the desired one. This 'error' in force can also appear when some lower area is present in the sample. In such a case the force will be lower than the set one which is also unwanted phenomenon. To avoid such a situation the current position of the cantilever has to be immediately adjusted. For this reason, AFM setups are equipped with a feedback mechanism which is usually divided in two types: proportional and integral. The proportional feedback loop gains simply the difference between the set-point value and the current force to estimate the degree of the correction needed. Integral correction is based on the integration of errors over the short period of time. In both cases, the gain of each method has to be optimised so that the system can react for the fast changes in the cantilever deflection. Setting the feedback gains too high leads usually to oscillation and also should be avoided.

Another scanning mode of AFM is the so-called intermittent contact mode. This mode the probe is not continuously with the sample. To avoid an application of a high force to the sample, the cantilever can be oscillated so that it touches the sample only in down position. This mode generally is called tapping mode and is commonly used in experiments involving soft biological samples. It usually requires cantilevers with much higher resonance frequency, hence usually higher force constant.

The output data recorder by AFM are not only a topographical information about sample surface. Other types of images are: error images, lateral deflection, phase and amplitude images. While topographic, error and lateral images are common for all types of modes, phase contrast and amplitude images are exclusive to tapping modes. Error image is simply the record of the deviations of the cantilever from the set-point. Usually this signal is elevated at the borders of the high features where the probe changes its position and the system is not able to correct on time (figure 4.1). Usually, this signal is stronger at low feedback gains setting. Lateral deflection images contains information about twisting of the cantilever along its longitudinal axis. While this signal does not provide any information about topography of the surface, it reflects the interaction between the tip of the probe and the

4. Atomic Force Microscopy

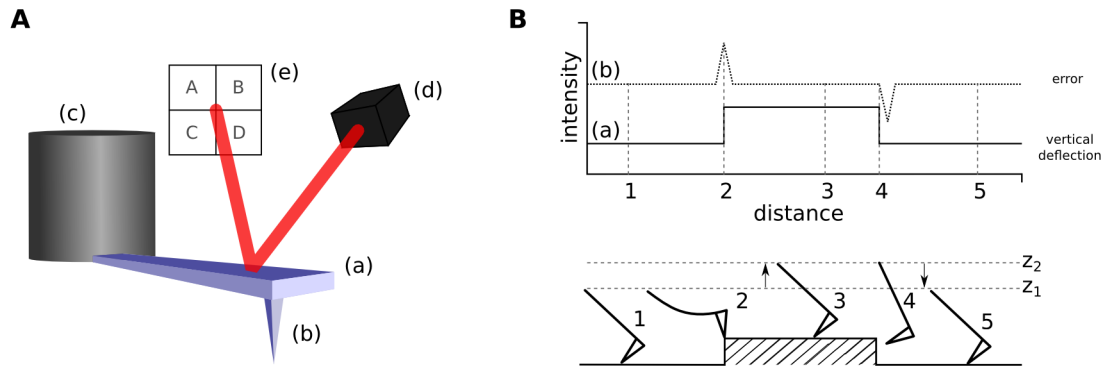


Figure. 4.1.: A) Main parts of the AFM setup. The cantilever (a) with a tip (b) is attached to the piezo scanner (c) which provides high spatial resolution and fine control. The laser (d) is directed on the back side of the cantilever and the reflection hits the photodiode (e) which is divided into four fields which give an information about the coordinates of the probe. B) Schematic representation of the scanning (the sketch below) and related vertical and error signal. At point 1. the piezo is position at height z_1 so that the desired force is generated by the cantilever on the sample. The recorded signal of the vertical (a) and error (b) channel does not change. Once the probe is scanned over the surface it hits the obstacle (2). The cantilever bends up what results in increase vertical deflection signal. Since at this point the piezo has not yet reacted for the spontaneous deviation from set-point the error signal also increases. After the feedback loop reacts the piezo is moving to the new z_2 position in order to relax the cantilever and reach the set point (3). This results in decrease of the error signal to the ground level. After the cantilever reaches the edge of the obstacle (3) the cantilever relax and its position is lowered. This is connected with deviation from the set point since the cantilever bends down and appears as a negative value in the error signal. Simultaneously, the change of the probe position is also reflected in the vertical deflection signal. After the feedback correction (5) (piezo moves from z_2 to z_1 position) the error and the vertical deflections signals reach their starting values.

sample. Hence it provides additional insight in to the chemical nature of the surface. Phase and amplitude images are connected strictly with the induced oscillations of the cantilever. Oscillations which are applied to the probe in the tapping mode have certain phase and amplitude. Upon the contact of the cantilever with the sample both phase and the amplitude are changed due to damping. This phenomenon depends mostly on the medium in which the experiment is conducted and the mechanical characteristic of the sample. Since samples are not homogeneous, spatial information about shifts in phase or amplitude can be very useful in further sample characterisation.

Part II.

Materials and Methods

5. Protein expression, purification and labelling of BAR domains

5.1. Vectors and bacterial expression systems

FCHo2 BAR domain mutants were a kind gift from prof. Harvey McMahon (Cambridge University, England). mFCHo2 1-327aa wild type, mFCHo2 1-261 K146E + R152E and mFCHo2 monoC C308 (C86S, C146S, C273S) were cloned into the pGEX-6P1 vector. In all of the cases the BAR domain was fused with glutathione S-transferase (GST) which was used as a binding domain to glutathione (GTT) Sepharose beads. Plasmids were transfected into bacterial host Escherichia coli, BL21 strain. The sequence of each construct was confirmed by PCR. To amplify the construct pGEX-5' and pGEX-3' primers were used (purchased from GE Healthcare).

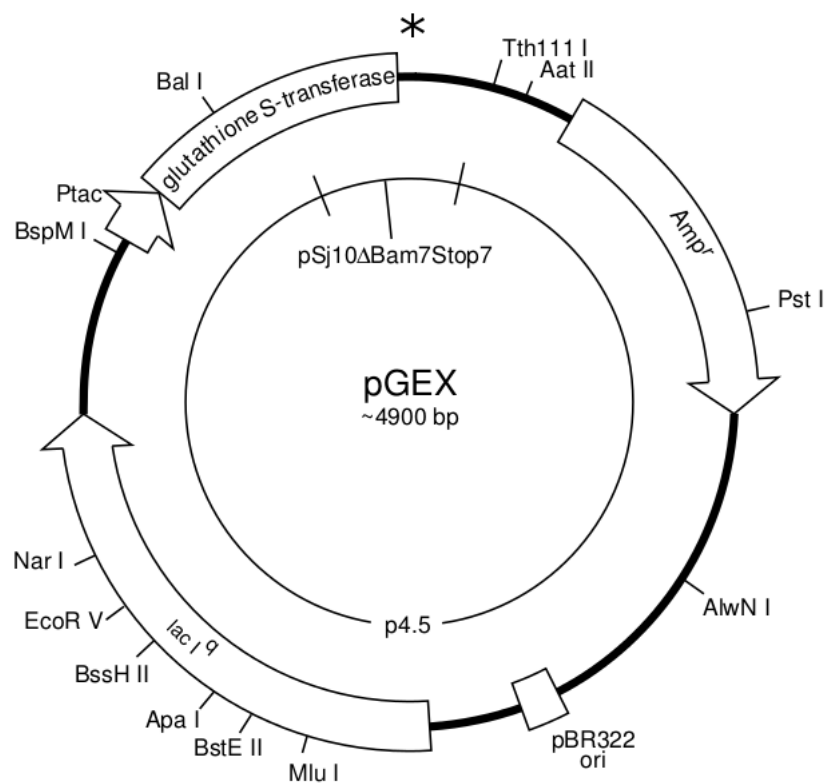


Figure 5.1.: The pGEX-6P1 plasmid map. Asterisk depicts multiple cloning site where BAR domains were localised.

5.2. Purification protocol

All constructs were purified by following the same protocol. First, bacteria were inoculated in 5ml LB medium overnight at 37 °C. Subsequently, 5 ml suspension of bacteria were transfer to 1 l of medium and grown at 37 °C till optical density (OD) reached 0.7. The protein expression was activated by adding isopropylthio-β-galactoside (IPTG) to the final concentration 0.5 mM. Overnight expression was carried out at 25 °C. Cells were subsequently spun at 4000 g for 10 min at 4 °C. Pellet was re-suspended in 50 ml of PBS buffer supplemented with protease inhibitors (Complete ULTRA tablets, Roche) and homogenised with a French press. Subsequently, lysate was spun at 10000 g for 15 min at 4 °C. The obtained supernatant was mixed with glutathione beads. Beads were prepared according to the manufacturer instruction. For 1 l of the initial inoculate 1000 µl of ready-to-use beads were used. Glutathione Sepharose beads were incubated with the lysate for 30 min at room temperature on the shaker. Then supernatant was decanted and beads were washed twice with 500 ul PBS containing 0.5 M NaCl. In order to sediment, beads were spun at 500g for 5 min at 4 °C. The washing buffer was removed with a pipette. To prevent aggregation and facilitate the following labelling procedure, the protein was subsequently washed twice with 500 µl of Tris buffer containing TCEP. Next, 1 ml of Tris-TCEP buffer was added to the final volume 2 ml. To such prepared beads 5 µl of PreScission 3C protease was added and the sample was incubated overnight at 4 °C on the rotary shaker. On the following day beads were spun at 500 g and supernatant containing protein was collected. Spinning/washing procedure with Tris-TCEP buffer was repeated three times. The whole procedure is summarised in the figure 5.2.

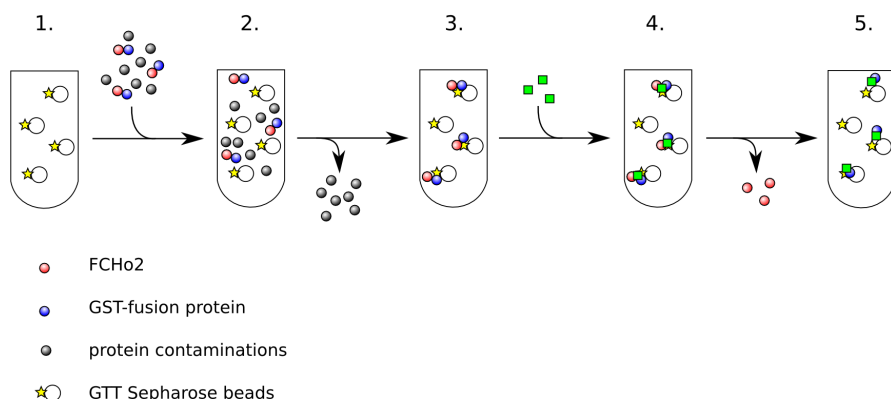


Figure 5.2.: The scheme of the purification procedure. 1. To freshly prepared GTT Sepharose 4B beads, lysate is added. 2. After the incubation, beads are washed with the fresh buffer so that only the GST-fusion protein stays bound to beads. 3. To the sample the protease is added, which recognises the sequence between the GST domain and the fusion protein. 4. After the cleavage, the protease stays bound to the GST domain and only the protein of interest is released to the solution. 5. By repeating washing step the fusion protein is collected.

The purification was always monitored by collecting small aliquots of the sample at each step and running a polyacrylamide 12,5 % gel. Gels were stained according to Kang's modified Coomassie staining procedure (68).

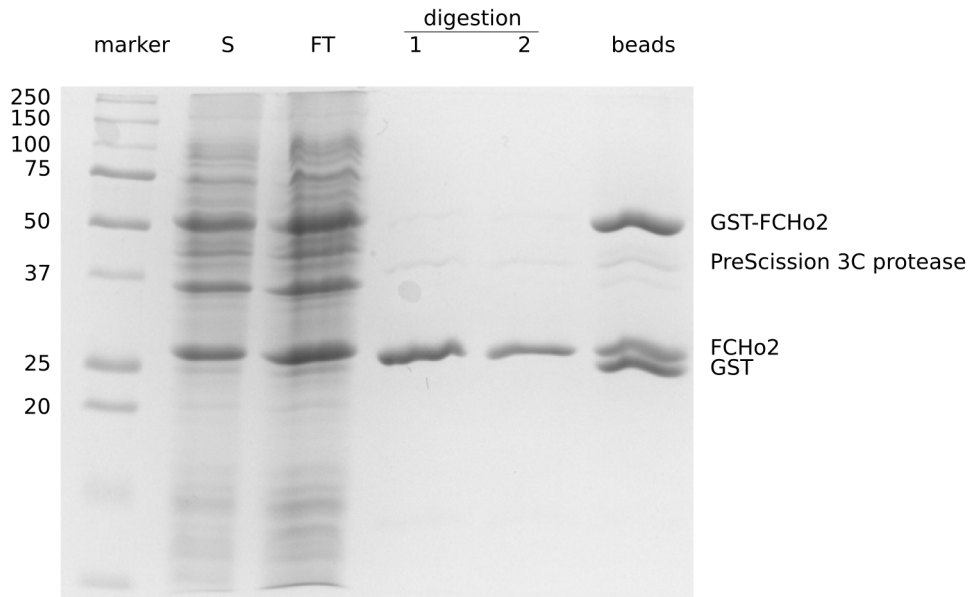


Figure. 5.3.: The figure shows a Coomassie stained gel from the example purification. S refers to the supernatant after spinning down the lysate. FT - is the flow trough after the first wash of beads upon the incubation with lysate. In case of this preparation the digestion was carried out in two separate tubes. The solution from each tube are indicated as a digestion 1 and 2. The last line shows the protein content of beads after whole purification. One can see that beads are still bearing not digested construct (GST-FCHo2), Bound GST domain and PreScission protease as well as cleaved FCHo2 domain.

5.3. Labelling procedure

The protein was labelled with maleimide Alexa 488 dye which was coupled to a cysteine residue. For labelling, instead of wild type FCHo2 domain, we used mutant in which all Cys were substituted with Ser. Additionally, one Cys was introduced at the 308 position. In such a construct only one dye can be attached. This is crucial in single molecule experiments, where exact labelling is needed and any deviation in this matter would lead to substantial errors in obtained data. The figure 5.4 shows steps of the labelling reaction. In order to simplify the protocol tris-(2-carboxyethyl)phosphine (TCEP) was used instead of dithiothreitol (DTT). Both of these molecules are reducing reagents. DTT is a standard chemical used successfully so far. It is used to reduced Cys what is required for the coupling reaction with maleimide. Unfortunately, maleimide reacts with DTT and has to be removed from the sample after Cys reductions. This requires additional step in the protocol and causes unwanted loss of the protein. Instead, TCEP can be used to reduced Cys residues. It does not react with maleimide and that is why does not have to be removed from the solution. It has to be mentioned, that TCEP is unstable in presents of phosphates and cannot be used in phosphate buffered solutions. To avoid any complications, we used Tris buffer in the last washing step during purification.

Protein was incubated with the dye (10 mM solution) overnight at 4 °C. After labelling the protein was separated from the free dye using dialysis tubes with a membrane of a pore size 10 kDa. The protein was spun at 14000 g for 30 min at 4 °C. The flow-through fraction was taken and the absorbance of it was measured. The procedure was repeated till the signal drop to negligible level. The example

5. Protein expression, purification and labelling of BAR domains

experimental data are show in the figure 5.4B.

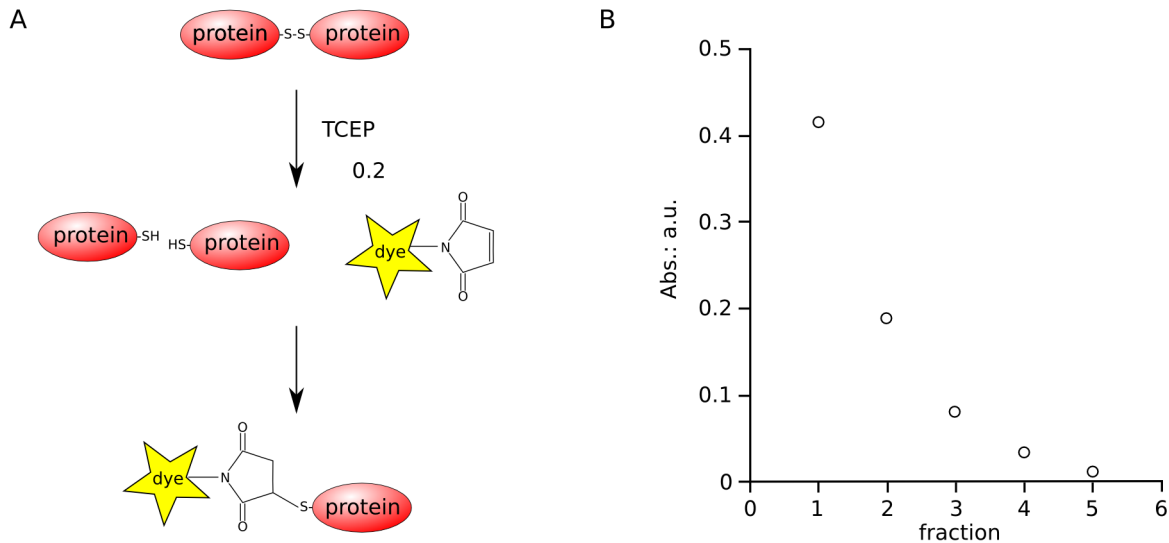


Figure 5.4.: A) Schematic representation of the coupling reaction of the dye to the protein through the Cys residue. **B)** Example data of the separation of the free dye from labelled protein. After each washing step (horizontal axis) the absorbence of the flow-through fraction was measured. The procedure was continue till completely clear solution was obtained.

5.4. Other proteins used in this studies

Cholera toxin subunit B conjugated with Alexa 488 and Streptavidin conjugated with AlexaFluor 488 were purchased from Invitrogen (Carlsbad, CA, USA) and were used without further purification. Proteins were aliquoted and stored at -20 °C temperature. When needed, small aliquots were thawed and kept on ice. At all times proteins were kept under the cover to avoid bleaching.

6. Model membrane systems

6.1. Lipid handling

For any kind of the membrane system pure lipids are needed. All lipids used in this studies were purchased from Avanti (Alabaster, AL, USA). Lipids were kept at -20 °C. Before use, lipids were solved in chloroform, aliquoted and kept at -20 °C. To prevent the oxidation of lipids, before closing, vials were filled with argon. This inert gas blocks lipid solution from oxygen and allows to keep stock solutions for extended period of time. All vials were always sealed with silicon tape to avoid any evaporation of stock solutions. All the lipid stocks were first bring to the room temperature before opening to avoid water condensation on inner walls of vials. On the daily basis, the lipid concentration was calculated upon the mass of the lipid and the added volume of the solvent. This method was validated using Rouser's assay which showed that precise pipetting provides enough accuracy. Concentration of stocks which was suspected to be changed over time or wrong was determined using Rouser's modified method.

6.1.1. Rouser's method to estimate phosphorus concentration

This method makes use of molybdate which under acidic conditions complexes with free phosphorus. Phospholipids incubated at high temp. in perchloric acid are decomposed into CO₂, H₂O and PO₄³⁻. In acidic condition orthophosphate makes complexes with molybdenum — ammonium phosphomolybdate (VI)[(NH₄)₃PMo₁₂O₄₀]. Next, this compound gets reduced by ascorbic acid and turns into the mixture of molybdenum oxides at oxidation states between +IV and +VI - MoO₂xMoO₃ (the so called molybdenum blue). The amount of the latter is estimated by the absorption measurement. It is important to notice that the Rouser assay cannot be used to measure lipid suspensions containing any phosphate since any form of inorganic phosphorus will sum up to the total mass of measured phosphorus. Proper amount of lipids (between 10 to 100 nmols) was pipetted into the glass test-tube and filled with 500 µl of water and 300 µl of perchloric acid. After short vortexing lipids were incubated at 180 °C for 3 hours. Such a long time is needed to fully mineralise lipids and release phosphorus. After the incubation test-tubes were quickly cooled down under the tap water stream. Then 2,5 ml of water, 400 µl of ammonium molybdate solution (1,25 % w/v) and 400 µl of fresh ascorbic acid solution (5 % w/v) was added to the test-tube which was subsequently vortexed and kept for 15 min at 100 °C. Samples were again quickly cooled down under the water stream and absorption of the solution was immediately measured using spectrophotometer at 812 nm (Varian, Cary). Simultaneously with the lipid samples the standardisation curve was prepared for which, instead of lipids, phosphorus standard solution was used. The example of mineralisation of the brain sphingomyelin and the standard curve are shown in 6.1.

6.2. Supported Lipid Bilayers (SLBs)

Supported lipid bilayers (SLBs) were formed according to (50). First, multilamellar vesicles (MLVs) made by drying lipids in the glass vial. Obtained thin lipid film was then hydrated with the so-called

6. Model membrane systems

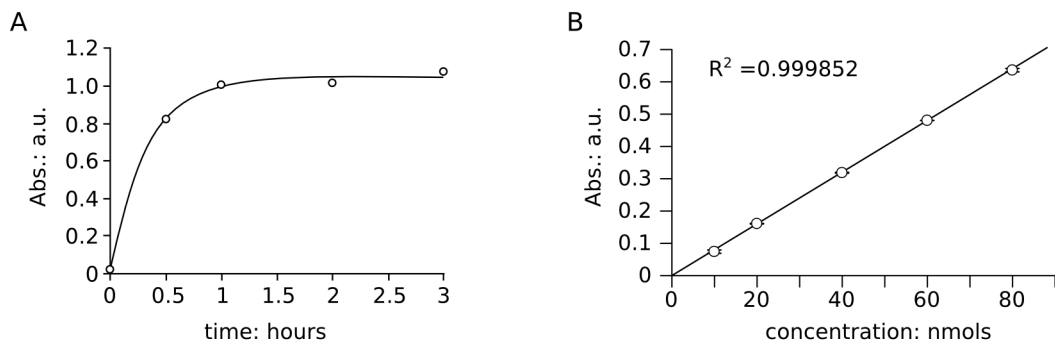


Figure. 6.1.: A) The mineralisation of brain sphingomyelin at 180 °C. The full mineralisation was achieved after approximately 2 h. B) The standard curve to determine phosphorus concentration. To estimated the amount of the lipid used in assay we assumed that mineralisation was complete and hence one mol of lipids equals one mol of free phosphorus (true for PC and PI and SM).

SLB buffer (50) so the final concentration was 2.5 mg/ml. The hydration always took place at temperature over the lipid mixture phase transition. Such prepared MLVs were aliquoted and kept at -20 °C. Liposomes were thawed just before SLBs preparation. Milky suspension of MLVs was diluted with SLB buffer to 0.3 mg/ml and sonicated in a batch sonicator for 10 min. After this step liposomes become small and unilamellar (small unilamellar vesicles - SUVs) and the suspension turns transparent. In order to form SLB vesicles were deposited on the freshly cleaved mica surface. Mica was attached to the glass surface with a UV-curable glue of low autofluorescence (63 Norland Products, Cranbury, NJ, USA). In figure 6.2 are shown two chambers which were used for SLBs preparation. Unless the AFM was used, chambers made of Eppendorf tube were used. For experiments requiring AFM, we used chamber provided by AFM manufacture (JPK Instruments, Berlin Germany).

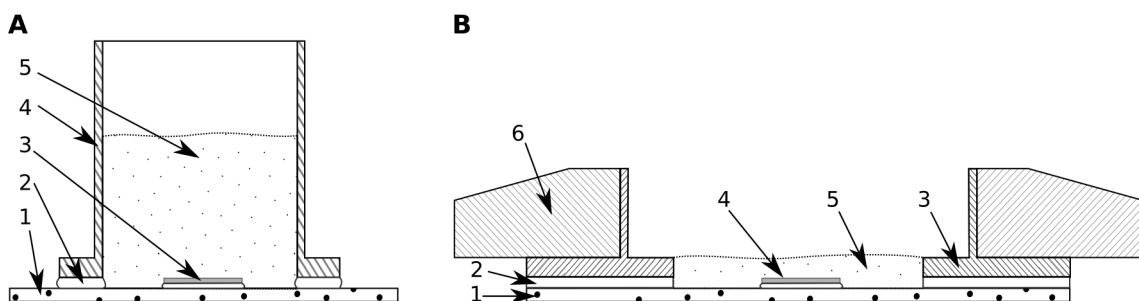


Figure. 6.2.: The schematic representation of chambers used in experiments involving SLBs. A) Home-built cell made of coverslip and Eppendorf tube. 1. Coverslip of nominal thickness 150 µm; 2. Optical glue; 3. the sheet of freshly cleaved mica glued to the glass; 4. Eppendorf tube with a cut-off bottom; 5. The sample solution. B) Biocell of the JPK AFM setup. 1. Round coverslip of a diameter 24 mm; 2. The rubber seal; 3. The metal ring which makes the wall of the cell; 4. The mica sheet glued to the glass; 5. The sample solution; 6. The clamp of the cell which keeps all the parts in the right position.

After deposition, the vesicles were incubated at 21 °C for 5 min. During this step vesicles were let to sink down and partially fuse at the mica surface. To accomplish the vesicles fusion we add 3 µl

of 0.1 M CaCl₂. After 5 min of the incubation with calcium, the sample volume was raised to 300 µl of SLB buffer and the sample was incubated for 15 min above the phase transition temperature. To achieve this goal, the sample was placed on the hot plate (in case of the Eppendorf tube chamber) or the built-in Peltier element was used (in case of the AFM cell). Newly formed SLB was washed with 4 ml of fresh buffer (of a temperature matching the temperature of the sample) and the sample was let to cool down for 30 min. In cases where membranes with the phase separation were used, the cooling procedure was prolonged to one hour. The whole procedure of SLBs formation is summarised in figure 6.2.

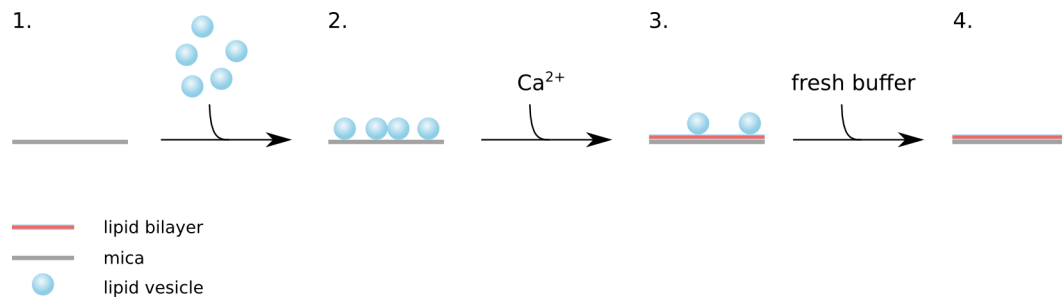


Figure. 6.3.: The schematic representation of the SLBs formation. 1. On the freshly prepared sheet of mica SUVs are deposited; 2. After letting the vesicles to sink down calcium is added to the sample in order to facilitate membrane fusion; 3. Non-fused vesicles and calcium ions are washed away using fresh buffer; 4. Ready lipid bilayers deposited on the mica.

6.2.1. SLBs tubulation experiment

Tubulation experiments were carried out using the confocal microscope equipped with laser scanning unit. Upon formations of the SLB, the known amount of the purified protein was added to the chamber. The microscope was used in time-series mode, where the first image was always taken before the protein was added. The analysis was based on the assumption that the membrane which is forming lipid tubes is equal to the area of defects appearing in SLBs. Since defects are free of the fluorescence dye, they can be easily detected and their total area can be estimated (figure 6.4 and 6.5).

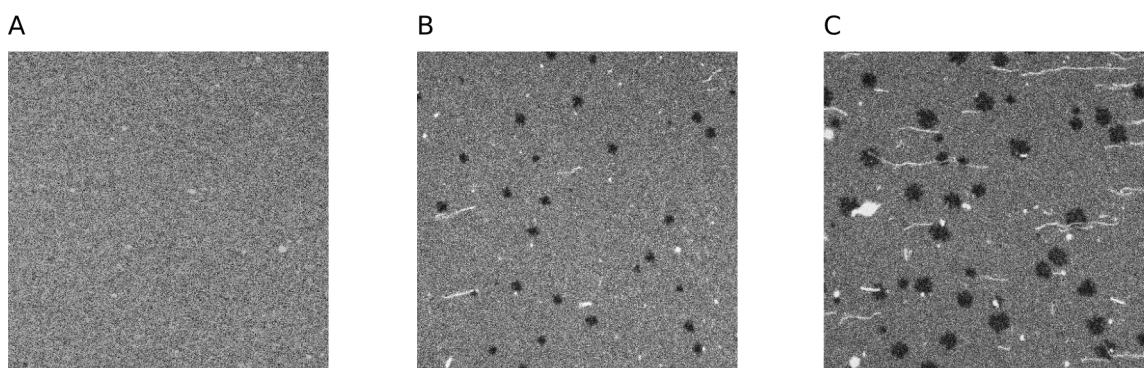


Figure. 6.4.: SLBs images take prior (A) and 5 (B) and 10 (C) minutes after the protein addition. Bright long structures are lipid tubes freely floating in the buffer solution and dark patches are defects of the SLBs caused by the protein activity.

6. Model membrane systems

ImageJ software was used to analyse the data. First the threshold was set so that only dark part of the images corresponding to membrane defects are considered. Then the total area of defects as a percentage of total image area was plotted versus time.

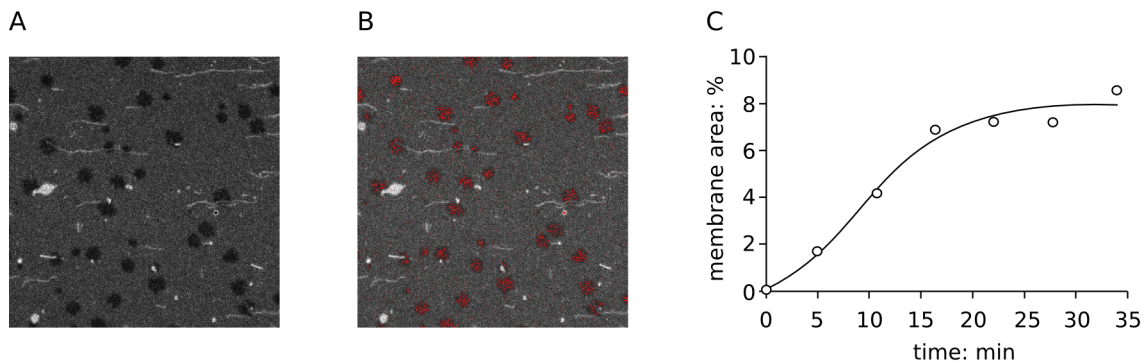


Figure. 6.5.: The example of the data analysis. A) The image of the SLBs after 10 min of the incubation with FCHo2 BAR domain. B) By using threshold option of ImageJ software, the area of defects is marked in red and the plot of it over time is shown in C.

6.3. Langmuir monolayers

Standard isotherms were taken using NIMA 112D Langmuir trough equipped with micro-balance. Each time before use, the trough was thoroughly cleaned. Firstly, wearing gloves and using the tweezers, the paper tissue (Kimwipes) was soaked with chloroform and the all PTFE surfaces were rubbed what was followed by a drying the remains of the solvent with the new clean tissue. Then procedure was repeated using ethanol. This two steps were repeated twice. Subsequently, trough was filled with pure water and the water-air interface was cleaned using vacuum. This step was repeated three times. Then a new Wilhelmy plate made of ash-free filtration paper was attached to the micro-balance and was let to soak with water for 15 min. After the mass of the plate reached equilibrium, barriers were closed with velocity of $150 \text{ cm}^2/\text{min}$ and the surface pressure was monitored. Unless the surface pressure at the smallest possible area (24 cm^2) was higher than 0.3 mN/m , the system was used for the experiment. Otherwise, the washing step with a water was repeated.



Figure. 6.6.: NIMA 112D Langmuir trough.

Isotherms were taken so that the starting surface pressure equalled zero. The compression rate was

set to 5 cm²/min. After each compression experiment the trough was thoroughly cleaned. Each lipid mixture was measured at least three times and the average of three isotherms is presented.

6.4. Monolayers troughs for FCS

6.4.1. Modified NIMA 112D Langmuir trough

Conventional Langmuir troughs are not designed to work with optical microscopes. In order to combined NIMA 112D trough with an inverted confocal microscope we modified it by placing special window with coverslip at the bottom of the device. Window is made of a high quality metal and has a form of a ring with a thread which allows for exchanging and washing the glass. The schematic drawing and the practical implementation is shown in figures 6.7 and 6.8.

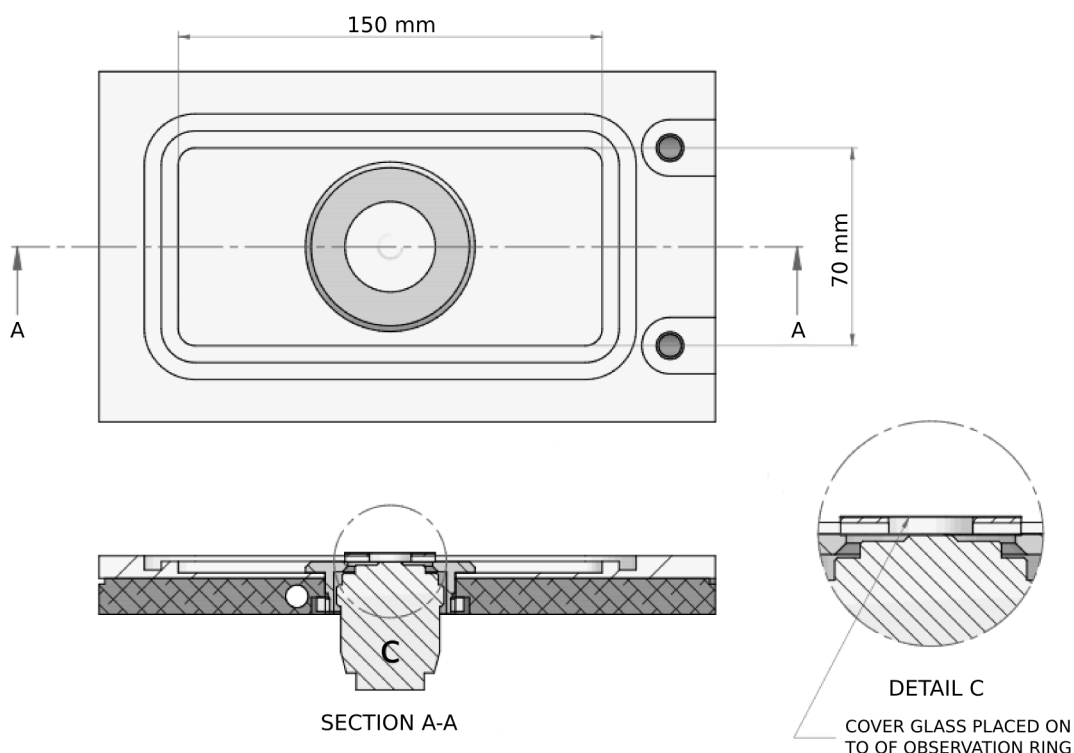


Figure. 6.7.: Schematic representation of the modification made on the conventional 112D NIMA Langmuir trough. At the top, top view of the trough with the clearly visible observation window for the light microscope. Bottom, left is shown the cross section of the device along A-A line with depicted microscope objective (C). Details of the window together with the objective are depicted on the right site. According to material provided by NIMA (Coventry, GB).

To be able to carry out fluorescence correlation spectroscopy (FCS), objectives with a high numerical aperture are used. The drawback of such objectives is their short working distance. For example, for the commonly used objective, C-Apochromat 40x 1.2 NA (Zeiss, Jena, Germany) the working distance is 240 µm. This is very problematic in experiments involving lipid monolayers, since it requires very low level of the subphase. It is very difficult to achieve and causes often monolayer collapsing.

6. Model membrane systems

To overcome this problem we used long distance LDC-Apochromat 40x objective of 1.1 NA (the working distance is 640 μm).

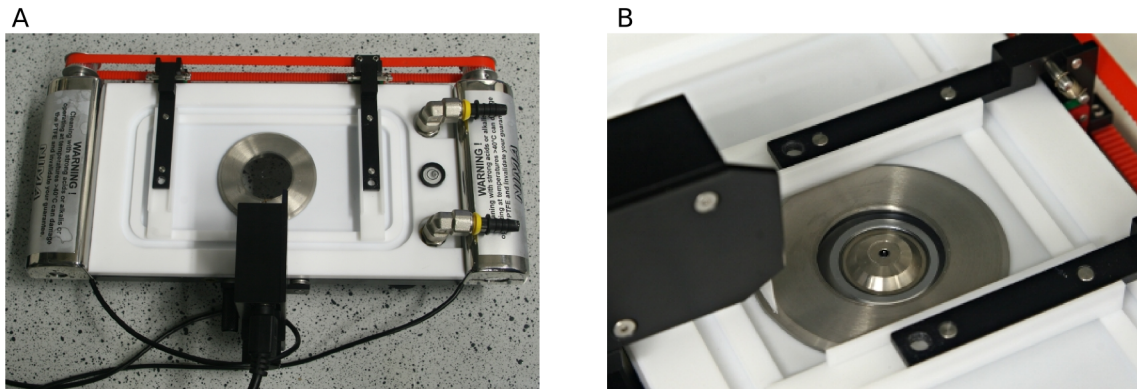


Figure. 6.8.: Photography of the modified Langmuir trough. A) Top view of the trough. With visible observation window. B) Close-up view of the window with LDC-Apochromat 40x 1.1 NA Zeiss objective below the trough. Picture shows closed position of barriers, with micro-balance seen from the left side.

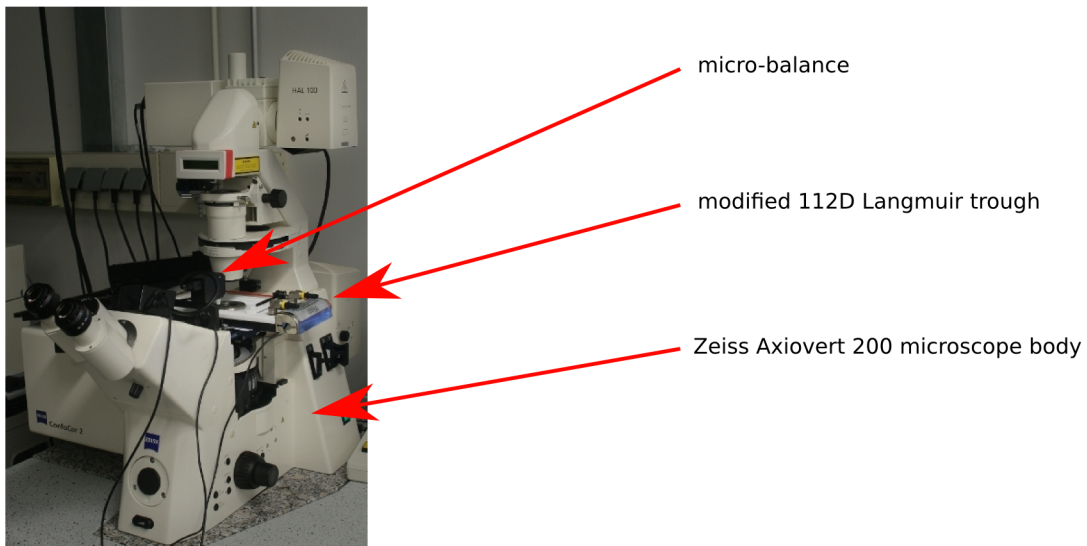


Figure. 6.9.: Picture of the monolayer trough mounted on the Zeiss Axiovert 200 microscope body. Arrows points the main parts of the setup.

FCS measurement were taken using the commercially available ConfoCor 2 setup equipped with laser scanning unit (Zeiss, Jena). After the lipid deposition, the trough was covered with Plexiglas plate which was freely laying on movable trough barriers. To further decrease the air flow over the monolayers we used paper tissues soaked in water and put in the proximity of the barriers, but still allowing for the compression of the monolayer. The mentioned procedure avoids the evaporation of the subphase and the uncontrolled drop of the monolayer level and was required for the precise positioning of the focus of the laser beam. In order to focus on the monolayers, we make use of the fact that the laser beam is scattered strongly at the interfaces, i.e. by moving the objective from the

most down position upwards we could detect three levels at which the intensity was increased. To do it we set laser power at the minimum value and allow the laser light to reach the PMT detector. The first intensity peak comes from the water-glass interface (the lower surface of the coverslip), the second one is the scattering of the light at the glass-water interface (upper coverslip surface) and the third peak is the reflection coming from water-air interface. Finally, we confirmed the right positioning of the objective by monitoring the fluorescence intensity of the fluorescent probe incorporated into the lipid monolayer. In all the experiments, the level of the water-air interface was kept between 350 and 600 μm above the glass surface. An example intensity scan over the Z-axis and the scheme of relative positions of system components are shown in the figure 6.10.

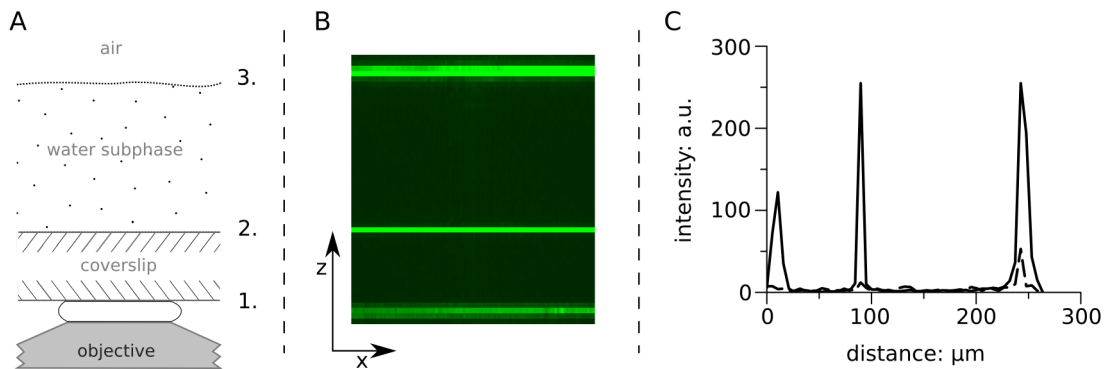


Figure. 6.10.: Schematic representation of the relative position of interfaces positioning and the experimental data showing scattering of the laser beam. A) The localisation of the interfaces with respect to the objective. 1. Water-glass interface between the lower surfaces of the coverslip and the immersion water; 2. Water-glass interface between the upper surface of the coverslip and the monolayer subphase; 3. Water-air interface on which the lipid monolayer is deposited. B) The line scan along the z axis. The optical path was set so that reflected laser light was collected at the PMT detector. Bright lines correspond respectively to interfaces depicted in A. C) Relative intensity of the light collected at different position in z direction. Solid line corresponds to reflected light of 543 nm HeNe laser. At the same time, fluorescence of the lipid dye (dashed line) was monitored by splitting the light of the wavelength longer than 545 nm and directing it to the second detector. It can be easily seen that laser light is reflected on every interface, while increased fluorescence is found only at water-air surface, where the monolayers is expected.

6.4.2. Micro-chamber for protein-monolayer studies

While modified trough can be used to measure properties of lipid monolayers, to carry out experiments involving proteins is a very challenging task. The main reason for that is the relatively big volume of the device, i.e. in the conventional trough the volume is usually bigger than 100 ml which requires large amount of the protein. This constrains experiments only to those proteins which are abundant in nature or are commercially available. Obviously, protein over-expressed in bacteria or other expression systems currently used in the laboratories cannot be easily produced in such quantities. Since the only reasonable source of proteins used by us is the bacterial expression system we had to look for an alternative that could allowed us to carry out binding experiments involving proteins and monolayers. The only solution was to miniaturise currently available devices. Since monolayers formation is based on the one of the most fundamental property of the lipids - their amphiphaticity, it is virtually possible to obtain monolayers on any water-air interface. Therefore we made PTFE seal which we then attached to the coverslip with a UV-curable glue. The seal works like a barrier for a drop of water solution

6. Model membrane systems

spread over the glass surface. The volume of a such system is over 1000x smaller than that one of the conventional instrument and gives opportunity to carry out experiments involving proteins without unnecessary loss of biological material. While PTFE provides proper contact angle for water solution, it was difficult to obtain evenly thin layer of water over the glass surface. To overcome this problem we treated glass with plasma for 10 min. This procedure makes the glass more hydrophilic and reduces the contact angle between the water and the glass surface. Such prepared chamber was filled with water. Subsequently, by using the pipette lipids in chloroform solution were deposited on the water surface. After 5 min of an incubation, the chamber was covered with $22 \times 22 \text{ mm}^2$ coverslip to avoid the evaporation and the air flow.

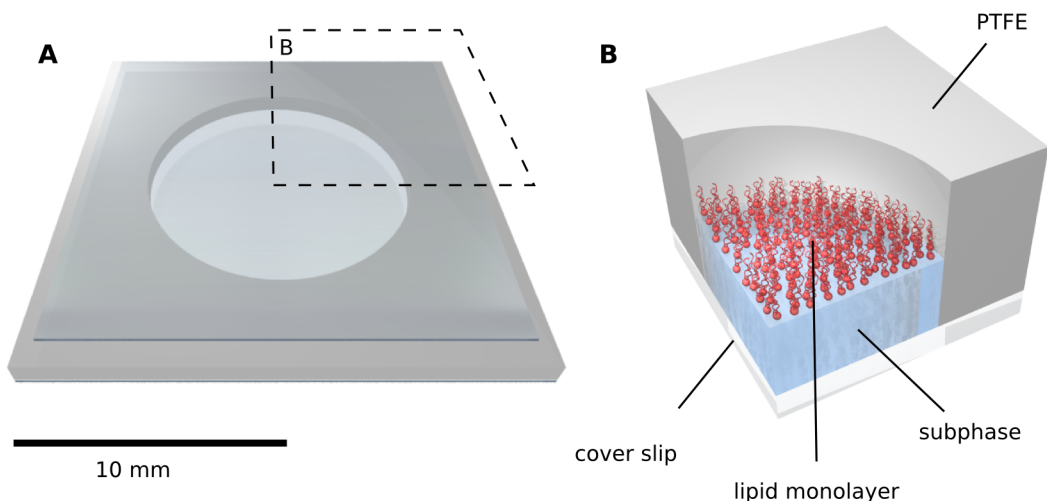


Figure. 6.11.: 3D projection of the micro-chamber. A) Overview of the chamber; B) The enlarged part marked with the dashed line in A.

The PTFE used to construct the chamber was 1 mm thick to provide enough space for the subphase. The area available for monolayers was 1.76 cm^2 . To obtain subphase depth not bigger than $500 \mu\text{m}$, $100 \mu\text{l}$ of water was used. Unfortunately, with this amount of water it was difficult to obtain monolayers since most of them immediately were collapsing. This was mostly due to very thin layer of water, which was expelled from the glass surface by the chloroform solution. To overcome this problem and to obtain more reproducible results, we firstly put $200 \mu\text{l}$ of the subphase solution into the chamber. After depositing the monolayer, $100 \mu\text{l}$ of the solution was removed from the subphase. The deposition protocol is summarised in figure 6.13. Because of the mechanical disturbance of the monolayer surface, we checked the morphology of the interface before and after the procedure (in this case $100 \mu\text{l}$ of solution was used, in order to ensure that the monolayer is within the working distance of the objective).

Additionally, we checked the mobility of the fluorescent dye incorporated into the lipid monolayer. Again, we could not see any significant changes of the diffusion of the lipids (figure 6.15).

After the experiment, the chamber was kept in water and washed alternatively with 80% v/v ethanol and deionised water. After washing the chamber was rinsed thoroughly with MiliQ water and dried with compressed air. While our new constructed chambers enables measurement of proteins in small volumes, it has to be mentioned, that because of its small dimension, it was not possible to implement

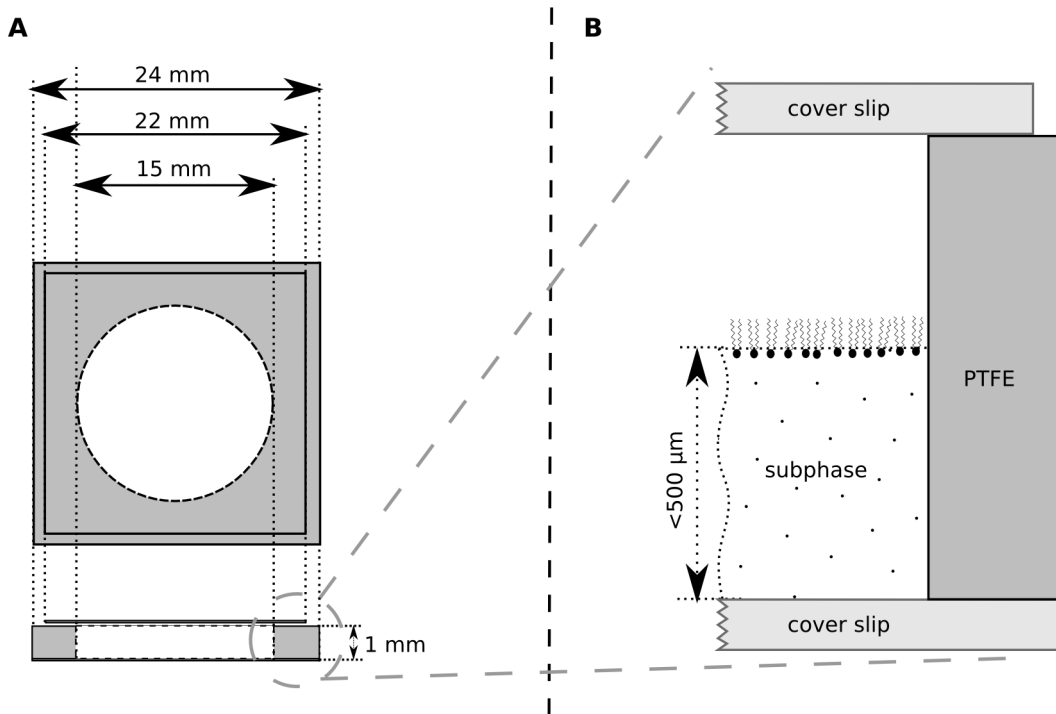


Figure. 6.12.: A) Schematic drawing of the micro-chamber for monolayers studies. B) Parts of the cell with respect to the monolayer.

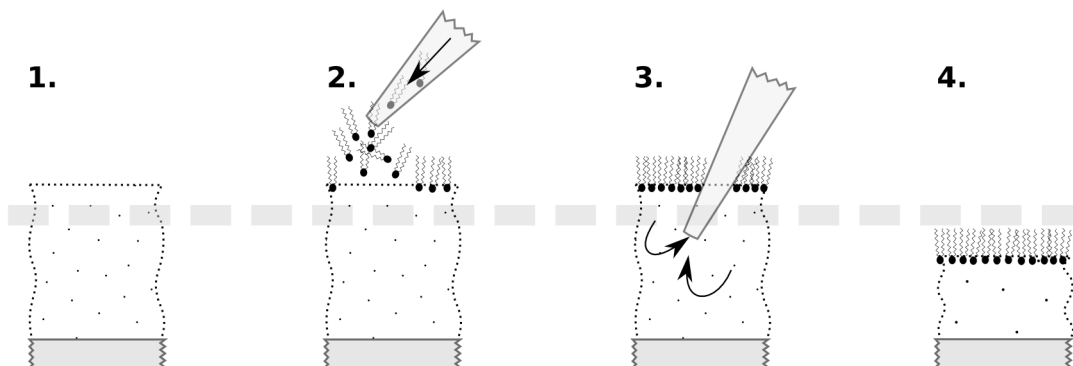


Figure. 6.13.: Scheme of the monolayer deposition. 1.) Filling of the chamber with 200 μl of subphase solution; 2.) Applying of lipids in chloroform solution with a pipette; 3.) Removing of the excess subphase; 4.) Ready to use monolayer within the working distance of the objective mark in the drawing by thick, dashed line.

neither the micro-balance nor the mechanical barriers. That is why it is not possible to directly measure the surface pressure using micro-chamber. Since we were interested mostly in influence of the mean molecular area of the lipids and molecule mobility on the protein binding, this was not the main issue for us. To extract information about surface pressure in this case, one has to perform the calibration curve on the modified NIMA trough where both surface pressure and the diffusion can be monitored.

6. Model membrane systems

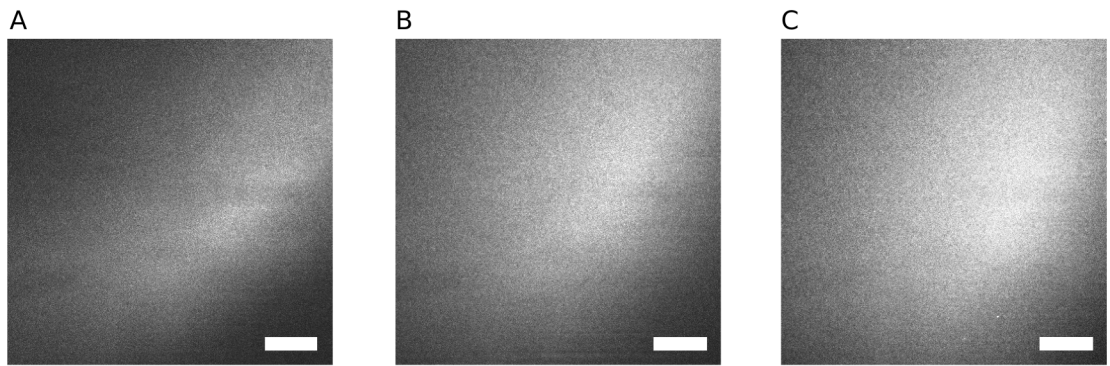


Figure. 6.14.: Fluorescence images of the monolayer before (A) and after 5 (B) and 10 (C) dipping events.

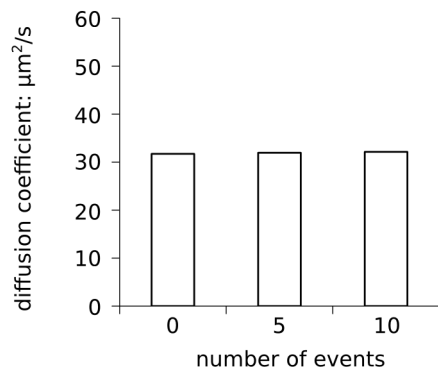


Figure. 6.15.: The control experiment showing no significant changes in the diffusion of the lipids within the monolayer upon the contact with the pipette tip. One 'event' is one touch of the monolayers surface with the pipette. 'Zero' events corresponds to the freshly prepared sample.

Since the surface pressure is strictly connected to the diffusion of the molecules in the monolayer, it is possible to derive one parameter knowing another one, i.e. to extract surface pressure knowing the diffusion of lipids using a calibration curve. Mobility of molecules in the monolayer was controlled by applying particular amount of lipids in chloroform solution.

7. Atomic force microscopy measurements

7.1. Instrumentation

All AFM measurements were conducted using NanoWizard I device purchased from JPK Instruments (Berlin, Germany). The system was combined with a confocal microscope equipped with LSM 510 Meta unit purchased from Zeiss (Jena, Germany). The standard stage supplied by Zeiss was replaced by JPK precision stage which allows for the precise positioning of the AFM head and the sample with respect to each other. For measurements of SLBs we used BioCell purchased from JPK and depicted in 6.2B. Cantilevers were purchased from MicroMash (Tallinn, Estonia). CSC38 model was used with typical spring constant 0.03 N/m.

7.2. Procedure

The measurement cell was assembled according to the user manual provided by JPK. SLBs were prepared as described earlier. After the mounting of the cantilever, the AFM laser was focus using IR-detector and keeping AFM head aside of the optical microscope in the vertical position. Subsequently, the signal at the AFM photo-diode was maximised by adjusting the mirror and the laser was centred by fine-tuning of the detector position. After placing the AFM head in its working position the mirror was readjusted. This is necessary since the difference of the reflectivity of air and water solution changes the laser path. Fine positioning of the laser beam was accomplished by using confocal microscope in continuous scanning mode. We used IR 640-710 band pass filter which allows only AFM laser to reach the PMT detector of the confocal microscope. Then following the spot of the AFM laser beam and the shadow of the cantilever, the laser beam was positioned in the middle of the cantilever in the proximity of the cantilever tip. Subsequently, the position of the AFM detector was refined so that the laser beam hit exactly the middle of the photo-diode. In order to approach the sample surface the optical microscope was operated using halogen lamp and transmitted light. The focus was placed just above the surface and the AFM was lowered stepwise till the cantilever was in the focus of the optical microscope. Then automatic procedure was launched provided by JPK software. System was approaching the surface till 0.5 V current was reached on the detector. The imaging was carried out at lowest possible force applied to the sample which typically corresponded to 0.05 V current at the photo-diode. System gain parameters were adjusted so that the trace and retrace profiles were overlaid. Typical values for the z-range set to 3 μm were IGain 1500-2500 and for PGain 0.005-0.02. The scan rate was typically set to 1.5 Hz and the image size to 512 x 512 px². In order to reduce the noise at 50 Hz frequency, during AFM measurements, control unit of LSM had to be switched off. In co-localisation studies, first AFM images were taken and then LSM control unit was switched on and the confocal image was take. On regular basis C-Apochromat 40x 1.2 NA Zeiss objective was used in these studies. In order to avoid unwanted detection of the laser light of the AFM, during imaging the laser was switched off. AFM images were analysed using Gwyddion program (www.gwyddion.org).

8. Confocal Microscopy

8.1. Fluorescent probes

For imaging the following dyes were used: 1,1'-Dioctadecyl-3,3,3',3'-Tetramethylindodicarbocyanine, 4-Chlorobenzenesulfonate Salt ('DiD'), 1,1'-Dilinoleyl-3,3,3',3'-Tetramethylindocarbocyanine Perchlorate (FAST DiI) and CholEsteryl 4,4-Difluoro-5-(4-Methoxyphenyl)-4-Bora-3a,4a-Diaza-s-Indacene-3-Undecanoate (543 cholesteryl). All dyes were purchased from Invitrogen (Carlsbad, NJ, USA). Besides lipid dyes, fluorescent proteins were used. FCHo2 BAR domain was labelled with Alexa 488 maleimide dye. Cholera toxin subunit B and streptavidin were labelled with AlexaFluor 488 and purchased from Invitrogen. For the calibration of the FCS setup Alexa 546 was used.

8.2. Imaging instrumentation

Imaging was carried out using LSM 510 Meta or LSM 510 ConfoCor 2 microscope (Zeiss, Jena, Germany). For two colour imaging microscopes were operated in the so called multitrack mode in which each channel has a separated optical path (two detectors and only one laser is engaged at the time. This procedure does not provide high temporal resolution, but provides better separation of the signal and prevents false-positive results due to cross-talk. For dyes excited with 488 nm laser, 505-550 or 505-530 nm band pass filter were used. In case of dyes with excitation of 543 nm, 560 nm long pass or 560-585 nm band pass filter were used. For infra-red dye - DiD, 640-710 nm band pass filter was used. After adjusting the laser power and the gain of the detector images were collected at a moderate scanning rate (typically 7 seconds per images) using averaging over two scans. All images were processed in ImageJ software.

8.3. Fluorescence correlation spectroscopy instrumentation

FCS measurements were carried out using LSM 510 ConfoCor 2 microscope. Dichroic 488/543 nm mirror was used in the optical path. Collimator was set to 16. Pinholes for APDs were set to 70 (for 488 laser line) and 80 (for 543 laser line). Before each measurement the correction ring of the objective was adjusted to maximise the signal. Then the system pinhole positions were automatically adjusted using microscope GUI. Before each alignment focus was placed at the monolayer. To do so, the motorised focusing mechanism was used with a step size set to 0.2 μm . For single measurements 5 second independent traces were averaged (typically 20) (figure 8.2). The 5 second period was long enough to obtain good quality data and allowed for a convenient correction of the focus. This was necessary, since the increased temperature at the measurement spot caused increased evaporation. Typically, such correction was done 2 to 3 times per measurement (100 second total). Traces over which the correction was done were discarded. Data were fitted using Zeiss software. Since monolayers are very pronounced to mechanical instability and inherent undulations due to thermal fluctuations the additional slow component was appearing in the correlation curve. To overcome this problem and to

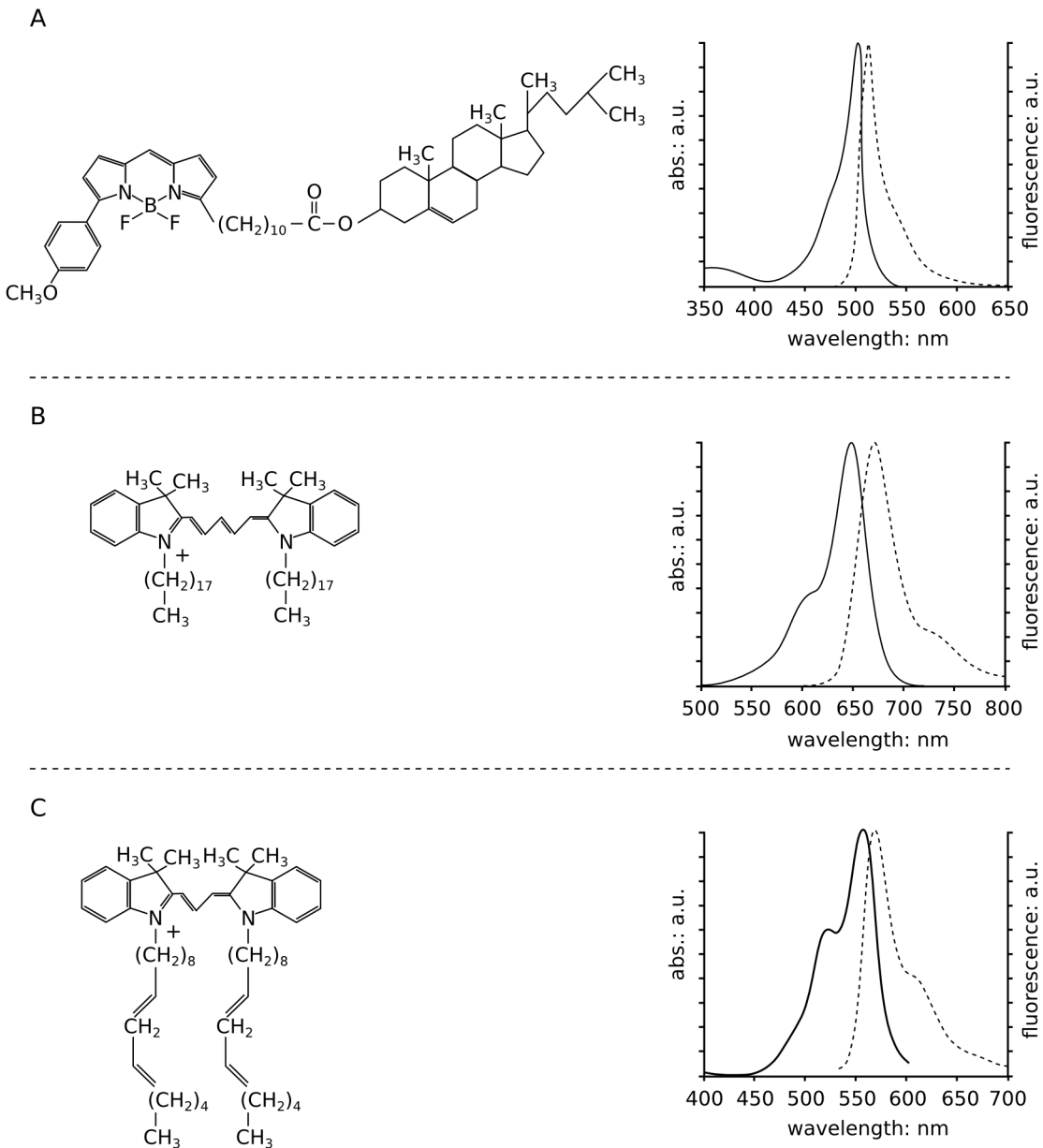


Figure. 8.1.: Chemical structures and optical spectra of fluorescence dyes used in our studies. Bodipy cholesterol (A), DiD (B) and FAST DiI (C). Spectra drawn with solid line correspond to absorption and dashed line refers to fluorescence emission spectra. Adopted from www.invitrogen.com

improve the accuracy of the determination of the lipid diffusion time, averaged data were fitted with a two component two dimensional diffusion model with a triplet state:

$$G(\tau) = \frac{1}{N} \left(1 + \frac{T}{1-T} e^{-\tau/\tau_T} \right) \left(\frac{F}{1+\tau/\tau_F} + \frac{1-F}{1+\tau/\tau_D} \right) \quad (8.1)$$

where N is the number of particles, T is a triplet state fraction, τ_D , τ_F are diffusion times for a lipid

8. Confocal Microscopy

dye and monolayer fluctuations respectively. F indicates the contribution of the monolayer fluctuations with respect to the lipid diffusion component (typically below 0.05). The faster component was used to determine the diffusion time of the lipid dye.

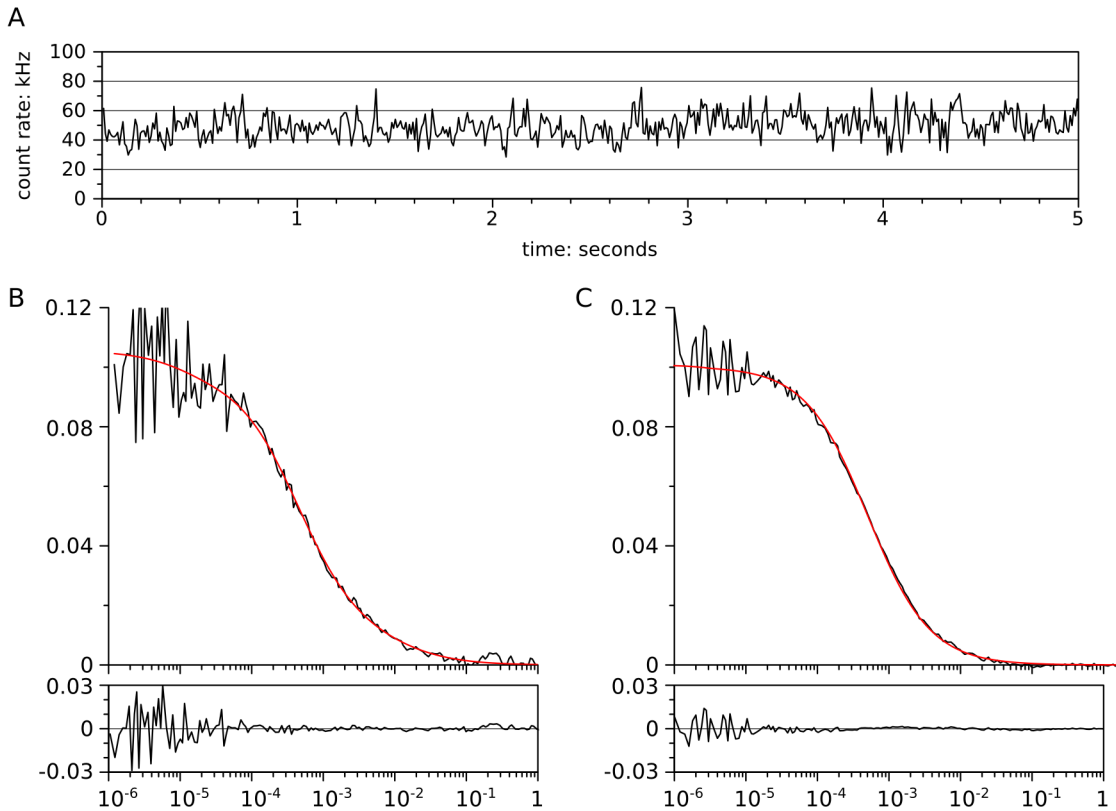


Figure. 8.2.: A) An example of the signal acquired by APD during FCS measurements In this particular case the sample was a DMPC monolayer with SLB buffer as a subphase. B) The auto-correlation of the trace in A. The red line represents fit to the equation 8.1. B) The average of auto-correlation curves with the fit the equation 8.1.

In order to calculate the diffusion coefficient, the system was calibrated with Alexa 546 dye of which D was taken from (69). Correlation curves were fitted in this case to one component three dimensional diffusion model with a triplet state:

$$G(\tau) = \frac{1}{N} \left(1 + \frac{T}{1-T} e^{-\tau/\tau_T} \right) \left(1 + \frac{\tau}{\tau_D} \right)^{-1} \left(1 + \frac{\tau}{S^2 \tau_D} \right)^{-1/2} \quad (8.2)$$

where T is a triplet state fraction, τ_T is the characteristic triplet time, τ_D is diffusion time for the dye and S is the structural parameter describing the shape of the detection volume. The waist of the focal volume was calculated according to the following equation (r_o refers to the radius of the focal spot):

$$D = \frac{r_o^2}{4\tau_D} \quad (8.3)$$

Part III.

Results

9. BAR protein binding to SLBs

9.1. Introduction

The starting point of the work was to find the most appropriate lipid system in which BAR domains could be investigated. The natural candidate was a SLB approach, in which the sample can be easily prepared providing large flat area of the membrane. This gives an opportunity for both: to study the kinetics of the protein-membrane interaction and to investigate the structural basis of this phenomenon. In this chapter the pioneering work on the BAR protein interactions with SLBs is presented. In addition to the qualitative overview of the FCHo2 tubulation activity, a quantitative analysis is proposed.

9.2. Tubulation of SLBs by FCHo2 BAR domain

Due to the evidence coming from recent publications (49), (11) that BAR domains have strong affinity to the negatively charged lipids, we chose DOPC:PI(4,5)P₂ 95:5 (mol:mol) as a lipid mixture for the experiment. While DOPC with a zwitterionic headgroup a standard lipid used for the SLB formation, phosphatidylinositols are negatively charged lipids abundant in commonly used polar fraction of Folch lipid extract. Since the mentioned extract contains substantial quantities of PIPs and that FCHo2 specifically interacts with this lipid we used membranes composed of 5 mol% of PI(4,5)P₂ and 95 mol% DOPC. It is the upper limit of the amount of this lipid which can be incorporated into SLBs. The figure 9.1 shows the homogeneous SLB made of DOPC:PI(4,5)P₂ mixture with 0.1 mol% of a fluorescent marker (DiD).

When the protein was added to the SLB the fast appearance of dark defects in the membrane (9.1B, 9.2) was observed. While this phenomenon can be observed at relatively high concentrations in the case of many proteins, in our experiment this effect occurs already at nanomolar concentrations. To confirm the specificity of this interaction we carried out a control experiment in which 0.7 µg/ml of BSA was used instead of a BAR domain solution. As it was expected, we did not observe any deformation of the bilayer in this case (figure 9.7). The other characteristic feature of the membrane deformation are elongated lipid structures which grow out of a SLB. Some of these structures adhere to the bare support, but many of them move freely in the buffer solution above the bilayer (figures 9.3 and 9.4) with one end anchored to the SLB. From earlier studies on BAR domain interacting with vesicles (48), (43), and taking into account general properties of lipid membranes we concluded that the mentioned structures are protein-scaffolded lipid tubes. It has to be noticed, that while in most of the studies cited above only tubular structures were shown to be formed, we cannot exclude that some of structures observed by us might be elongated micelles similar to those reported by Mizuno and co-workers (46). Unfortunately, the confocal microscopy cannot provide enough high resolution needed to distinguish between these two different lipid structures.

While the membrane tubulation is a pronounced process, we noticed that in some cases other, more subtle changes in the SLB morphology appeared. Before the formation of SLB defects we observed

9. BAR protein binding to SLBs

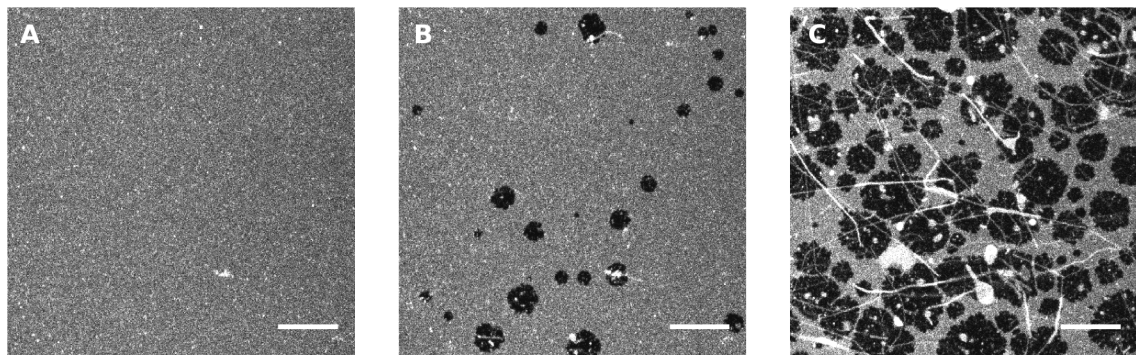


Figure. 9.1.: Series of time-lapse images presenting the SLB rupture and the tube formation in presence of the FCHo2 BAR domain. A) The fluorescence image of the homogeneous membrane composed of DOPC:PI(4,5)P2 95:5 (mol:mol) mixture with 0.1 mol% of DiD in the absence of the protein. B). The same sample shortly (60 seconds) after the addition of the FCHo2 BAR domain . Small defects of very low fluorescence signal are randomly distributed over the whole surface. C) The late stage of the membrane deformation (25 minutes). Large patches of a bare mica can be seen. Additionally, elongated lipid structures of a different width and length. While some of lipid tubes are stretched over the support, many of them are anchored to the membrane by one end what allows for pivoting of the tube in the buffer solution. The scale bars are 20 μ m.

a temporal change in fluorescence brightness. It has a form of bright concentric rings growing from the spot where the defect in the bilayer will finally be formed. Described changes in the brightness have the form of waves spreading after its appearance. Although very interesting, this effect did not converge with the main aim of the work hence it was not thoroughly investigated. We speculate that the source of this phenomenon might be dewetting of the membrane induced by high protein density at the lipid-water interface. Changes in the amount of a solvent penetrating the lipid membrane would alter the polarity of the membrane environment and could lead to fluctuations of the fluorescence signal. Another probable source of the ring-effect might be lower lipid mobility at sites where proteins molecules bind to the membrane. If we would assume, that each BAR domain interacts strongly with a certain number of lipids, a cumulative interaction of many domains at neighbouring sites can substantially diminish the mobility of lipids in the whole area. The used lipophilic dye, DiD, is very sensitive to the lipid packing of the membrane and it partitions mostly in fluid, liquid disordered phase. Once the BAR domains bind to the deformation spot with high densities, the increased order of lipids might lead to the exclusion of the DiD from this region. It also has to be noticed that the BAR domain (see figure 1.11A) and the DiD (see figure 8.1B) are both positively charged molecules. In this case repulsive forces between the protein and the lipid dye what might be reflected in the mentioned ring-like exclusion of the fluorophore from the region of a higher protein density.

9.3. Quantitative tubulation assay

In order to get better insight into the mechanism of the tubulation process, we designed a quantitative assay which allows for a precise monitoring of the membrane deformation. In our experiment the bilayer rearrangement was typically accomplished within 30 minutes upon the protein addition. We noticed that independently from total protein concentration the plot of the area percentage of the tubulated membrane versus time has sigmoidal shape (figure 9.6) and the saturation character of curves

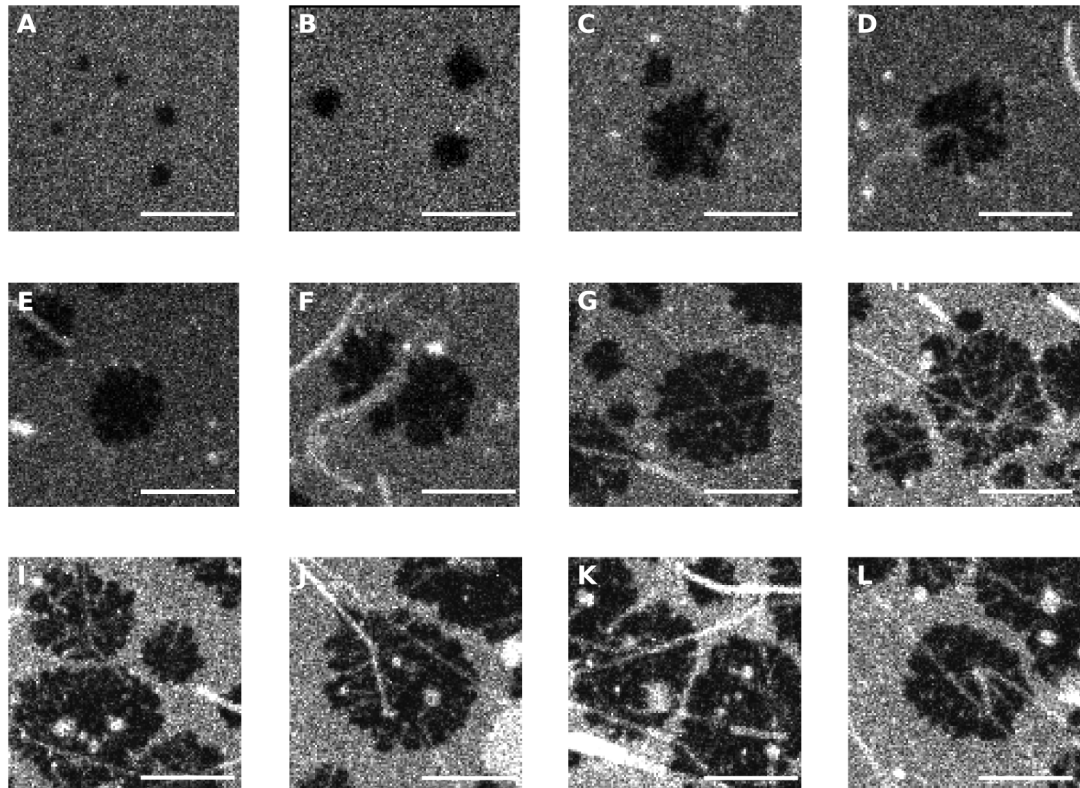


Figure. 9.2.: Morphology of DOPC:PIP(4,5)2 (95:5) membrane deformations at different stage of the SLB tubulation. Images show fluorescence micrographs on membrane containing 0.1 mol% of DiD. The initial stage of the of the membrane rupture is shown in A and B. The appearance of tubes is shown in D, E and F. Shape of the defects and lipid tubes at the final stage of the deformation process are shown in G to L. The scale bars are 10 μ m.

was obtained within the range of protein concentration used. The final saturation level is proportional to the amount of the protein used in the experiment (the total area of the available lipid membrane was considered as constant) and reaches the maximum value of about 50 %. Since the fluorescence signal coming from any lipid structures in our test does not differ significantly, it is not possible to distinguish between intact lipid bilayer and tubular structure located at the surface. That is why the theoretical maximum defects area of 100 % of the total sample area is never reached. The time after which the tubulation is accomplished directly depends on the protein concentration. It is a result of the equilibrium shift between free and membrane bound fraction of the protein. This equilibrium is reached much faster at higher protein concentrations, thus the overall rate of the process increases (figure 9.7). Considering the K_D measured for FCHo2 BAR domain (11) which equals 2.4 μ M, one could expect that substantial changes of the tubulation process would appear while approaching this concentration. In our case the x_0 equals 1.5 μ g/ml (0.06 μ M) and significantly deviates from K_D value. While it is difficult to draw solid conclusions out of this result, we speculate that this shift towards lower concentrations might be a result of the addition attractive forces between the protein and the support used in our system. This would lead to higher apparent affinity of the protein to the SLB. The experiments described further in this chapter supports this hypothesis and will be broadly discussed later.

9. BAR protein binding to SLBs

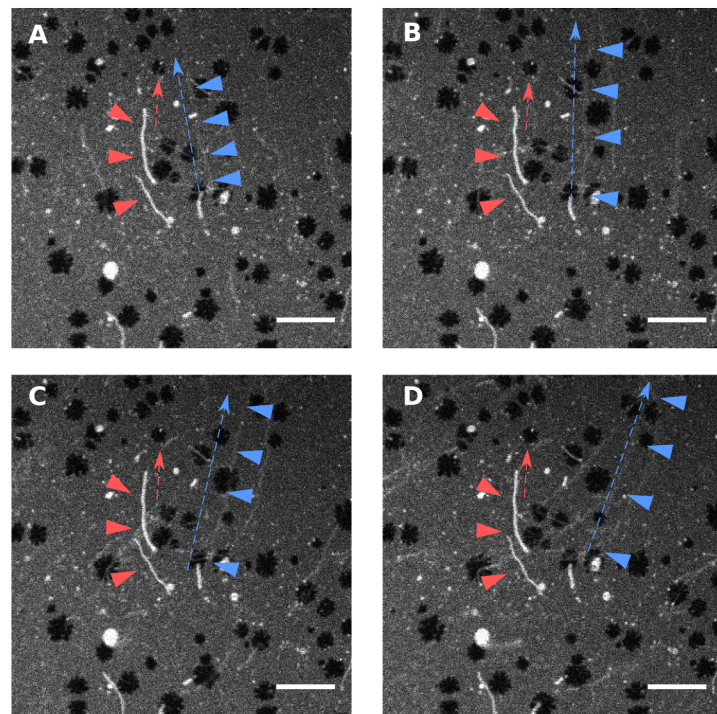


Figure. 9.3.: Different types of membrane tubes induced by BAR domain. Images are the part of the time-lapse imaging. While large bright tubes are 'crawling' over the surface (mark in red), thin long tubes are attached to the bilayer only by one (mark in blue). The direction of growth and the tube orientation are pointed out by dashed arrows. It can be seen that lipid tubes stuck to the SLB surface are growing relatively slowly and do not change their orientation. Since floating tubes are relatively thin and mobile they appear to be much darker. These tubes turn freely in clockwise direction. This synchronised movement of almost all tubes is probably the result of the thermal drift occurring in the sample.

9.4. Influence of negatively charged lipids on protein affinity

While previous experiments were carried out using one lipid mixture, it was interesting to investigate whether the composition of a lipid membrane can regulate the activity of BAR proteins. In order to study the specificity of the FCHo2 binding towards different lipid species we employed three additional types of phospholipids to our experimental system. We kept the zwitterionic nature of the headgroup of the main membrane component (95 mol%) by using DOPC. Since results published so far are based on the usage of Folch lipid extract, we decided to test the influence of its major component - phosphatidylserine (PS). This is a negatively charged lipid, with smaller head group when compared to PI(4,5)P₂ and has only one net charge per molecule. Besides PS, we tested another negatively charged lipid - phosphatidylglycerol (PG). The influence of negatively charged lipids on the tubulation induced by FCHo2 BAR domain is summarised in figure 9.8. Sample with PI(4,5)P₂ shows relatively small tubular structures with homogeneous distribution over whole surface (9.8 D and D'). In contrast, PG and PS samples exhibit rather heterogeneous lipid structures (9.8 B and C). In both cases lipid tubes are abundant and exhibit variety of shapes. It has to be noticed that besides relatively elongated lipid tubes, vesicular-like structures are present in these samples. Although the rate of the process does not differ significantly among these three cases, there is a visible difference in the morphology of formed lipid structures. While membranes containing PI(4,5)P₂ with three net

9.4. Influence of negatively charged lipids on protein affinity

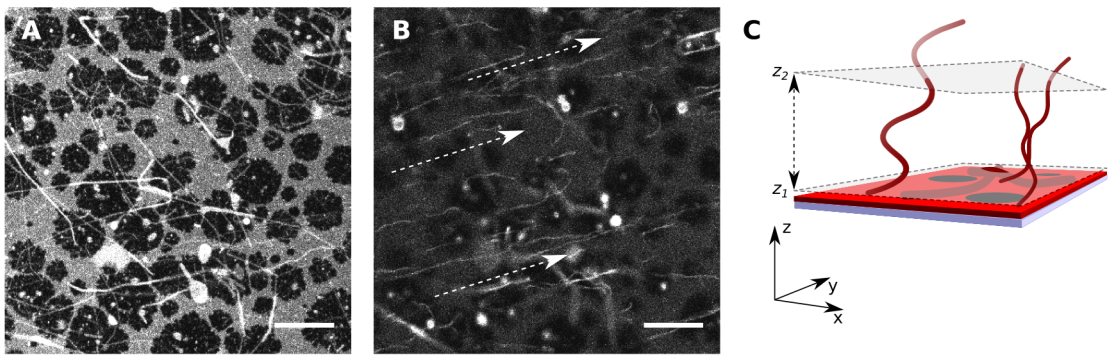


Figure. 9.4.: To better illustrate different kinds of tubes generated by the FCHo2 BAR domains we took images at different z positions. This is schematically shown in part C. Standard measurements is taken so that the focal plane is positioned at the level of the SLB (A, z_1). At this position shallow depth of field does not allow for imaging objects (e.i. lipid tubes) which are above the membrane. Therefore we acquired additional images at the level z_2 above the surface where mostly signal from lipid tubes is collected (B). In B thin stretched tubes are aligned in one directions (pointed by arrows). As mentioned earlier floating tubes turn clockwise with respect to the end by which they are attached to the SLB.

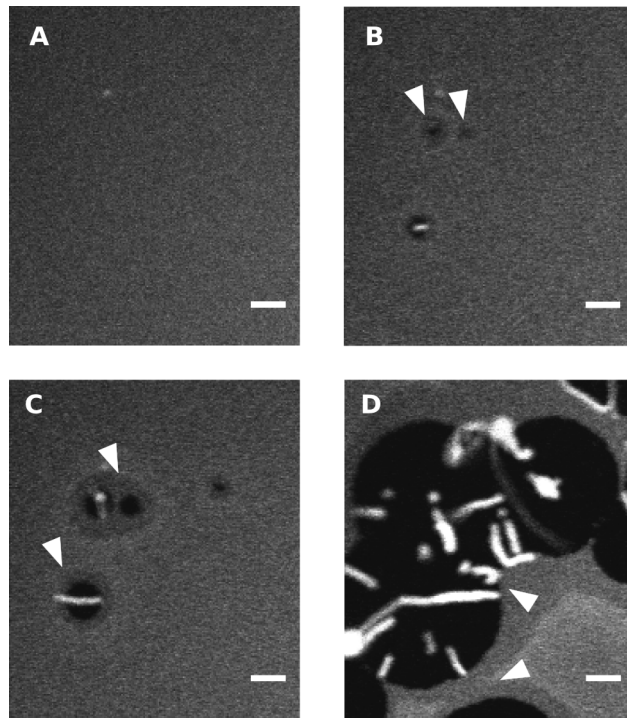


Figure. 9.5.: Rings of different brightness appeared on SLB. A) The lipid membrane composed of DOPC:DOPS (95:5) in absence of the protein (t_0). B) Generated defects in the lipid membrane upon the FCHo2 addition. Arrows point dark spots at the region of the membrane rupture (t_1). C) Two earlier generated defects merged together. Additionally, the growth of tubes can be seen (t_2). D) The late stage of the tubulatation process when the area of the bare mica surface become relatively big. One arrow points out the region where two defects were merged. The second arrow points out merging of dark rings (t_3).

9. BAR protein binding to SLBs

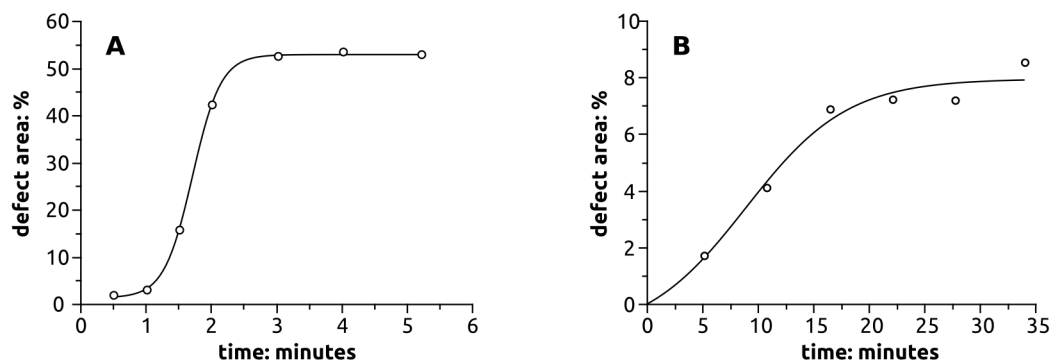


Figure 9.6.: The change of the SLB area in the presence of FCHo2 BAR domain in time. Vertical axis shows the increase of the total defect area over time upon the addition of the protein. A shows the experimental data for the final concentration of 5 $\mu\text{g}/\text{ml}$ of FCHo2. The final total defect area levels out at 50 % and the process is accomplished within 3 minutes after the addition of the BAR domain. B) the same experiment repeated at 0.63 $\mu\text{g}/\text{ml}$ of FCHo2 BAR domain. In contrast to previous case, the saturation level is reached after 25 minutes after the protein addition. Moreover, the total area of defects is much lower and equals 8 %.

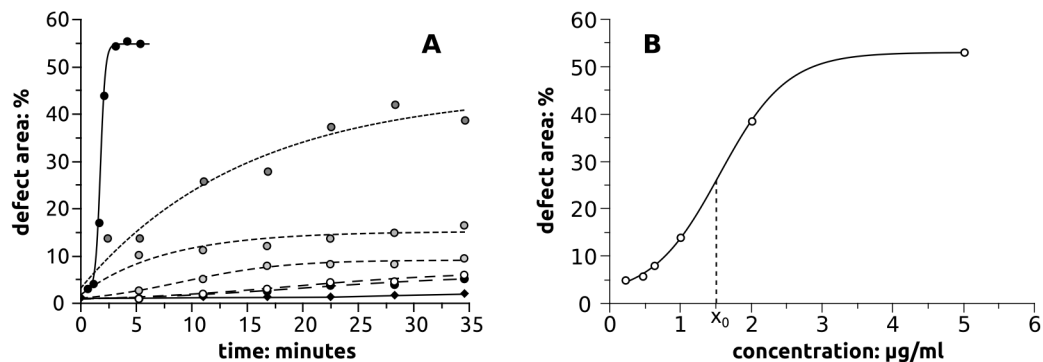


Figure 9.7.: Comparison of the tubulation rate at different final concentrations of protein. To the SLB composed of DOPC:PI(4,5)P₂ 95:5 (mol:mol) FCHo2 BAR domain was added to the final concentration of: 5, 2, 1, 0.63, 0.47 and 0.22 $\mu\text{g}/\text{ml}$. The data are shown in A where the brightness of points and the size of the dashed lines increase respectively. Diamonds represent the effect of BSA on he changes in monolayer morphology. The concentration was 0.6 $\mu\text{g}/\text{ml}$. B) Plot of the total defect area versus the protein concentration. The curve has a sigmoidal shape what implies cooperative nature of the tubulation process. The characteristic x_0 value points the concentration of the protein at which the the rate of the tubulation equals half of the maximal possible rate.

negative charges form very small regular structures, bilayers containing PG and PS (both with the one net negative charge per molecule) are transformed into big heterogeneous vesicle-like structures. Interestingly, we could not observe any difference between PG and PS, what might indicate that in this case the FCHo2 BAR domain is sensitive to the density of the charges at the surface rather than the specific shape of these particular lipids.

Subsequently we carried out the control experiment in which pure DOPC bilayers was studied. Taking into account the recently published work (49) we expected that the tubulation activity of the BAR domain would be suppressed in this case. Surprisingly, we observed the membrane deformation

also in this case. While formed structures were relatively heterogeneous, resembling that of PS and PG membranes, almost no tubular structures could be seen (figure 9.8 A). Typically, vesicles are induced with an eventual narrower equatorial area (figure 9.8 A'). These results support the hypothesis that the overall charge density is a very important factor in the membrane deformation induced by the FCHo2 BAR domain.

It also has to be noticed, that while the SLB system give a possibility to quantify the BAR domains activity, it also bares some disadvantages. We speculate that the tubulation of the pure DOPC membrane is mostly caused by the additional attractive forces generated by the support. This is reflected by the fact that the tubulation of the SLBs occurs on the mica, but not on glass surface.

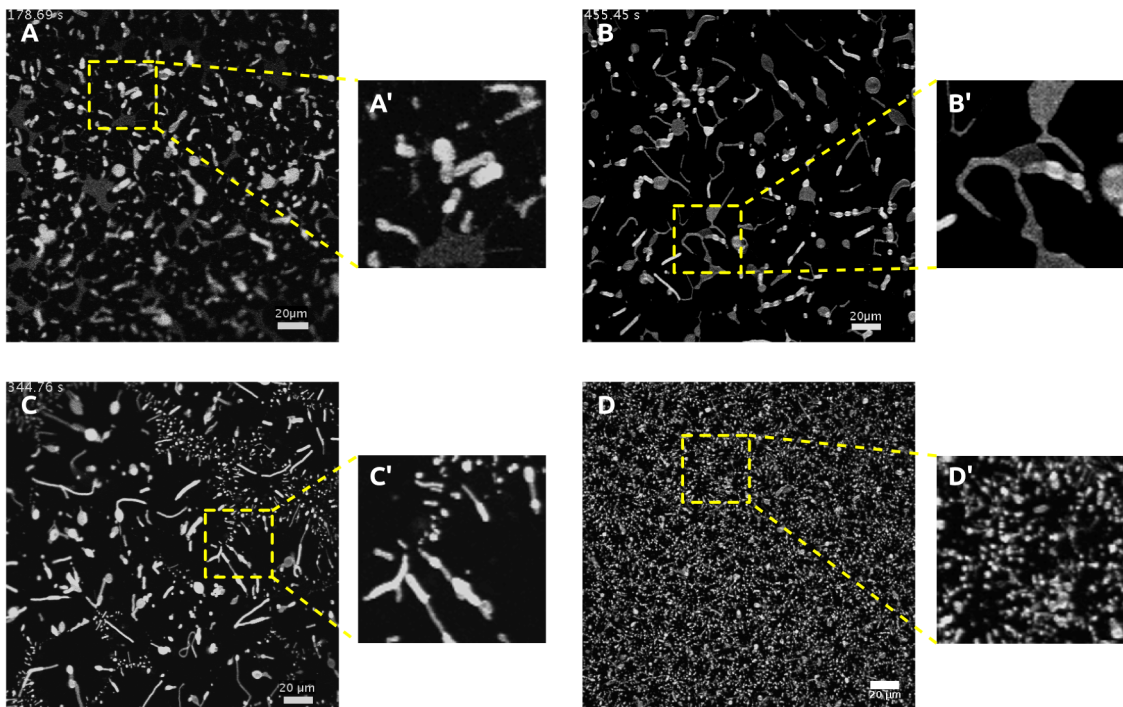


Figure. 9.8.: Patterns of lipid structures generated by the FCHo2 BAR domain. A) 100 mol % DOPC bilayer upon complete deformation. Typical structures are shown in A'. B) DOPC: DOPG 95:5 (mol:mol) SLB after the tubulation. C) structures generated by BAR domain from the DOPC:DOPS 95:5 (mol:mol) membrane. D) Pattern of lipid structures upon complete DOPC:PI(4,5)P2 95:5 (mol:mol) SLB tubulation.

9.5. Phase separation and membrane tubulation

Together with the development in biology which followed the concept of lipid rafts (25), it became obvious that the modulation of the fluidity of the native membrane might be one of the mechanisms by which many biochemical processes in the cell can be controlled. Therefore we tested how the phase coexistence in the lipid membrane can influence the tubulation activity of the BAR domain. First we prepared the lipid bilayer composed of DPPC:DOPC:cholesterol 2:2:1 (mol:mol:mol) mixture. Such a SLB exhibits phase separation at room temperature and only two types of lipid headgroups (phosphatidylcholine and cholesterol) are present in such a membrane. This approach excludes the

9. BAR protein binding to SLBs

possibility of specific interaction between lipids and allows to focus on the thermodynamic properties of the bilayer. Pictures of time-lapse imaging are shown in figure 9.9. The general increase of a size of lipid domains is the first change in the membrane morphology following the addition of the protein. This indicates that at this stage the protein binds to the membrane and induces changes in the surface tension. Shortly after, the first rupture of the bilayer takes place. The tubulation of the phase separated membrane is characterised by a low number of generated tubes. Additionally, the merging of liquid ordered domains can be observed. This effect has been never observed in a SLB system, since lipid domains are rather static structures which diffusion is arrested due to membrane interactions with a support. Thus, such dramatic changes in the SLB morphology indicate substantial remodelling of lipids.

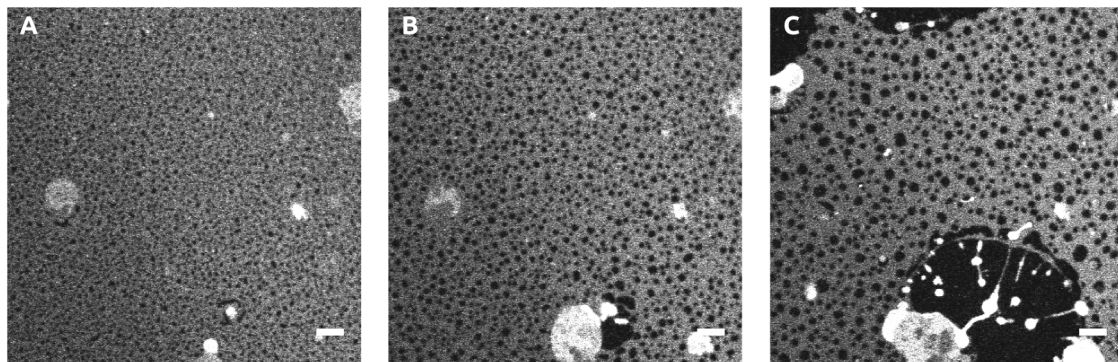


Figure. 9.9.: A deformation of phase separated SLB composed of DPPC:DOPC:chol 2:2:1 (mol:mol:mol) mixture. The membrane shows the phase separation in the absence of the protein (A). Shortly upon the protein addition, the domain size substantially increases (B) and the first rupture of the bilayers occurs. C) The advanced stage of the membrane tubulation where merge domains around the defect can be easily seen.

To get better insight into changes induced by the FCHo2 BAR domain on phase separated membranes we used AFM. This raster scanning technique gives an opportunity to collect structural information of the sample. Since the scanning of a conventional AFM system is relatively slow with respect to the tubulation process, it was necessary to arrest the membrane deformation. To achieve that, we prepared 5 M NaCl solution which was added to the sample after first defects of the membrane appeared (1 M NaCl final concentration). As expected, the process was completely arrested within several second upon NaCl addition. This agrees with experiments of Henne et al. (11) who showed that the binding of the FCHo2 BAR domain depends strongly on an ionic strength of the solution. The AFM image co-localised with fluorescent micrograph is presented in figure 9.10.

Figure 9.10 A shows the typical appearance of the defect generated in phase separated SLBs. While it is difficult distinguish between the bare mica and liquid ordered domains by applying confocal microscopy, one can conclude that the bright ring (pointed out by red arrows in figure 9.10) is the rim of the defect and the uneven dark region around is composed of fused L_o domains. This hypothesis is supported by AFM images which clearly show that the rim of the defect is composed of thinner, liquid disordered phase and it is surrounded by fused liquid ordered domains. From this we conclude that the phase, hence the mobility of the lipid environment is an important factor in the tubulation process. Our results indicate that the liquid disordered phase is prone to deformation, while liquid ordered phase is rather passive. This implies that phase heterogeneity of the cell membrane might be one way of the BAR protein regulations.

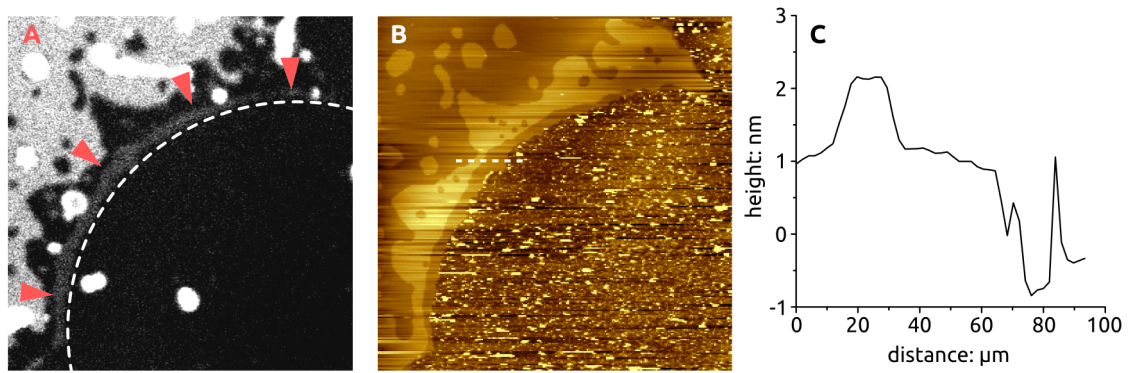


Figure. 9.10.: Co-localisation of the fluorescene and AFM images of the membrane defect. The SLB is composed of DPPC:DOPC:chol 2:2:1 (mol:mol:mol) and 0.1mol % of DiD. A) Fluorescence image of the defect. The edge of the membrane is marked by dashed line. B) Co-localised AFM image of A. Upper left part of the image shows the phase separated membrane with merged domains around the defect. The surface of the defect appears uneven due to transformed membrane and proteins. Red arrows point out the area of higher fluorescence signal at the rim of the defect (dashed line). C) The topographical profile along the line mark in B.

9.6. Discussion

While earlier work of Frost and co-workers (48) revealed the protein alignment at the SLBs surface by electron microscopy, here we present, to our knowledge, for the first time the evidence that BAR domains not only can bind to entirely flat membranes but they also can induce their deformation. This is especially interesting with respect to the dispute which takes place in the BAR domains field about functionality of BAR domains, e.i. whether the BAR protein can sense or induce the curvature of the membrane (13), (12), (70). Because of their shape and the ability to tubulate the membrane, BAR domains are intuitively seen as an example of the direct relation between the structure and the function. However, our results imply that the activity of BAR domains might be regulated by additional factors. We presented that when BAR domains deform the bilayer with a co-existence of two phases, the tubulation is restricted to liquid disordered region of the membrane. This indicates that the heterogeneity of the cell membrane can be used as an alternative way of controlling the specific activity of BAR domains. Although it was shown that BAR proteins have higher affinity towards smaller lipid vesicles, there is no evidence for any specific surface undulations in the cell. Thus, while hypothetically plausible it is still unclear how the cell could regulate the recruitment of BAR domains by inducing high local curvature of the bilayer. According to literature and our results, it is clear that BAR domains are able to generate lipid tubes. This process can occur on the membrane with any curvature and it is driven by the affinity of the protein to the membrane. This affinity is an result of ionic interactions between the FCHo2 domain and lipids where attractive forces are generated between the positively charged protein and negatively charged lipids. While our results show the general influence of the charge density on formed lipid structures, it has to be noticed that the quantitative analysis is influenced by the surface charge of the support.

10. BAR domain binding to monolayers

10.1. Introduction

Since in the SLB system membrane properties are substantially altered by the support, we decided to use another approach. The prerequisite of a new system was the possibility of implementation a confocal microscopy to be able to acquire spatial data of the sample. Therefore we were looking for a model system which provides entirely flat and a relatively big interface. Another important feature of the new approach was the absence of any kind of supports which can interfere with obtain results. All these features can be found in the monolayer system. There is no support, the interface is entirely flat and the area of the model membrane can reach tens of centimetres squared. Additionally, a monolayer gives an opportunity to control mean molecular area of lipids at the interface. This is especially helpful, since it allows us to study the influence of the surface pressure on the BAR domain binding.

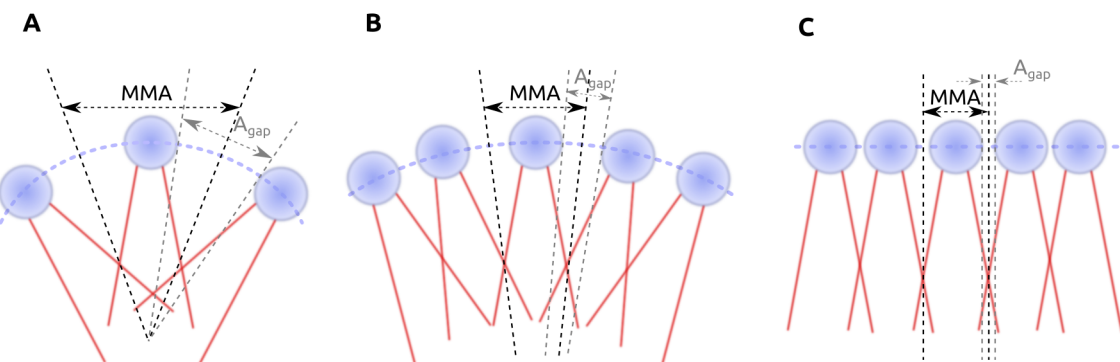


Figure. 10.1.: Orientations of lipids in the outer leaflet at different curvatures of the bilayer. A) The high curvatures (which occurs in small vesicles) molecules are splayed far from each other what gives rise to a relatively high area of gaps between lipids headgroups A_{gap} and results in relatively big mean molecular area (MMA) of lipids. Once the diameter of the vesicle increases (B), the bend of the membrane gets smaller and the lipid headgroups become aligned more closely which decreases the average area of the gaps. In GUVs (where the membrane is almost flat) or in SLBs with entirely flat bilayer the splay between the lipids is minimal thus the gap between headgroups is relatively small.

While the role of negatively charged lipids in the regulation of the activity of FCHo2 BAR domains was our goal in the previous part of this project, the recent work of Dimitrios Stamou group (71), (72), (73) and our intriguing results of the experiment with phase separated SLBs provoked us to focus on the curvature aspect of the FCHo2 activity. Group of Stamou designed a new assay in which the size of the vesicles can be measured (74) by confocal microscope. Additionally, it is possible to measure the amount of the protein bound to vesicles of known size. With this approach it was shown that BAR domains have higher affinity towards smaller vesicles, hence higher membrane curvature. Moreover, when the surface of vesicles was saturated with detergent-like molecules, proteins lost

their selectivity and bound independently of the vesicles size. It is worth noticing that the saturation of the vesicles surface with detergent did not change significantly the size of vesicles. This gave rise to the conclusion that BAR domains do not sense curvature *per se* but rather respond to another factor correlated with membrane bending. It was proposed that the reason for a higher affinity of BAR proteins to smaller vesicles is driven by defects in the lipid alignment in the bilayer. The size of such hydrophobic gaps in the membrane is proportional to the curvature of the bilayer and hence the protein binds to vesicles with smaller diameter (71), (72) (figure 10.1). In this context it became very interesting for us to investigate this hypothesis using monolayers. Since it is possible to change the density of lipid molecules at the air-water interface, monolayers give opportunity to directly measure how the FCHo2 binds to lipid monolayers at different mean molecular area (MMA) (figures 10.2, 10.3).

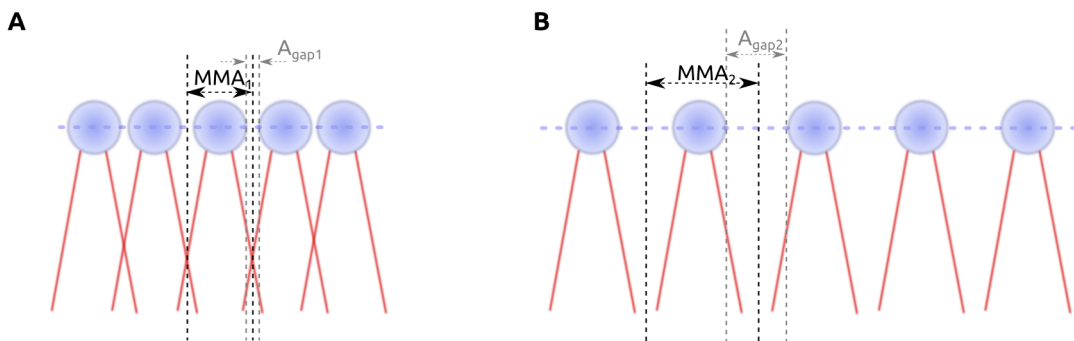


Figure. 10.2.: Changes of the MMA at two different compression states of the monolayer. A) The sketch shows the alignment of lipids in the monolayers at the relatively high compression. Molecules are very close to each other (high surface density) so the average area occupied by a single molecule is small (MMA_1). When the monolayer is decompressed (B), the same amount of lipids is evenly distributed over the larger area hence the average area per lipid molecule increases ($MMA_2 > MMA_1$). While the composition of a monolayer does not change (lipid molecules are characterised by the same core area), the only parameter which changes is the excess of MMA - A_{gap1} .

During our studies on monolayers we found out that the variation in mean molecular area is related to a change of the mobility of lipid molecules in the monolayers. In fact, the recent work of Gudmand et al. (77) provides an evidence of the dependence between lipid mobility and MMA. Molecules of the decompressed monolayer exhibit relatively high mobility. Once, the monolayer is compressed lipids experience less freedom due to increased surface density what results in their slower diffusion. This means that while in the vesicle the curvature is the main factor determining the size of the hydrophobic gaps, in flat membranes similar effect can be achieved by variation in lipid mobility.

In the following sections we describe the measurement of the lipid diffusion in our system as well as the approach which we used in order to monitor the binding of the protein to the lipid monolayer together with results of these experiments.

10.2. Mobility of lipids in monolayers

In order to measure the binding of the FCHo2 to the monolayer we chose PC as the only component of the system. Phosphocholine does not have any net charge per molecule. This is important, since

10. BAR domain binding to monolayers

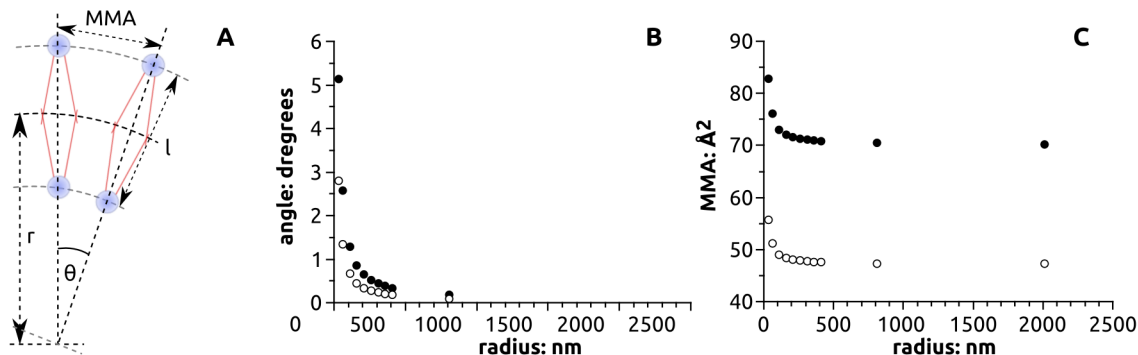


Figure. 10.3.: Calculations of the geometric properties of the vesicles made of DOPC and DMPC. A) Shows schematically lipids in the membrane (of a thickness l) of a vesicle with a radius r . θ is the angle between two adjacent lipids in the outer leaflet. B) Plot of the θ versus radius of the vesicle for DOPC (black circles) and DMPC (open circles). Taking in to account the recent work (75), (76) we assumed that values for the hypothetical vesicles core value 70 Å and 47 Å for DOPC and DMPC respectively. The change of the angle reflects lipid alignment. The bigger the angle the farther away are the headgroups of lipids. This results in the larger mean area of the molecule (C) which can be directly measured in monolayer system.

we aim at the investigation of the hydrophobic gaps between the lipids and any additional factor (like headgroup charges) would alter the protein behaviour. Since mono-molecular layers of lipids composed of one species can separate into liquid expanded (LE) and liquid condensed (LC) phases (figure 10.4), we decided to use DMPC which does not exhibit phase separation at room temperature (77). To validate DMPC monolayers we carried out a standard compression experiment in which the surface pressure was recorded. The phase separation in monolayers is manifested by a plateau region in compression isotherm. As expected, DMPC monolayers in contrast to DPPC, do not show any coexistence region in isotherm curve (figure 10.4A and B). Additionally,to test the morphology of the monolayers we collected the fluorescence images at arbitrary MMA using 543 Cholesteryl dye. While in case of DPPC there is a clear phase separation visible at lower surface pressures, DMPC appears homogeneous over whole tested MMA range (figure 10.4 B'.)

Subsequently, we carried out FCS measurements on DMPC monolayers at different MMA values (10.5). We could observe that the characteristic diffusion time of a dye decreases proportionally to the MMA. This result is in agreement with theoretical by (78) and it was shown experimentally (77) that for monolayers far from phase transitions the diffusion coefficient scales linearly with the MMA of lipids. This relation for DMPC measured in our system is shown in figure 10.5B. According to the free area model (FAM) data-points of such a plot should fall on a strait line (79). The intersection of this line with the horizontal axis is the so-called critical point (a_c) — the theoretical MMA value at which the molecules in the lipid monolayer turn from a diffusive into the non-diffusive state ($D = 0$). In our case $a_c = 42 \pm 10 \text{ \AA}^2$ and agrees very well with the literature value obtained for the same lipid mixture (77). Since in our micro-chamber the area of the monolayer is more than ten times smaller than in any conventional Langmuir trough, we carried out a control experiment in order to exclude any potential influence of the trough size on the experimental results. To do this we repeated the previous experiment using a specially modified Langmuir trough with an area of the monolayer set to 85 cm². The control experiment showed no significant difference ($a_c = 43 \pm 5 \text{ \AA}^2$) between results obtained by using systems of various monolayer dimensions. This shows that physical properties of the monolayer

in our case do not depend on trough dimensions and that monolayers formed in our system exhibit the same features as these formed in conventional troughs.

In a next step, we carried out the control experiment in which we tested the influence of the buffer solution on lipids mobility in the monolayer. This aspect is especially important in studies involving proteins, in which variety of buffers is used. As a subphase we tested the commonly used 10 mM HEPES buffer, 150 mM NaCl, pH 7.4. As previously, we observed that D scales linearly with MMA and the slopes in both experiments are nearly identical ($1.32 \pm 0.15 \cdot 10^8$ and $1.37 \pm 0.12 \cdot 10^8 \text{ s}^{-1}$, respectively for buffer and pure water subphase) showing that the influence of the buffer on the diffusion of the molecules in lipid monolayer is relatively small. This finally validated our system for the measurement of the protein binding.

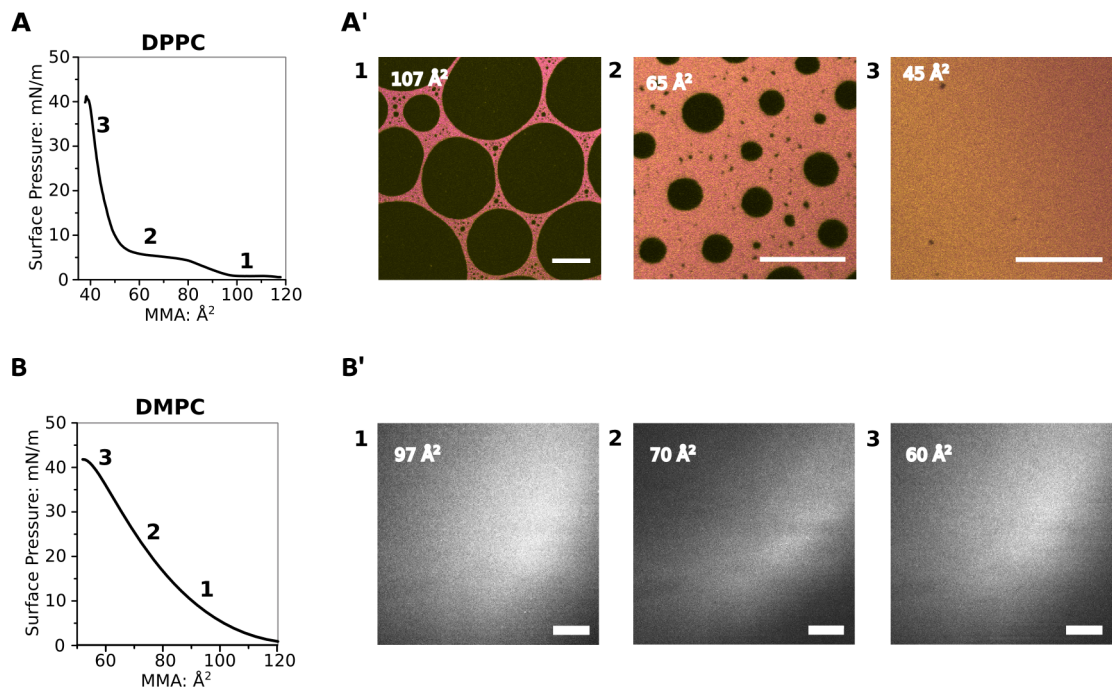


Figure. 10.4.: Isotherms and fluorescence images of DPPC (A) and DMPC (B) monolayers. In both case 543 Cholestryly dyes was used. According to recently published work, these dye will partition mostly to more fluid, LE phase (80), (81). Graphs A and be show typical compression isotherm of DPPC monolayer. It exhibits plateau (2) which implies the coexistence of two liquid phases at this range of MMA. In fact, the fluorescence images taken at that MMA value shows dark domains of LC phase (B', 2). In contrast, compression isotherm of DMPC monolayer (B) do not show any plateau which could indicate phase coexistence. This result was confirmed by fluorescence imaging and finally validated DMPC monolayers for the binding assay of FCHo2 BAR domain.

10.3. FCHo2 binding assay

In order to measure the FCHo2 binding to the monolayer, we decided to use the FCS method in which the amount of the protein in the subphase and at the interface is estimated by the fitting procedure. First

10. BAR domain binding to monolayers

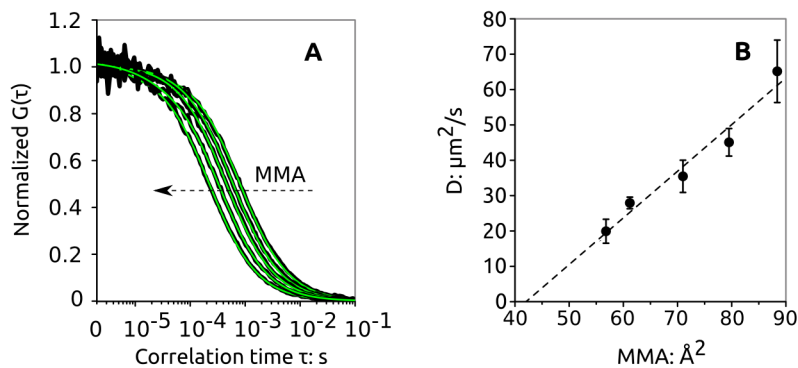


Figure. 10.5.: Autocorrelation curves of the fluorescent dye measured on the DMPC monolayer (A). The drop of the characteristic diffusion times is a result of increasing lipid density at the surface (indicated as MMA). Using equation 8.3 we were able to calculate the corresponding diffusion coefficients which are plotted in B. Obtained data points were fitted with the linear (dashed line). The extrapolation of the fit to $D = 0 \mu\text{m}^2/\text{s}$ give a critical point a_c

step in this approach is to measure the mobility of particles in the subphase (figure 10.6B). In this case three dimensional one component model is used and it allows for the estimation of average number of molecules in the focal volume. Then the experiment is repeated at the monolayers, so the laser beam is focused exactly at the interface (figure 10.6A). In this case two component model is used in which one describes three dimensional movement of the protein in the solution while another one is the approximation of the two dimensional diffusion in the plane of the monolayer. Since in such a model the number of free parameters substantially increases, these referring to three dimensional diffusion are fix with the value obtained from the measurements carried out in the subphase. Such a protocol increases accuracy of the analysis. Unfortunately, while the quality of the data obtained from the FCS measurements of FCHo2 BAR domains in the solution was good, results of experiments carried out at the interface did not allow for proper analysis. This was mostly due to strong aggregation of the protein upon binding to the interface. Since intensity of the fluorescent species in the FCS is one of the most important parameter which is assumed to be constant, any aggregations of molecules which give rise to fluorescence fluctuations will strongly disturbed the signal correlation.

In such a situation we had to use another approach. We decided to use FCS data, but instead of correlating recorded fluorescence signal we used a countrate to estimate the relative amount of the protein bound to the monolayer and freely diffusing in the solution. To accurately estimate the amount of the protein in the subphase and at the monolayer we had to consider the nature of fluorescence signal collected by FCS. When measured in the solution, fluorescence signal comes entirely from the protein diffusion in the subphase. On the other hand, signal recorded at the water-air interface has more complex origin. We assumed the the fluorescence collected at the interface has apparent intensity C_{app} . In an ideal case, the focal spot is positioned in such a way that the effective volume is 'divided' by a monolayer into two equal parts (figure 10.6). One half of the focal spot is above whereas the second half is below the interface. Since the signal is collected not only from the monolayer but from the whole effective volume, the C_{app} is the sum of the fluorescence intensity of a monolayer itself C_{inter} plus the signal coming from lower part of the focal volume. Giving C_{sub} as a intensity of the solution which is equal at any point in the subphase we can conclude that the contribution of the signal from the subphase to the C_{app} equals $C_{sub}/2$ and thus $C_{app} = C_{inter} + C_{sub}/2$.

The results of the experimental data are shown in the figure 10.7. We expressed the binding in

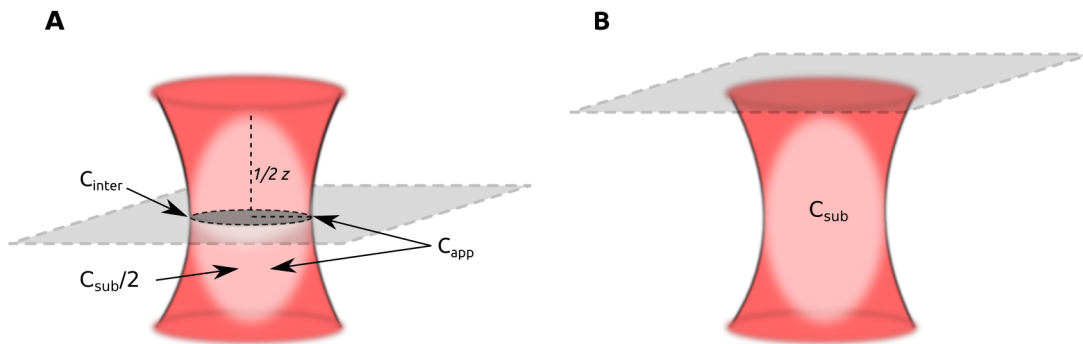


Figure. 10.6.: Schematic representation of the positioning of the effective focal volume at the monolayer (grey). A) When the focal spot is positioned at the interface, the monolayer is oriented in such a way that the half of effective volume is above the water surface and second half is in submersed in the subphase. The signal collected in this position is a sum of monolayer intensity C_{inter} and the signal coming from the lower part of the focal volume $C_{\text{sub}}/2$. B) When the laser beam is focused in the solution below the interface, the entire signal comes from the solution of the protein.

therms of $C_{\text{inter}}/C_{\text{sub}}$. The BAR domain bind relatively weakly at the MMA similar to that one estimated for native bilayers (76). Once the MMA increases, the binding increase substantially showing an exponential behaviour (figure 10.7). At very low lipid densities the measurement error significantly increases what is mostly due to the aggregation of the protein at the monolayer. Interestingly, when protein was added to the subphase in the absence of lipids, the strong localisation of the FCHo2 at the interface could be observed. This implies very high surface activity of the protein. To exclude any artifacts connected with used setup we additionally carried out the control experiment, where a labelled streptavidin was added to the subphase. This protein was used as a control protein in mentioned published experiments (72). It was shown that streptavidin is not sensitive to the membrane curvature and does not bind preferentially to smaller vesicles. Our experiment in the absence of lipids confirmed that in fact, streptavidin is not surface active and does not bind to the water-air interface.

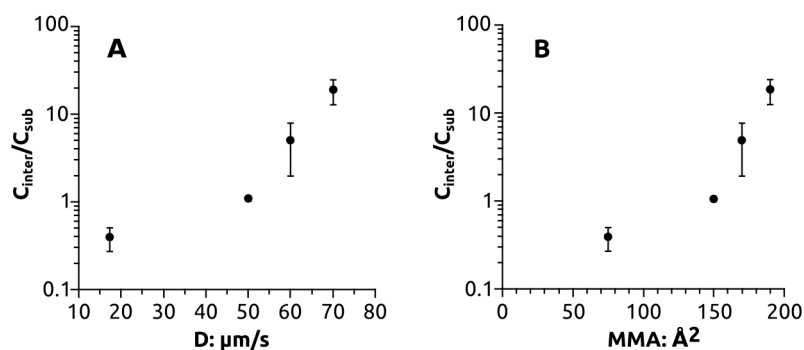


Figure. 10.7.: Binding of FCHo2 BAR domain to DMPC monolayer. Protein at final concentration of 100 nM was added to the subphase at different MMA/lipid mobility. A) plot of the $C_{\text{inter}}/C_{\text{sub}}$ versus diffusion of lipids. B) The same data plot versus MMA.

Interestingly, when data were plotted versus diffusion coefficient of lipids instead of MMA, the characteristic shape was conserved. This shows, that while the MMA was considered so far in therms

10. BAR domain binding to monolayers

of the membrane curvature, it also can be analysed from the point of view of the lipid diffusion.

10.4. Discussion

Presented results indicate that the current view on the regulation of the BAR proteins activity is too simplified. The functionality of BAR domains seems to be rather emerged from many properties of both: the protein and its binding partner - lipid bilayer. While the membrane curvature might be one of the ways by which the BAR proteins are recruited to the specific bilayer area, this hypothesis still needs to be proofed. On the other hand, our results imply that the BAR domain of FCHo2 is a surface active unit which is sensitive to increased hydrophobicity of the surface. This hydrophobicity might be a result of a higher membrane curvature but also it might be connected to the fluidity of the bilayers. This finding is especially interesting in context of the lipid raft model, in which the bilayer heterogeneity is postulated as the one of methods of the organisation of the biochemical pathways. It was already shown that the coexistence of different phases in the cell membrane might be used to segregate proteins and lipids (82), (83), (84). This implies that the modulation of the membrane fluidity by cells can be a tool in specific recruitment of BAR domains to the sites of interest.

11. Quaternary structure of BAR ensemble investigated by high-speed AFM

To gain the knowledge about the structural organisation of BAR domains during the tubulation process, we collaborated with the group of prof. Toshio Ando (Knazawa University, Japan). We used high-speed AFM (hsAFM), which allows to monitor processes taking place on surfaces with very high spatio-temporal resolution (85), (86), (87). Therefore, hsAFM was the technique of choice by which we could follow the membrane deformation induced by BAR domains. hsAFM measurement was carried out in the SLB system under the same conditions used in the tubulation assay discussed above. We did not observed lipid tubes in any of the carried out experiments. This might be due to the design of the hsAFM itself. In this particular model, the cantilever is static and the sample is attached to the piezo scanner. While the scan rate is very high in such a microscope, it might be that the tubes were torn of the membrane due to shearing forces.

Fortunately, high spatial resolution of the AFM allowed to observe BAR domains assembling on the membrane surface (DOPC:PI(4,5)P2 95:5 mol:mol). FCHo2 BAR domains bound to the SLB are shown in figure 11.1A. Seen high density packing of domains usually was followed by membrane rupture. In this particular image many different orientations of BAR domains are visible. While in images 1, 2 and 3 domains adhere to each other side by side, in pictures 4 an 5 the protein is organised more loosely. Similar orientation of another F-BAR domain (FBP17) was observed by Frost et al. (48) using electron microscopy. While that studies shows the *post factum* situation, we demonstrate the first steps of the protein coat assembling. Interestingly, reported earlier generation of lipid tubes with different diameter (11) might be a result of a different orientation of domains (46). While close packing of the protein might lead to smaller tubes, loose interactions between BAR domains can give rise of relatively big tubes.

11. Quaternary structure of BAR ensemble investigated by high-speed AFM

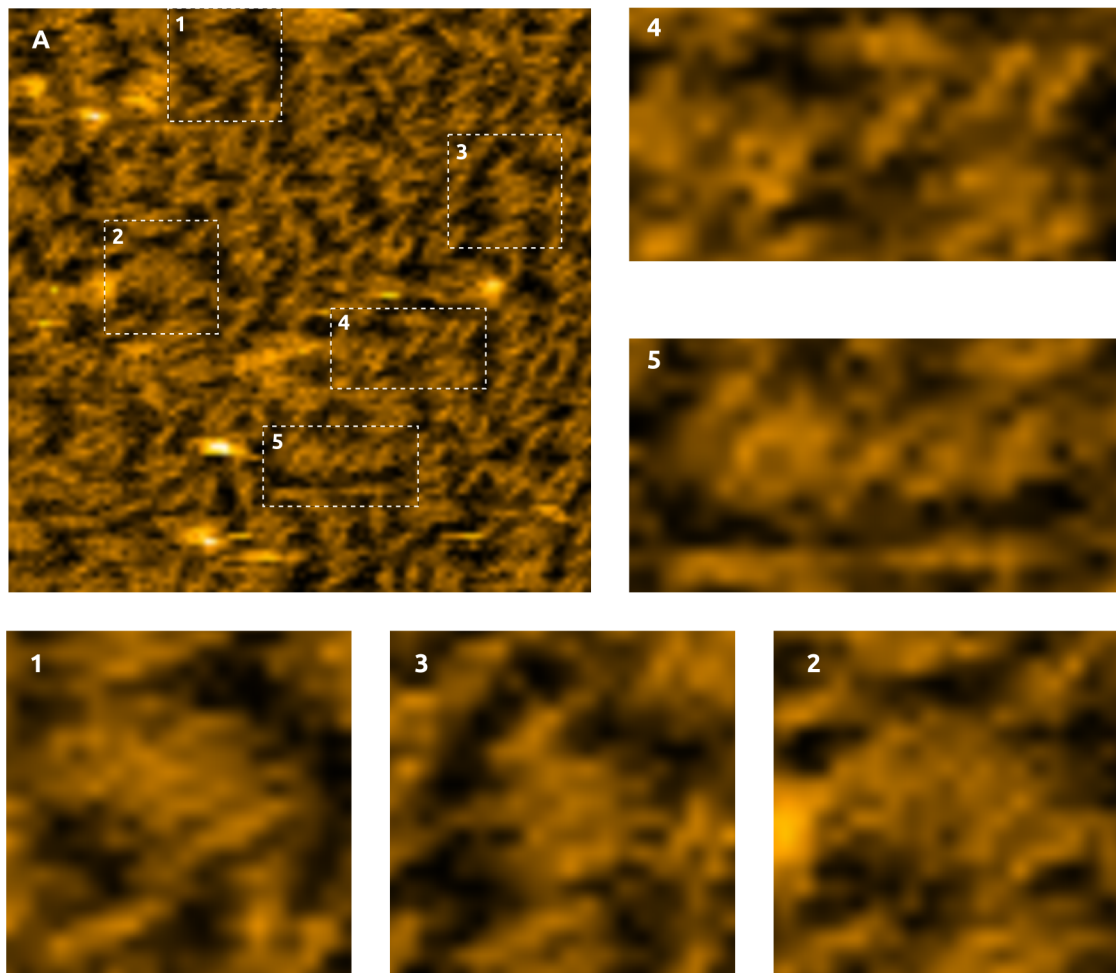


Figure. 11.1.: High resolution image of FCHo2 BAR domains assembled on SLB. A) Image showing broad distribution of domains interactions. Among randomly oriented proteins two most pronounced orientation can be seen. Tightly stacked domains (pictures 1, 2 and 3) are oriented with their concave (positively charged) site towards the membrane. In this conformation domains interact with themselves with sides. The second orientation (pictures 4 and 5) is rather loose and proteins are twisted with respect to its longitudinal axis.

Conclusions and outlook

Since their discovery, BAR proteins became one of the most intriguing group of proteins. Their presents in many biochemical processes and the characteristic membrane tubulation activity rise questions about the molecular basis of specific binding and the exact function of this group of proteins. We demonstrated *in vitro* systems which can be used as a tools to address such questions. We presented the quantitative assay of the tubulation activity. We demonstrated that the BAR domain of FCHo2 can bind to flat interfaces. Moreover, this BAR domain can tubulate these flat membranes in a concentration dependent manner. Using supported lipid bilayers we showed that the FCHo2 is sensitive to charge density at the membrane. We observed that the tubulation of the phase separated membrane induced by BAR domains leads to dramatic lipid reorganisation and that the membrane deformation is restricted to liquid disordered phase. We also demonstrated that the tubulation leads to the fusion of liquid ordered domains.

We established the monolayer system in which the diffusion of lipids at the interface can be monitored. The new approach allows to study lipid-protein interactions by fluorescence techniques without unnecessary loss of the protein. Using this system, we confirmed previously published results which indicate that the BAR domains are surface active and that their binging depends on the relative area of hydrophobic gaps in between lipid headgroups. Additionally, we carried out FCS measurements and by this we correlated MMA with a diffusion of the lipids. We demonstrated that the FCHo2 has higher affinity to the interface with a less packed lipids and also that the higher binding is directly connected with the mobility of the lipids in the monolayer.

In collaboration, we used hsAFM to gain the insight into structural changes taking place during the tube formation. Although, we could not observer the formation of tubular structures, we were able to recorded assembling of the FCHo2 BAR domains at the membrane. We observed that the protein exhibits more than one stable assemble pattern.

Although, we demonstrated three different approaches to facilitate studies on BAR domains, many questions about molecular basis of the tubular activity remain unknown. At the moment there is still not sufficient understanding of the mechanistic nature of the membrane tubulation. Moreover, we cannot explain how structural differences between BAR domains influence their functionality. This is mostly a result of lack good *in vitro* methods where single elements of biochemical pathways can be investigated. Therefore, we believe that established methods will help in future in studies on BAR proteins what will lead to better understanding of the role of these proteins in cell biology.

Acknowledgements

Here, I would like to thank all the people who made it possible to accomplish this thesis:

At most, I would like to thank Petra. She gave me an opportunity to work in an exciting scientific environment and providing the magic laboratory full of any kind of equipment.

I would not be able to finish this work without help of Salvo. You were great tutor at the beginning of my work in Petra's group, but first of all you were great friend.

Special thanks go to Fabian with whom I spent countless hours trying to fix AFM and our beloved scanning FCS setup. Fabian you were always there to answer all my questions and to patiently listen to all my crazy ideas — thanks!

I would like to thank Eugene and Zdenek who always had time to explain me details of FCS and FIDA analysis.

This work would not be possible without wonderful technical support. Karin, thank you for all your efforts to make my laboratory life easier. Working with you was always a great pleasure. I would like to thank Anke, Sabine and Sahara - you were always there ready to help me.

I would like to thank Harvey McMahon from Cambridge University for providing all necessary plasmids of FCHo2.

I would like to thank also prof. Toshio Ando and Takayuki Uchihashi from Kanazawa University for the collaboration on hsAFM.

I was introduced to wet-lab protocols of monolayers by fantastic people for the group of prof. Patrycja Dynarowicz-Latka from Jagiellonian University.

Special thanks go to Fabian, Olek and Jens for proofreading parts of this thesis.

Over this four years of work I spend a lot of time in the office. Here, I would like to thank all the people I have been sharing this wonderful 326 room on the 3rd floor of Biotec: Ana, Jonas, Salvo, Robert, Viktoria, Fabian, Hare, Franzi, Sonal and Hetvi. Thanks all of you guys. There was always time for fruitful discussions, jokes and chatting. I will never forget these countless cups of coffee, packages of potato chips and amazing cakes baked by Franzi.

I would like to thank my closest friends: Senthil, Hetvi, Viktoria, Alex, Jens, Carina and Remi. I was always enjoying your company irrespectively whether it was on the trail in Sachsische Schweiz or in dark and cold rooms of our laboratory.

I would like to thank all the people who always were there ready to relax at the kicker table and all the members of our joint kicker league: Senthil, Jens, Jörg, Erdinc, Christoph H., Thomas, Christian, Mohamed, Fabian, Sven, Paul, Janine, Franziska, Ilaria and Christoph F.

11. Quaternary structure of BAR ensemble investigated by high-speed AFM

This group would not be the same without our Brightness and Contrast band of which I was a proud member. It was always fun playing with you guys: Remi, Erdinc, Le Mu and Robert.

I would like also to thanks all the photographers in our group who always were ready to go out to take some shots: Senthil, Jens, Remi.

I would like to thank Jörg who was always great companion for easy jogs in Ostragehegen and for tough 100km duathlons around Dresden.

Kristina, thank you for introducing me to the subtle world of tango. Thank you for your patience in teaching me and for all your passion of dance. I would like to thank at this occasion all my dancing partners with whom I enjoyed so much the last year of my stay in Dresden: Janine, Sonal (and for 'all this Jazz about salsa'), Louise and Hetvi.

I wound not be able to accomplish my PhD without help and support of my family. Thank you for being all this time with me.

At the end I would like to thank Bela - for being my ultimate motivation for this time.

Abbreviations

ADP	adenosine 5‘-(trihydrogen diphosphate)
AFM	atomic force microscopy
APPL1	DCC-interacting protein 13-alpha
BAR	BIN/Amphyphisin/Rvs homology domain
BIN	box-dependent myc-interacting protein-1
BSA	bovine serum albumin
CIP4	Cdc42-interacting protein 4
Cys	cysteine
DiD	1,1‘-Dioctadecyl-3,3,3‘,3‘-Tetramethylindodicarbocyanine, 4-Chlorobenzene
DiI	1,1‘-Dilinoleyl-3,3,3‘,3‘-Tetramethylindocarbocyanine Perchlorate
DMPC	1,2-dimyristoyl-sn-glycero-3-phosphocholine
DOPC	1,2-dioleoyl-sn-glycero-3-phosphocholine
DOPG	1,2-dielaidoyl-sn-glycero-3-phosphoglycerol)
DOPS	1,2-1,2-dioleoyl-sn-glycero-3-phospho-L-serine
DPPC	1,2-dipalmitoyl-sn-glycero-3-phosphocholine
EEA1	early endosome adaptor protein 1
DTT	dithiothreitol
ENTH	epsin N-terminal homology domain
FAM	free area model
FAT	freezing after thawing
F-BAR	Fer/CIP4 BAR domain
FBP17	formin binding domain 17
FCHo2	Fer/CIP4 Homology domain only protein
FCS	fluorescence correlation spectroscopy
FYVE	Fab1/YOTB/Vac1/EEA1 homology domain
GST	glutathione S-transferase
GTT	glutathione
GUI	graphic user interface
GUVs	giant unilamellar vesicles
HEPES	4-(2-hydroxyethyl)-1-piperazineethanesulfonic acid
hsAFM	high-speed atomic force microscopy
I-BAR	IMD/BAR homology domain
IMD	IRSp53/MIM homology domain
IPTG	isopropyl-β-D-thiogalactopyranosid
IRSp53	insulin receptor tyrosine kinase substrate p53
ITO	indium tin oxide
LC	liquid condensed
LE	liquid expanded
LSM	laser scanning microscope

11. Quaternary structure of BAR ensemble investigated by high-speed AFM

LUVs	large unilamellar vesicles
NA	numerical aperture
N-BAR	BAR domain with adjacent amphipatic α -helix
NLS	nuclear localisation sequence
N-WASP	neuronal Wiskott Aldrich Syndrome protein
MBD	membrane binding domain
MLVs	multilamellar vesicles
MMA	mean molecular area
PBS	phosphate-buffer solution
PDZ	PSD95/Dlg1/o-1 homology domain
PG	phosphoglycerol
PH	pleckstrin homology domain
PI	phosphoinositol
PI(4,5)P ₂	1,2-dioleoyl-sn-glycero-3-phospho-(1'-myo-inositol-4',5'-bisphosphate)
PIP _s	phosphoinositol phosphates
PKC	phosphokinase C
PMT	photomultiplier tube
PS	phosphoserine
PTFE	polytetrafluoroethylene
Rvs	Reduced viability on starvation protein
SDS-PAGE	Sodium dodecyl sulfate polyacrylamide gel electrophoresis
SH3	Src homology domain 3
SLB	supported lipid bilayers
SUVs	small unilamellar vesicles
SNX9	Sorting nexin-9
TCEP	tris(2-carboxyethyl)phosphine
TIRF	total internal reflection fluorescence

Bibliography

1. Doherty GJ, McMahon HT (2009) Mechanisms of endocytosis. *Annu Rev Biochem* 78:857–902.
2. Henne WM, Boucrot E, Meinecke M, Evergren E, Vallis Y, Mittal R, McMahon HT (2010) Fcho proteins are nucleators of clathrin-mediated endocytosis. *Science* 328:1281–4.
3. Schmid EM, McMahon HT (2007) Integrating molecular and network biology to decode endocytosis. *Nature* 448:883–8.
4. Ford MG, et al. (2001) Simultaneous binding of ptdins(4,5)p2 and clathrin by ap180 in the nucleation of clathrin lattices on membranes. *Science* 291:1051–5.
5. Ford MGJ, Mills IG, Peter BJ, Vallis Y, Praefcke GJK, Evans PR, McMahon HT (2002) Curvature of clathrin-coated pits driven by epsin. *Nature* 419:361–6.
6. Taylor MJ, Perrais D, Merrifield CJ (2011) A high precision survey of the molecular dynamics of mammalian clathrin-mediated endocytosis. *PLoS Biol* 9:e1000604.
7. Gallop JL, Jao CC, Kent HM, Butler PJG, Evans PR, Langen R, McMahon HT (2006) Mechanism of endophilin n-bar domain-mediated membrane curvature. *EMBO J* 25:2898–910.
8. Reider A, Barker SL, Mishra SK, Im YJ, Maldonado-Báez L, Hurley JH, Traub LM, Wendland B (2009) Syp1 is a conserved endocytic adaptor that contains domains involved in cargo selection and membrane tubulation. *EMBO J* 28:3103–16.
9. Milosevic I, et al. (2011) Recruitment of endophilin to clathrin-coated pit necks is required for efficient vesicle uncoating after fission. *Neuron* 72:587–601.
10. Mattila PK, Pykäläinen A, Saarikangas J, Paavilainen VO, Vihinen H, Jokitalo E, Lappalainen P (2007) Missing-in-metastasis and irsp53 deform pi(4,5)p2-rich membranes by an inverse bar domain-like mechanism. *J Cell Biol* 176:953–64.
11. Henne WM, et al. (2007) Structure and analysis of fcho2 f-bar domain: a dimerizing and membrane recruitment module that effects membrane curvature. *Structure* 15:839–52.
12. Peter BJ, Kent HM, Mills IG, Vallis Y, Butler PJG, Evans PR, McMahon HT (2004) Bar domains as sensors of membrane curvature: the amphiphysin bar structure. *Science* 303:495–9.
13. Shimada A, et al. (2007) Curved efc/f-bar-domain dimers are joined end to end into a filament for membrane invagination in endocytosis. *Cell* 129:761–72.
14. Weissenhorn W (2005) Crystal structure of the endophilin-a1 bar domain. *J Mol Biol* 351:653–61.
15. Arkhipov A, Yin Y, Schulten K (2008) Four-scale description of membrane sculpting by bar domains. *Biophys J* 95:2806–21.
16. Yin Y, Arkhipov A, Schulten K (2009) Simulations of membrane tubulation by lattices of amphiphysin n-bar domains. *Structure* 17:882–92.
17. Arkhipov A, Yin Y, Schulten K (2009) Membrane-bending mechanism of amphiphysin n-bar domains. *Biophys J* 97:2727–35.
18. Arumugam S, Chwastek G, Schwille P (2011) Protein-membrane interactions: the virtue of minimal systems in systems biology. *Wiley Interdiscip Rev Syst Biol Med* 3:269–80.

Bibliography

19. Loose M, Fischer-Friedrich E, Ries J, Kruse K, Schwille P (2008) Spatial regulators for bacterial cell division self-organize into surface waves in vitro. *Science* 320:789–92.
20. Arumugam S, Chwastek G, Fischer-Friedrich E, Ehrig C, Mönch I, Schwille P (2012) Surface topology engineering of membranes for the mechanical investigation of the tubulin homologue ftsz. *Angew Chem Int Ed Engl.*
21. Rytömaa M, Kinnunen PK (1994) Evidence for two distinct acidic phospholipid-binding sites in cytochrome c. *J Biol Chem* 269:1770–4.
22. Saarikangas J, Zhao H, Pykäläinen A, Laurinmäki P, Mattila PK, Kinnunen PKJ, Butcher SJ, Lappalainen P (2009) Molecular mechanisms of membrane deformation by i-bar domain proteins. *Curr Biol* 19:95–107.
23. Gorter E, Grendel F (1925) On bimolecular layers of lipoids on the chromocytes of the blood. *J Exp Med* 41:439–43.
24. Singer SJ, Nicolson GL (1972) The fluid mosaic model of the structure of cell membranes. *Science* 175:720–31.
25. Simons K, Ikonen E (1997) Functional rafts in cell membranes. *Nature* 387:569–72.
26. McMahon HT, Boucrot E (2011) Molecular mechanism and physiological functions of clathrin-mediated endocytosis. *Nat Rev Mol Cell Biol* 12:517–33.
27. Vijay-Kumar S, Bugg CE, Cook WJ (1987) Structure of ubiquitin refined at 1.8 Å resolution. *J Mol Biol* 194:531–44.
28. Zhang RG, Scott DL, Westbrook ML, Nance S, Spangler BD, Shipley GG, Westbrook EM (1995) The three-dimensional crystal structure of cholera toxin. *J Mol Biol* 251:563–73.
29. Takai Y, Kishimoto A, Iwasa Y, Kawahara Y, Mori T, Nishizuka Y (1979) Calcium-dependent activation of a multifunctional protein kinase by membrane phospholipids. *J Biol Chem* 254:3692–5.
30. Dumas JJ, Merithew E, Sudharshan E, Rajamani D, Hayes S, Lawe D, Corvera S, Lambright DG (2001) Multivalent endosome targeting by homodimeric eel. *Mol Cell* 8:947–58.
31. Lichte B, Veh RW, Meyer HE, Kilimann MW (1992) Amphiphysin, a novel protein associated with synaptic vesicles. *EMBO J* 11:2521–30.
32. Stahelin RV (2009) Lipid binding domains: more than simple lipid effectors. *J Lipid Res* 50 Suppl:S299–304.
33. Manna D, Albanese A, Park WS, Cho W (2007) Mechanistic basis of differential cellular responses of phosphatidylinositol 3,4-bisphosphate- and phosphatidylinositol 3,4,5-trisphosphate-binding pleckstrin homology domains. *J Biol Chem* 282:32093–105.
34. Gaullier JM, Simonsen A, D'Arrigo A, Bremnes B, Stenmark H, Aasland R (1998) Fyve fingers bind ptdins(3)p. *Nature* 394:432–3.
35. Sakamuro D, Elliott KJ, Wechsler-Reya R, Prendergast GC (1996) Bin1 is a novel myc-interacting protein with features of a tumour suppressor. *Nat Genet* 14:69–77.
36. Modregger J, Ritter B, Witter B, Paulsson M, Plomann M (2000) All three pacsin isoforms bind to endocytic proteins and inhibit endocytosis. *J Cell Sci* 113 Pt 24:4511–21.
37. Qualmann B, Roos J, DiGregorio PJ, Kelly RB (1999) Syndapin i, a synaptic dynamin-binding protein that associates with the neural wiskott-aldrich syndrome protein. *Mol Biol Cell* 10:501–13.
38. Itoh T, Erdmann KS, Roux A, Habermann B, Werner H, De Camilli P (2005) Dynamin and the actin cytoskeleton cooperatively regulate plasma membrane invagination by bar and f-bar proteins. *Dev Cell* 9:791–804.

39. Yamagishi A, Masuda M, Ohki T, Onishi H, Mochizuki N (2004) A novel actin bundling/filopodium-forming domain conserved in insulin receptor tyrosine kinase substrate p53 and missing in metastasis protein. *J Biol Chem* 279:14929–36.
40. Lee YG, Macoska JA, Korenchuk S, Pienta KJ (2002) Mim, a potential metastasis suppressor gene in bladder cancer. *Neoplasia* 4:291–4.
41. Lee SH, Kerff F, Chereau D, Ferron F, Klug A, Dominguez R (2007) Structural basis for the actin-binding function of missing-in-metastasis. *Structure* 15:145–55.
42. Rao Y, et al. (2010) Molecular basis for sh3 domain regulation of f-bar-mediated membrane deformation. *Proc Natl Acad Sci U S A* 107:8213–8.
43. Takei K, Slepnev VI, Haucke V, De Camilli P (1999) Functional partnership between amphiphysin and dynamin in clathrin-mediated endocytosis. *Nat Cell Biol* 1:33–9.
44. Ho HYH, Rohatgi R, Lebensohn AM, Ma L, Li J, Gygi SP, Kirschner MW (2004) Toca-1 mediates cdc42-dependent actin nucleation by activating the n-wasp-wip complex. *Cell* 118:203–16.
45. Takano K, Toyooka K, Suetsugu S (2008) Efc/f-bar proteins and the n-wasp-wip complex induce membrane curvature-dependent actin polymerization. *EMBO J* 27:2817–28.
46. Mizuno N, Jao CC, Langen R, Steven AC (2010) Multiple modes of endophilin-mediated conversion of lipid vesicles into coated tubes: implications for synaptic endocytosis. *J Biol Chem* 285:23351–8.
47. Jao CC, Hegde BG, Gallop JL, Hegde PB, McMahon HT, Haworth IS, Langen R (2010) Roles of amphipathic helices and the bin/amphiphysin/rvs (bar) domain of endophilin in membrane curvature generation. *J Biol Chem* 285:20164–70.
48. Frost A, Perera R, Roux A, Spasov K, Destaing O, Egelman EH, De Camilli P, Unger VM (2008) Structural basis of membrane invagination by f-bar domains. *Cell* 132:807–17.
49. Tsujita K, Suetsugu S, Sasaki N, Furutani M, Oikawa T, Takenawa T (2006) Coordination between the actin cytoskeleton and membrane deformation by a novel membrane tubulation domain of pch proteins is involved in endocytosis. *J Cell Biol* 172:269–79.
50. Chiantia S, Kahya N, Ries J, Schwille P (2006) Effects of ceramide on liquid-ordered domains investigated by simultaneous afm and fcs. *Biophys J* 90:4500–8.
51. Kahya N, Brown DA, Schwille P (2005) Raft partitioning and dynamic behavior of human placental alkaline phosphatase in giant unilamellar vesicles. *Biochemistry* 44:7479–89.
52. Israelachvili JN, Marcelja S, Horn RG (1980) Physical principles of membrane organization. *Q Rev Biophys* 13:121–200.
53. Chiantia S, Ries J, Kahya N, Schwille P (2006) Combined afm and two-focus sfcs study of raft-exhibiting model membranes. *Chemphyschem* 7:2409–18.
54. Bangham AD, Standish MM, Watkins JC (1965) Diffusion of univalent ions across the lamellae of swollen phospholipids. *J Mol Biol* 13:238–52.
55. Herold C, Chwastek G, Schwille P, Petrov EP (2012) Efficient electroformation of supergiant unilamellar vesicles containing cationic lipids on ito-coated electrodes. *Langmuir* 28:5518–21.
56. Lasic DD (1988) The mechanism of vesicle formation. *Biochem J* 256:1–11.
57. Olson F, Hunt CA, Szoka FC, Vail WJ, Papahadjopoulos D (1979) Preparation of liposomes of defined size distribution by extrusion through polycarbonate membranes. *Biochim Biophys Acta* 557:9–23.
58. Pick U (1981) Liposomes with a large trapping capacity prepared by freezing and thawing of sonicated phospholipid mixtures. *Arch Biochem Biophys* 212:186–94.

Bibliography

59. Angelova M, Dimitrov D (1986) Liposome electroformation. *Faraday Discuss. Chem. Soc.* 81:303–311.
60. Tamm L, McConnell H (1985) Supported phospholipid bilayers. *Biophysical journal* 47:105–113.
61. Ira, Zou S, Ramirez DMC, Vanderlip S, Ogilvie W, Jakubek ZJ, Johnston LJ (2009) Enzymatic generation of ceramide induces membrane restructuring: Correlated afm and fluorescence imaging of supported bilayers. *J Struct Biol* 168:78–89.
62. Müller DJ, Schabert FA, Büldt G, Engel A (1995) Imaging purple membranes in aqueous solutions at sub-nanometer resolution by atomic force microscopy. *Biophys J* 68:1681–6.
63. Magde D, Elson E, Webb WW (1972) Thermodynamic fluctuations in a reacting system measurement by fluorescence correlation spectroscopy. *Phys. Rev. Lett.* 29:705–708.
64. Rigler R, et al. (1999) Specific binding of proinsulin c-peptide to human cell membranes. *Proc Natl Acad Sci U S A* 96:13318–23.
65. Schwille P, Kummer S, Heikal AA, Moerner WE, Webb WW (2000) Fluorescence correlation spectroscopy reveals fast optical excitation-driven intramolecular dynamics of yellow fluorescent proteins. *Proc Natl Acad Sci U S A* 97:151–6.
66. Petrov E, Schwille P (2008) State of the art and novel trends in fluorescence correlation spectroscopy. *Standardization and Quality Assurance in Fluorescence Measurements II* pp 145–197.
67. Binnig G, Quate C, Gerber C (1986) Atomic force microscope. *Phys Rev Lett* 56:930–933.
68. Kang D, Gho YS, Suh M, Kang C (2002) Highly sensitive and fast protein detection with coomassie brilliant blue in sodium dodecyl sulfate-polyacrylamide gel electrophoresis. *Bull. Korean Chem. Soc.* 23:1511.
69. Petrásek Z, Schwille P (2008) Precise measurement of diffusion coefficients using scanning fluorescence correlation spectroscopy. *Biophys J* 94:1437–48.
70. Sorre B, Callan-Jones A, Manzi J, Goud B, Prost J, Bassereau P, Roux A (2012) Nature of curvature coupling of amphiphysin with membranes depends on its bound density. *Proc Natl Acad Sci U S A* 109:173–8.
71. Bhatia VK, Madsen KL, Bolinger PY, Kunding A, Hedegård P, Gether U, Stamou D (2009) Amphipathic motifs in bar domains are essential for membrane curvature sensing. *EMBO J* 28:3303–14.
72. Hatzakis NS, et al. (2009) How curved membranes recruit amphipathic helices and protein anchoring motifs. *Nat Chem Biol* 5:835–41.
73. Madsen KL, Bhatia VK, Gether U, Stamou D (2010) Bar domains, amphipathic helices and membrane-anchored proteins use the same mechanism to sense membrane curvature. *FEBS Lett* 584:1848–55.
74. Kunding AH, Mortensen MW, Christensen SM, Stamou D (2008) A fluorescence-based technique to construct size distributions from single-object measurements: application to the extrusion of lipid vesicles. *Biophys J* 95:1176–88.
75. Feller SE, Yin D, Pastor RW, MacKerell ADJ (1997) Molecular dynamics simulation of unsaturated lipid bilayers at low hydration: parameterization and comparison with diffraction studies. *Biophys J* 73:2269–79.
76. Mills TT, Toombes GES, Tristram-Nagle S, Smilgies DM, Feigenson GW, Nagle JF (2008) Order parameters and areas in fluid-phase oriented lipid membranes using wide angle x-ray scattering. *Biophys J* 95:669–81.
77. Gudmand M, Fidorra M, Bjørnholm T, Heimburg T (2009) Diffusion and partitioning of fluorescent lipid probes in phospholipid monolayers. *Biophys J* 96:4598–609.
78. Doolittle A (1952) Studies in newtonian flow. iii. the dependence of the viscosity of liquids on molecular weight and free space (in homologous series). *Journal of Applied Physics* 23:236–239.

79. Galla HJ, Hartmann W, Theilen U, Sackmann E (1979) On two-dimensional passive random walk in lipid bilayers and fluid pathways in biomembranes. *J Membr Biol* 48:215–36.
80. Dietrich C, Bagatolli LA, Volovyk ZN, Thompson NL, Levi M, Jacobson K, Gratton E (2001) Lipid rafts reconstituted in model membranes. *Biophys J* 80:1417–28.
81. Karttunen M, Haataja MP, Säily M, Vattulainen I, Holopainen JM (2009) Lipid domain morphologies in phosphatidylcholine-ceramide monolayers. *Langmuir* 25:4595–600.
82. Sezgin E, Kaiser HJ, Baumgart T, Schwille P, Simons K, Levental I (2012) Elucidating membrane structure and protein behavior using giant plasma membrane vesicles. *Nat Protoc* 7:1042–51.
83. Duman M, et al. (2010) Improved localization of cellular membrane receptors using combined fluorescence microscopy and simultaneous topography and recognition imaging. *Nanotechnology* 21:115504.
84. Wieser S, Moertelmaier M, Fuertbauer E, Stockinger H, Schütz GJ (2007) (un)confined diffusion of cd59 in the plasma membrane determined by high-resolution single molecule microscopy. *Biophys J* 92:3719–28.
85. Ando T, Kodera N, Takai E, Maruyama D, Saito K, Toda A (2001) A high-speed atomic force microscope for studying biological macromolecules. *Proc Natl Acad Sci U S A* 98:12468–72.
86. Kodera N, Kinoshita T, Ito T, Ando T (2003) High-resolution imaging of myosin motor in action by a high-speed atomic force microscope. *Adv Exp Med Biol* 538:119–27.
87. Milhiet PE, Yamamoto D, Berthoumieu O, Dosset P, Le Grimellec C, Verdier JM, Marchal S, Ando T (2010) Deciphering the structure, growth and assembly of amyloid-like fibrils using high-speed atomic force microscopy. *PLoS One* 5:e13240.

Declaration (Erklärung)

Declaration according to §5.5 of the doctorate regulations.
Erklärung entsprechend §5.5 der Promotionsordnung.

I herewith declare that I have produced this paper without the prohibited assistance of third parties and without making use of aids other than those specified; notions taken over directly or indirectly from other sources have been identified as such. This paper has not previously been presented in identical or similar form to any other German or foreign examination board.

The thesis work was conducted from September 2008 to August 2012 under the supervision of Prof.Dr. Petra Schwille in Biophysics research group, at Biotec, Dresden University of Technology, Germany.

I declare that I have not undertaken any previous unsuccessful doctorate proceedings.

I declare that I recognise the doctorate regulations of the Fakultät für Mathematik und Naturwissenschaften of the Technische Universität Dresden.

Hiermit versichere ich, dass ich die vorliegende Arbeit ohne unzulässige Hilfe Dritter und ohne Benutzung anderer als der angegebenen Hilfsmittel angefertigt habe; die aus fremden Quellen direkt oder indirekt übernommenen Gedanken sind als solche kenntlich gemacht. Die Arbeit wurde bisher weder im Inland noch im Ausland in gleicher oder ähnlicher Form einer anderen Prüfungsbehörde vorgelegt.

Die Dissertation wurde im Zeitraum vom September 2008 bis August 2012 verfasst und von Prof. Dr. Petra Schwille, Biophysik Forschungsgruppe, Biotec, Technische Universität Dresden betreut.

Meine Person betreffend erkläre ich hiermit, dass keine früheren erfolglosen Promotionsverfahren stattgefunden haben.

Ich erkenne die Promotionsordnung der Fakultät für Mathematik und Naturwissenschaften, Technische Universität Dresden an.

.....

Dresden, 31.08.2012